MODIFIED VIRTUAL INTERNAL BOND MODEL FOR CONCRETE SUBJECTED TO DYNAMIC LOADING

A THESIS IN

Civil Engineering

Submitted to the Faculty of the University of
Missouri-Kansas City in partial fulfillment of
Requirements for the degree of
MASTER OF SCIENCE

by

MAYURI PATIL

Bachelor of Technology- Civil Engineering (2011)

Veermata Jijabai Technological Institute

(Autonomous: Affiliated to Mumbai University)

University of Missouri-Kansas City

2014

© 2014
MAYURI RAJENDRA PATIL
ALL RIGHTS RESERVED

MODIFIED VIRTUAL INTERNAL BOND MODEL FOR CONCRETE SUBJECTED TO DYNAMIC LOADING

Mayuri Rajendra Patil, Candidate for the Master of Science Degree,
University of Missouri- Kansas City

ABSTRACT

Concrete is often used as a primary material to build protective structures. There is a wide range of research work being performed to simulate the behavior of reinforced concrete under impact and blast loading. This behavior is studied from both material and structural points of view. The research study presented in this thesis focuses on material aspects of modeling. LS-DYNA® is an effective software for modeling and finite element analysis of structural members. It allows the user to define the material through commercially available or user-defined constitutive material models. Each material model has a distinct set of parameters to define a material which is further assigned to elements and used for simulations. This research study presents a user defined material model called Modified Concrete Virtual Internal Bond Model (MC-VIB). The basic constitutive model of VIB assumes the body as a collection of randomly oriented material points interconnected by a network of internal bonds. The model was modified by several researchers for different purposes. This research presents the MC-VIB for concrete under dynamic loading and studies its implementation into LS-DYNA®. The modifications include incorporation of shear behavior and accounting for the difference in behavior of concrete in tension and compression.

This project includes the calibration of the model based on stress-strain behavior of single element and cylinder model of concrete. The parameters are based on concrete with a uniaxial compressive strength of 27.6 MPa (4 ksi). These numerical curves are compared to those obtained from conventionally used material models for concrete and standard curves obtained by accepted equations to check the accuracy of prediction.

The material model available in LS-DYNA® requires a number of input parameters to define concrete behavior. These properties are normally derived from actual tests performed on the concrete under consideration. Often the properties are based on past experiments performed and the values are automatically generated by the material model. This study has attempted to keep the number of variables and hence the number of tests to minimum. This study has derived the values for the input parameters of the MC-VIB and has successfully simulated the stress-strain response of concrete in tension and compression under dynamic loading.

APPROVAL PAGE

The faculty listed below, appointed by the Dean of the School of Computing and Engineering have examined a thesis titled "Modified Virtual Internal Bond Model for Concrete Subjected To Dynamic Loading" presented by Mayuri Rajendra Patil candidate for Master of Science in Civil Engineering, and certify that in their opinion it is worthy of acceptance.

Supervisory Committee

Ganesh Thiagarajan, Ph.D., P.E., Committee Chair
Department of Civil and Mechanical Engineering

Ceki Halmen, Ph.D.
Department of Civil and Mechanical Engineering

ZhiQiang Chen, Ph.D.
Department of Civil and Mechanical Engineering

TABLE OF CONTENTS

LIST OF ILLUSTRATIONS

Figure Page

LIST OF TABLES

Table Page

ACKNOWLEDGEMENTS

I would like to express my gratitude to everyone who was involved with me to complete this thesis.

I am grateful to my advisor Dr. Ganesh Thiagarajan for the opportunity to work with him on this research project, continuous guidance and support. It has been a great learning process. I am thankful to Dr. Ceki Halmen and Dr. ZhiQiang Chen for serving as a supervisor committee. I sincerely thank my colleagues at Desai Nasr Consulting Engineers for support and my supervisor Marc Steinhobel for motivation and understanding in to complete my thesis while working.

I am thankful for my lab mates Gunjan Shetye, Timothy Hines, Qiwei Cao, Bhargav Javvaji, and Kavya Thadisina for maintaining a positive working environment in Computational Mechanics lab. I would also like to mention my friends Tejas, Kuldeep and Wahid to keep up my spirit for completing my thesis.

I owe my thanks to my family, Rajendra Patil, Anupama Patil and Omkar Patil for continuous encouragement in my higher studies abroad.

I would like to acknowledge financial support by National Science Foundation through award number 0748085 and School of Computing and Engineering.

Chapter 1.

INTRODUCTION

1.1. An Overview: Research for Developing Blast Resistant Concrete Structures

With the increase in terrorist attacks on civilian structures, there is huge demand for research to develop blast resisting structures. Extensive research is being conducted at the University of Missouri Kansas City for design of structures for blast and impact loading. A major part of the study focuses on design of reinforced concrete structures subjected to blast and impact loading. One aspect of the study is to model structural members like column, slab or beam using commercially available finite element analysis software such as LS-DYNA® and try to simulate the behavior with changing reinforcement, loading, strain rate, grade of materials etc. While focusing on structural analysis, it is equally important to understand the theory behind the behavior of concrete as a material and pay attention to its properties used for the analysis.

1.2. Material Models in LS-DYNA®

This particular project presented in this thesis, addresses the material aspect of the study. It involves, simulating a cylinder model with 27.6 MPa (4 ksi) concrete under velocity loading using LS-DYNA®, an effective software for modelling and finite element analysis of structure for dynamic loading. This program allows user to specify the material properties using any material model. It can be commercially available or it can be user defined. For instance, Concrete_Damage_Model_Release_3 or Continuous_Surface_Cap_Model (CSCM)

are two material models already defined in the LS-DYNA® library and require different set of input parameters to describe a 27.6 MPa or 4 ksi concrete. Depending on the purpose of the simulation or study, any of these material models can be used. More insight is given on these material models in a later part of the thesis.

Material models involve the set of input parameters based on the sequence of equations which define the material constitutive model. For example, unconfined compressive strength of concrete, elasticity modulus, Poisson's ratio are the input parameters used to calculate the axial stress produced in the elements of concrete cylinder under the velocity loading. LS-DYNA® also allows users to supply their own subroutines defining material models by writing a user material subroutine called by the LS-DYNA® user material interface, creating a custom executable which includes material subroutine, Invoking that subroutine by defining a part in the keyword input deck that uses *MAT_USER_DEFINED_MATERIAL_MODELS with appropriate input parameters.

1.3. Proposed User Defined Material Model

One such user defined material model called the Modified Concrete Virtual Internal Bond Model (MC-VIB) proposed by Thiagarajan is at the core of this project. The basic Virtual Internal Bond (VIB) model assumes that the body is collection of randomly oriented material points interconnected by a network of internal bonds. The Literature study behind the theory, development and modifications to this VIB model is presented in Chapter 2. The original VIB model for concrete [1] was capable of only simulating axial tension behavior of concrete for simulating cracking and assumed an elastic compression behavior. The MC-VIB focuses on incorporating shear behavior of concrete and addresses the issue that behavior of concrete

differs in compression and tension. The stress-strain results from the proposed model have been compared with an existing analytical model which is described by Hognestad's Equation and another concrete model in LS-DYNA® called CONCRETE_DAMAGE_MODEL_RELEASE3 (CDMR3).

1.4. Scope of the Project:

In order to achieve the objectives of the research project, the following best describes the scope of the project.

Task 1: Obtain stress-strain curve for 27.6 MPa (4 ksi) concrete using Hognestad's Equation.

Task 2: Run single element simulations for 4 ksi concrete using CONCRETE_DAMAGE_MODEL_RELEASE_3 under velocity loading of 5 mm per sec under Unconfined Uniaxial Compression (UUC) and Unconfined Uniaxial Tension (UUT).

Task 3: Run single element simulations implementing MC-VIB subroutine in LS-DYNA® to study the effect of change in seven parameters, designated by E, EPS_C, BETA_C, EPS_T, BETA_T, EN, EC explained later in the thesis.

Task 4: Perform the single element simulations for cases consistent with those in Task 2 with several trial combinations of these seven parameters stated in Task 3. Compare the curves with those with their respective case for CDMR3 and Hognestad's Equation. Obtain a best combination of these seven variables, which can simulate closest possible behavior to concrete with unconfined compressive strength of 27.6 MPa (4 ksi) concrete under the given velocity loading.

Task 5: Proceed with this set of parameters to run simulations for 24 Cylinder models, twelve for each concrete model, CDMR3 and MC-VIB respectively. Analyze the results from UUC and UUT and base the conclusion on three criteria namely, % difference in peak stress and strain value with those from Hognestad's Equation and CDMR3, effect of mesh size on peak stress and strain value for a cylinder size, effect of cylinder size on peak stress and corresponding strain value for a mesh size.

1.5. Thesis Organization

The Chapter 2 describes the literature survey done on the development and modification of Virtual Internal Bond (VIB) model. It explains theory and its implementation in the Elasticity in LS-DYNA® user-defined concrete material model. It refers to the literature to substantiate the theory and to use it in practice.

The Chapter 3 describes the procedure to study the parameters of MC-VIB model based on single element simulations. One of the popular commercially available material model *MAT_CONCRETE_DAMAGE_RELEASE3 is used for calibration of the newly proposed MC-VIB model which is also explained in this chapter. It gives idea about the generation of single element and cylinder models, assumptions of properties, Boundary conditions assumed and value and mode of application of loads to the model. It also explains how the stress-strain curves are obtained and studied from the models. It briefly explains effect of each parameter on stress-strain curve.

The Chapter 4 presents comparison of stress-strain curves between MC-VIB and CDMR3 under same velocity loading for two cases namely UUC and UUT. The effect of mesh size and size of the cylinder on the stress-strain behavior of the cylinder is also presented in

graphical form in this chapter. It also presents summary of all the results obtained from comparison of curves from new model and the reference models. It contains discussion and interpretation of results.

The Chapter 5 talks about conclusion drawn from all the results from study. Once the model is generated, there will be scope to study the material model further and analyze it to confirm its suitability for further use in the simulations.

Chapter 2.

DEVELOPMENT OF MODIFIED CONCRETE VIRTUAL INTERNAL BOND MODEL

2.1 Literature Survey

This thesis presents the theoretical aspects of the material model Modified Concrete Virtual Internal Bond (MC-VIB), its parameters and implementation in LS-DYNA®. The focus of this particular thesis is the calibration of the model based on stress-strain behavior. In wider scope, objective to develop this model is for prediction and numerical simulation of fracture, crack initiation and propagation in concrete. A literature study has been performed to understand the development of VIB theory, on the background of other approaches used for the same purpose and the modifications done by the researchers over the years on this VIB model to use it for different objectives.

The materials can be ductile or brittle, composite, functionally graded or nanomaterial. There are three primary approaches to simulate fracture in variety of materials [1]. The first is based on molecular dynamics (MD) method which can be combined with finite element method. The other two approaches are finite element based known as cohesive bond theory for modeling fracture and the virtual internal bond (VIB).

The molecular dynamics method uses the interatomic potentials to simulate millions of atoms with appropriate boundary conditions. The choice of the interatomic potential and the availability of supercomputing facilities to model around 10^{23} items to simulate 1 cm^3 of a solid are critical parts of this approach [1]. The cohesive surface approach is based on defining discrete cohesive surfaces. The nonlinear cohesive law defines the traction and separation at

the boundaries eliminating the need for a separate fracture criteria. But this approach requires defining these cohesive surfaces lying in between the element boundaries and introduction of separate cohesive elements in between the boundaries of regular finite elements.

Gao [2] proposed a theory that, the hyperelastic description of the crack tip behavior in the Lagrangian framework provides a better explanation of crack tip instabilities. Based on his this theory, Gao [3] put forward the third approach or materials undergoing brittle fracture. It is multiscale approach connecting atomistic and continuum scales and incorporates the fracture criterion directly into the constitutive formulation of the material. Gao and Klein [4] developed virtual internal bond (VIB) method, in which cohesive type law is directly incorporated into the constitutive model by treating the body as a collection of randomly oriented material points interconnected by a network of cohesive bonds. With the Cauchy-Born rule of crystal elasticity, constitutive relations can be derived by equating the strain energy of the bonds to the potential energy stored in continuum due to applied loads and deformations. The bridging of scales between the continuum and atomistic levels is done by relating the bond length between the atoms to the continuum based Green Lagrange strain tensor. The second Piola-Kirchoff stress tensor can be computed from the potential energy expression.

Implicit and explicit are the two integration schemes which can be used to implement VIB model into finite element methods. Zhang et al. [5] used implicit method to integrate VIB ABAQUS 2000 using UMAT subroutine. Preconditions such as incorporating stiff elements adjoining the VIB layer may be required to implement this scheme successfully. It is very similar to pre-specifying the crack path. This proves its suitability for implicit fracture situations in which the elements on both the sides of the interface are relatively stiff throughout the deformation process.

These numerical issues were eliminated by Thiagarajan et al. [6] with explicit integration of cohesive models in ABAQUS with UMAT subroutine and they found it to be better suited finite element implementation than implicit integration. They studied the effect of mesh size, loading rate and other factors in quasi-static and dynamic loading cases on crack initiation, propagation and branching. They also verified and validated VIB model for dynamic fragmentation of brittle materials (alumina) under impact loading with experiments in Thiagarajan et al. [6]

To extend this VIB fracture model to ductile materials, the plasticity was incorporated at the continuum level by Thiagarajan et al [7]. It was achieved by blending together the two models, one is VIB model for tensile fracture and failure behavior at the atomistic level and the other is continuum level plasticity model.

Thiagarajan and Misra [7] introduced the bond density function at atomistic level and modeled that using the spherical harmonic expansion to apply VIB model to anisotropic materials. They recognized that the bond densities are different in different directions and introduced the anisotropy as a directional distribution of bond density function.

Zhang and Ge [8] presented a modified VIB model incorporating Poisson's effect into the model by introducing R-Bonds. This feature allows the definition of bond stiffness using both the elastic modulus and Poisson's ratio. Crack initiation and propagation under tensile loading was simulated.

Zhang et al [9] then proposed the virtual multi-dimensional internal bond (VMIB) model by incorporating the shear bond into VIB model to associate the macro mechanical properties of material with the microscopic mechanical properties of discrete structure. In [9] they presented simulation of the shear fracture of heterogeneous materials using VMIB.

Thiagarajan [1] applied the VIB model to the dynamic fracture simulation of plain concrete. To compare the simulation results the Experimental work on the dynamic tensile behavior of plain concrete Gran et al. [8] was the chosen for that study.

Zhang [11] developed a technique to model the pre-existing cracks distributed in heterogeneous materials. The fracture criteria was incorporated into the constitutive relationship via bond evolution function. In the paper [12] Zhang used equivalent cohesive zone (ECZ) method to represent a pre-existing crack which has same micromechanical properties as the surrounding material. He assigned an initial deformation to the ECZ to make the interaction between two faces of pre-existing crack negligible. He found this technique efficient as it does not need to consider the geometrical integrity of a cracked body in meshing procedure and does not need to modify the mesh configuration when crack propagates.

In another study, Zhang et al. [13] applied three node contact element (TCE) to VMIB model successfully to simulate the fracture propagation and coalescence behavior subjected to the compressive and shear stress field. The study proved the method to be efficient for pre-existing and newly extended fracture, which can be incorporated without remeshing. The drawback of this method is, large number of elements are needed to be modeled for accuracy.

In his recent study, Zhang [14] discretized the continuous VIB model for nonlinearity and developed a discrete system composed of unit cell in which the bonds are discretely distributed and the bond number is finite. This method is efficient to simulate fracture in a nonlinear elastic material.

2.2 Theoretical Framework

2.2.1 Development of VIB Model

2.2.1.1 Elements of Virtual Internal Bond Model

A material behaves differently at different scales [9]. It has discrete interaction in microscopic or atomic level while it is continuous at macroscopic or mechanical level. The theory of continuum mechanics emerges from hypothesis of continuous field. When using this theory to solve mechanical engineering problems for solid materials, it is common practice to consider its continuous nature at macroscopic level and ignore the freedom of each atom at microscopic level. To better solve the problem, it is necessary to combine both the scales in one approach, which is successfully achieved by VIB theory. In the VIB theory assumes that solid material is a collection of micro-particles with mass connected with virtual internal bonds, thus combining both the scales as following description.

At macroscopic level, based on theory of hyper-elastic continuum, the location of each microscopic particle is defined by deformation gradient using Cauchy-Born Rule. To denote initial and deformed configuration, Lagrangian coordinates $\bar{X} = \bar{X}_\iota$ and the Eulerian coordinates $x = x(\bar{X}, t) = x_i(\bar{X}_\iota, t)$ respectively are used. In this thesis, capital letter subscripts denote initial configuration and the lower case subscripts denote the deformed configuration. Lagrangian description the deformation gradient is as given by Eq. 1 and Eq. 2 defines the Green-Lagrange strain tensor, where, *I* is the second order identity tensor.

$$F = \frac{\partial x}{\partial X} \; or \; F_{iI} = \frac{\partial x_i}{\partial X_I} \qquad \text{Eq. 1}$$

$$E = \frac{1}{2}(F^T F - I) \quad \text{Eq. 2}$$

At atomistic or level, the potential energy function $U(l)$ can be used to describe the bond, where l = bond length. Consider an arbitrary microstructural bond which is oriented at an angle θ with respect to vertical positive axis and an angle ϕ in the horizontal plane with respect to vertical axis. The expression, $\xi = (sin\theta cos\phi, sin\theta sin\phi, cos\theta)$ gives the unit vector along this direction with respect to the undeformed configuration. Equating the stretch of bond at micro scale to deformation at continuum level, the Eq. 3 is obtained.

$$l = l_0\sqrt{1 + 2\xi_I E_{IJ}\xi_J} \quad \text{Eq. 3}$$

Cauchy-Born Rule

Cauchy-Born rule is helpful to derive, the macroscopic strain energy density function shown in the Eq. 4.

$$U(E_{IJ}) =< U(l) > \quad \text{Eq. 4}$$

Where, <> represents the weighted average with respect to the bond density function D_d and $U(l)$ is the bond potential energy function. Assuming that all the bonds have the same initial length l_o, for the general case the weighted average is given by Eq. 5.

$$< \cdots > = \int_0^{2\pi}\int_0^{\pi} .. D_d(\theta, \phi) sin\theta d\theta d\phi \quad \text{Eq. 5}$$

The term $D_d(\theta, \phi) sin\theta d\theta d\phi$ represents the number of bonds per unit volume between the bond angles $(\theta, \theta + d\theta)$ and $(\phi, \phi + d\phi)$.

2.2.1.2 Constitutive Elements and Cohesive Force Law

As explained in [1] using the strain energy density function U given in Eq. 4, the symmetric second Piola-Kirchoff stress S_{IJ} and the elastic modulus C_{IJKL} can be expressed as shown in Eq. 6.

$$S = \frac{\partial \Phi}{\partial E} \; or \; S_{IJ} = \frac{\partial \Phi}{\partial E_{IJ}} \qquad \text{Eq. 6}$$

$$C_{IJKL} = \frac{\partial^2 \Phi}{\partial E_{IJ} \partial E_{KL}}$$

The modulus derived from this potential satisfies the major and minor symmetries, $C_{IJKL} = C_{JIKL} = C_{IJLK} = C_{KLIJ}$, and Cauchy symmetry, $C_{IJKL} = C_{IKJL}$. As the Cauchy symmetry is satisfied by the fourth order isotropic elasticity tensor only for the case $\lambda = \mu$, where λ and μ are the two Lame's constants, for isotropic material it needs only one elastic constant.

It is difficult to derive a generalized closed form solution for the elastic stiffness tensor. But derivations of analytical forms of elastic stiffness tensor are given by Gao and Klein [4] for few simple cases. These cases can be used as guideline to correlate isotropic material properties to the model parameters. For the plane stress isotropic solid, the Eq. 7 can give the shear modulus *G*.

$$G = \frac{\pi D_0 {l_0}^2 U"(l_0)}{4} \qquad \text{Eq. 7}$$

Derivative of bond potential energy with respect to bond length gives bond potential or cohesive force $U'(l)$ which can be expressed as in

Eq. 8 using the classical two parameters cohesive law.

$$U'(l) = A(l - l_0)e^{-\frac{l-l_0}{B}} \quad \text{Eq. 8}$$

For equibiaxial stretching condition, the constant $\boldsymbol{A}$ can be related to the initial shear modulus by Eq. 7 . In the Eq. 8 the parameter $\frac{l-l_0}{B}$ is related to the strain at which the cohesive stress is attained.

2.2.1.3 Physical Consideration of Material Behavior

The mass particles are connected with virtual bonds embedded in the body assumed to obey the cohesive law [8]. For two coupled particles, there are axial and rotational degrees of freedom which are restricted by L-bond and R-bond respectively. The interaction in VIB model is nonlinear elastic for the interaction in the both L-bond and R-bond. The mean values of the stiffness coefficients for normal and rotational bond are expressed as shown in Eq. 9 and Eq. 10 respectively.

$$\bar{k} = \frac{3E}{4\pi(1-2\nu)} \quad \text{Eq. 9}$$

$$\bar{r} = \frac{3(1-4\nu)E}{4\pi(1+\nu)(1-2\nu)} \quad \text{Eq. 10}$$

The L-bond stretch in a certain direction ξ is given by Eq. 11.

$$l = l_0 \xi_i \varepsilon_{ij} \xi_j \qquad \text{Eq. 11}$$

Where, $\xi = (sin\theta cos\phi, sin\theta sin\phi, cos\theta)$is the unit orientation vector of L-bond in the sphere coordinate system, ε_{ij} is the strain tensor and l_0 is the original length of the L-bond. The rotation angles of L-bond with orientation ξ towards three coordinate axes are given by Eq. 12.

$$\begin{aligned} \beta_1 &= \xi_i \varepsilon_{ij} \eta'_j \\ \beta_2 &= \xi_i \varepsilon_{ij} \eta''_j \\ \beta_3 &= \xi_i \varepsilon_{ij} \eta'''_j \end{aligned} \qquad \text{Eq. 12}$$

Where η is the unit vector perpendicular to ξ and $\overrightarrow{x_i}$ is the unit orientation vector of coordinate-x_i. The detailed expression of η is

Eq. 13.

$$\begin{aligned} \eta' &= \xi \times (\overrightarrow{x_1} \times \xi) = (sin^2\theta sin^2\phi + cos^2\theta, -sin^2\theta cos\phi sin\phi, -sin\theta cos\phi cos\theta) \\ \eta'' &= \xi \times (\overrightarrow{x_2} \times \xi) = (-sin^2\theta cos\phi sin\phi, cos^2\theta + sin^2\theta cos^2\phi, , -sin\theta sin\phi cos\theta) \\ \eta''' &= \xi \times (\overrightarrow{x_1} \times \xi) = (-sin\theta cos\phi cos\theta, -sin\theta sin\phi cos\theta, sin^2\theta) \end{aligned} \qquad \text{Eq. 13}$$

The energy potential stored in single L-Bond can be expressed as Eq. 14.

$$U_L = \frac{1}{2} k l^2 = \frac{1}{2} \lambda \bar{k} (\xi_i \varepsilon_{ij} \xi_j)^2 \qquad \text{Eq. 14}$$

$$U_{R1} = \frac{1}{2} r {\beta_1}^2 = \frac{1}{2} \lambda \bar{r} \left(\xi_i \varepsilon_{ij} {\eta'}_j \right)^2$$
$$U_{R2} = \frac{1}{2} r {\beta_2}^2 = \frac{1}{2} \lambda \bar{r} \left(\xi_i \varepsilon_{ij} {\eta''}_j \right)^2 \quad \text{Eq. 15}$$
$$U_{R3} = \frac{1}{2} r {\beta_3}^2 = \frac{1}{2} \lambda \bar{r} (\xi_i \varepsilon_{ij} {\eta'''}_j)^2$$

Where,$U_{Ri} = (i = 1,2,3)$ is the energy potential of the R-Bond corresponding to the coordinate-x_i such that β_i is the rotation angles of L-bond towards co-ordinate- x_i . Hence, the energy potential within two-coupled particles $i - j$ could be expressed as

Eq. 16.

$$U = U_L + U_{R1} + U_{R2} + U_{R3}$$
$$\Phi = \int_0^{2\pi} \int_0^{\pi} U_L D(\theta, \phi) \sin(\theta)\, \mathrm{d}\theta \mathrm{d}\phi + \int_0^{2\pi} \int_0^{\pi} (U_{R1} + U_{R2} + U_{R3}) D(\theta, \phi) \sin(\theta)\, \mathrm{d}\theta \mathrm{d}\phi \quad \text{Eq. 16}$$

As per quasi-continuum method, a continuum volume element can be made equivalent to a discrete microstructure by equating strain energies. If a random element under consideration has volume V, the total strain energy stored in L-Bond can be denoted by

Eq. 17

$$\Phi_L = \int_{L_1}^{L_2} \int_0^{2\pi} \int_0^{\pi} U_L D_L(l_0, \theta, \phi) \sin(\theta)\, \mathrm{d}\theta \mathrm{d}\phi \mathrm{d}l_0 \quad \text{Eq. 17}$$

Where, $D_L(l_0, \theta, \phi)$ is the spatial distribution density of length bond l_0; $D_L(l_0, \theta, \phi) \sin(\theta)\, \mathrm{d}\theta \mathrm{d}\phi$ is the number of l_0-length bonds per unit volume between the bond angle $(\theta, \theta + d\theta)$ and $(\phi, \phi + d\phi)$ in spherical coordinates; L_1, L_2 represent the minimum and

maximum original length of L-bond respectively. The total strain energy stored in R-bond can thus be expressed as in Eq. 18.

$$\begin{aligned} \mathrm{U}_R = & \int_{L_1}^{L_2}\int_0^{2\pi}\int_0^{\pi} U_{R1} D_{R1}(l_0,\theta,\phi)\sin(\theta)\,\mathrm{d}\theta\mathrm{d}\phi\mathrm{d}l_0 \\ & + \int_{L_1}^{L_2}\int_0^{2\pi}\int_0^{\pi} U_{R2} D_{R2}(l_0,\theta,\phi)\sin(\theta)\,\mathrm{d}\theta\mathrm{d}\phi\mathrm{d}l_0 \\ & + \int_{L_1}^{L_2}\int_0^{2\pi}\int_0^{\pi} U_{R3} D_{R3}(l_0,\theta,\phi)\sin(\theta)\,\mathrm{d}\theta\mathrm{d}\phi\mathrm{d}l_0 \end{aligned} \qquad \text{Eq. 18}$$

Where, $D_{R_i}(l_0,\theta,\phi)(i=1,2,3)$ is distribution function of R-bond related to the L-bond with original length, l_0. The term U_{R_i} is the corresponding R-bond energy given in Eq. 15. The total strain energy stored in bond is given by Eq. 19.

$$\mathrm{U} = \mathrm{U}_L + U_R \qquad \text{Eq. 19}$$

Equating the strain energy function at continuum level to the potential energy stored in the cohesive bonds due to an imposed deformation, the stress tensor can be expressed as the relations used in the hyper-elastic theory as shown in Eq. 20. The elastic modulus can be expressed as in Eq. 22 and Eq. 22.

$$\begin{aligned} \sigma_{ij} = \frac{\partial(\frac{\Phi}{\mathrm{V}})}{\partial\varepsilon_{ij}} = & \frac{1}{V}\int_{L_1}^{L_2}\int_0^{2\pi}\int_0^{\pi} k{l_0}^2(\xi_m\varepsilon_{mn}\xi_n)\xi_i\xi_j D_L(l_0,\theta,\phi)\sin(\theta)\,\mathrm{d}\theta\mathrm{d}\phi\mathrm{d}l_0 \\ & + \frac{1}{V}\int_{L_1}^{L_2}\int_0^{2\pi}\int_0^{\pi} r\beta_1\xi_i{\eta'}_j D_{R1}(l_0,\theta,\phi)\sin(\theta)\,\mathrm{d}\theta\mathrm{d}\phi\mathrm{d}l_0 \\ & + \frac{1}{V}\int_{L_1}^{L_2}\int_0^{2\pi}\int_0^{\pi} r\beta_1\xi_i{\eta''}_j D_{R2}(l_0,\theta,\phi)\sin(\theta)\,\mathrm{d}\theta\mathrm{d}\phi\mathrm{d}l_0 \\ & + \frac{1}{V}\int_{L_1}^{L_2}\int_0^{2\pi}\int_0^{\pi} r\beta_1\xi_i{\eta'''}_j D_{R3}(l_0,\theta,\phi)\sin(\theta)\,\mathrm{d}\theta\mathrm{d}\phi\mathrm{d}l_0 \end{aligned} \qquad \text{Eq. 20}$$

$$C_{ijkl} = \frac{\partial^2 \left(\frac{\Phi}{V}\right)}{\partial \varepsilon_{ij} \partial \varepsilon_{kl}} \quad \text{Eq. 21}$$

$$\begin{aligned} C_{ijkl} = \frac{1}{V}\int_{L_1}^{L_2}\int_0^{2\pi}\int_0^{\pi} k{l_0}^2 \xi_i \xi_j \xi_k \xi_l D_L(l_0,\theta,\phi)\sin(\theta)\,\mathrm{d}\theta\mathrm{d}\phi\mathrm{d}l_0 \\ + \frac{1}{V}\int_{L_1}^{L_2}\int_0^{2\pi}\int_0^{\pi} r\xi_i {\eta'}_j \xi_k {\eta'}_l D_{R1}(l_0,\theta,\phi)\sin(\theta)\,\mathrm{d}\theta\mathrm{d}\phi\mathrm{d}l_0 \\ + \frac{1}{V}\int_{L_1}^{L_2}\int_0^{2\pi}\int_0^{\pi} r\xi_i {\eta''}_j \xi_k {\eta''}_l (l_0,\theta,\phi)\sin(\theta)\,\mathrm{d}\theta\mathrm{d}\phi\mathrm{d}l_0 \\ + \frac{1}{V}\int_{L_1}^{L_2}\int_0^{2\pi}\int_0^{\pi} r\xi_i {\eta'''}_j \xi_k {\eta'''}_l (l_0,\theta,\phi)\sin(\theta)\,\mathrm{d}\theta\mathrm{d}\phi\mathrm{d}l_0 \end{aligned} \quad \text{Eq. 22}$$

For the isotropic material, the bond density distributed uniformly in spatial. So, both the L-bond density and the R-bond density could be taken as constant and $D_L(\theta,\phi) = D_{R1}(\theta,\phi) = D_{R2}(\theta,\phi) = D_{R3}(\theta,\phi)$. Consider $\int_0^{2\pi}\int_0^{\pi} D(\theta,\phi)\sin(\theta)\,\mathrm{d}\theta\mathrm{d}\phi = 1$ such that the bond density can be written as: $D_L(\theta,\phi) = D_{R1}(\theta,\phi) = D_{R2}(\theta,\phi) = D_{R3}(\theta,\phi) = \frac{1}{4\pi}$.

The elastic tensor C_{IJKL} may take the matrix form as Eq. 23. The relationship is given by in Eq. 23, Eq. 24 and Eq. 25.

$$\Omega = \begin{bmatrix} C_{1111} & C_{1122} & C_{1133} & \frac{1}{2}(C_{1112} + C_{1121}) & \frac{1}{2}(C_{1132}+C_{1123}) & \frac{1}{2}(C_{1113}+C_{1131}) \\ C_{2211} & C_{2222} & C_{2233} & \frac{1}{2}(C_{2212}+C_{2221}) & \frac{1}{2}(C_{2232}+C_{2223}) & \frac{1}{2}(C_{2213}+C_{2231}) \\ C_{3311} & C_{3322} & C_{3333} & \frac{1}{2}(C_{3312}+C_{3321}) & \frac{1}{2}(C_{2232}+C_{3323}) & \frac{1}{2}(C_{3313}+C_{3331}) \\ C_{1211} & C_{1222} & C_{1233} & \frac{1}{2}(C_{1212} + C_{1221}) & \frac{1}{2}(C_{1232}+C_{1223}) & \frac{1}{2}(C_{1213}+C_{1231}) \\ C_{2311} & C_{2322} & C_{2333} & \frac{1}{2}(C_{2312}+C_{2321}) & \frac{1}{2}(C_{2332}+C_{2323}) & \frac{1}{2}(C_{2313}+C_{2331}) \\ C_{1311} & C_{1322} & C_{1333} & \frac{1}{2}(C_{1312}+C_{1321}) & \frac{1}{2}(C_{1332}+C_{1323}) & \frac{1}{2}(C_{1313}+C_{1331}) \end{bmatrix} \quad \text{Eq. 23}$$

$$\sigma = \Omega.\varepsilon \quad \text{Eq. 24}$$

Where,

$$\sigma = [\sigma_{11}, \sigma_{22}, \sigma_{33}, \sigma_{12}, \sigma_{23}, \sigma_{13}] \qquad \text{Eq. 25}$$

$$\varepsilon = [\varepsilon_{11}, \varepsilon_{22}, \varepsilon_{33}, 2\varepsilon_{12}, 2\varepsilon_{23}, 2\varepsilon_{13}]^{\mathrm{T}}$$

Where the terms $\sigma_{ij}$and ε_{ij} are the components of stress and strain tensor, respectively. The Equations from Eq. 22 through Eq. 25 are combined to obtain the Eq. 26.

$$\Omega = \frac{1}{15V}\begin{bmatrix} 3kl_0^2 + 2r & kl_0^2 - r & C_{1133} & 0 & 0 & 0 \\ & 3kl_0^2 + 2r & C_{2233} & 0 & 0 & 0 \\ & & C_{3322} & 3kl_0^2 + 2r & 0 & 0 & 0 \\ & & & & kl_0^2 + 1.5r & 0 & 0 \\ & & Symmetry & & & kl_0^2 + 1.5r & 0 \\ & & & & & & kl_0^2 + 1.5r \end{bmatrix} \qquad \text{Eq. 26}$$

To quantitatively describe the density reduction with the deformation increasing, the bond density can be phenomenological expressed. With reference to the L-bond density, it can be shown as in Eq. 27.

$$D_{LC}(\theta, \Phi) = \begin{Bmatrix} \frac{1}{4\pi} & if\ l' \le \varepsilon_c \\ \frac{1}{4\pi}\exp[-\frac{\lambda(l' - \varepsilon_c)^2}{\varepsilon_c^2} & if\ l' > \varepsilon_c \end{Bmatrix} \qquad \text{Eq. 27}$$

Where, $l' = |\xi_i \varepsilon_{ij} \xi_j|$. To simplify, the distribution density $D(\theta, \Phi)$ can be taken as unity for the isotropic solid.

A heterogeneous material, like concrete, may have the micro components with different strain strength even though having same stiffness value [15]. Macroscopic fracture behavior can also be affected by the varying value of strain strength. If ε_b shown in Eq. 28 is the strain

strength assigned to the bond at which the bond is assumed to break and $\overline{\varepsilon_b}$ is its mean value for all these bonds.

$$\varepsilon_b = \lambda \overline{\varepsilon_b} \qquad \text{Eq. 28}$$

2.2.1.4 Implementation of Shear Fracture in Bond Evaluation

The macro response of the material is the effect of bond evaluation function incorporated at the microscopic level. Simple version of bond evaluation function can only account for normal deformation and evaluate tensile fracture. To implement shear fracture, both normal and rotation deformations should be integrated together. A comprehensive description of bond deformation can be made by employing the integrated deformation bond index (δ) as shown in Eq. 29.

$$\delta = \frac{l}{\varepsilon_b} + \frac{\beta}{0.5(1+\nu)\varepsilon_b} \qquad \text{Eq. 29}$$

Where, $l = |\xi_i \varepsilon_{ij}^d \xi_j|, \beta = |\xi_i \varepsilon_{ij} \eta_j|$, Here, ε_{ij}^d is the corresponding deviatoric tensor of strain tensor ε_{ij} and ε_b is the uniaxial strain strength.

The discrete element undergoes linear deformation and then experiences breaking state. As per the criteria defined in [16] for discrete element, the case δ<1 signifies linear deformation and at $\delta \geq 1$ the discrete element is assumed to break. The Eq. 30 is implemented in to account for the pre-peak strengthening effect and the post-peak softening effect.

$$\begin{Bmatrix} \bar{k} \\ \bar{r} \end{Bmatrix} = \begin{Bmatrix} \bar{k}_0 \\ \bar{r}_0 \end{Bmatrix} \exp(-c.\delta^n) \qquad \text{Eq. 30}$$

Where, c, n are model parameters, which governs different characters of macro response; $\bar{k}_0$ and $\bar{r}_0$are the initial bond stiffness, which can be determined respectively by Eq. 9 and Eq. 10. The effect of n and c on macro response are discussed in section 3.3.3 and 3.3.4

The R-bond density can be expressed as:

In Compression, $D_{Ric}(\beta_i) = \begin{Bmatrix} \frac{1}{4\pi} & if\ \beta'_i \le \beta_c \\ \frac{1}{4\pi}\exp[-\frac{\lambda(\beta'-\beta_c)^2}{\beta_c^2}} & if\ \beta'_i > \beta_c \end{Bmatrix}$

Where β'_i is the absolute value of the L-bond rotation angle towards the coordinate-x_i; i.e. $\beta'_i = |\beta'_i|$; β_c and β_t is the critical value of L-bond rotation angle.

2.2.2 Modifications for MC-VIB Model

In this thesis, the MC-VIB model is incorporated to be used so that same model can be used for compression and tension loading. The modifications implemented in the equations for tension are given as

$$D_{Rit}(\beta_i) = \begin{Bmatrix} \frac{1}{4\pi} & if\ \beta'_i \le \beta_t \\ \frac{1}{4\pi}\exp[-\frac{\lambda(\beta'-\beta_t)^2}{\beta_t^2}} & if\ \beta'_i > \beta_t \end{Bmatrix}$$

$$D_{LT}(\theta,\phi) = \begin{Bmatrix} \frac{1}{4\pi} & if\ l' \le \varepsilon_t \\ \frac{1}{4\pi}\exp[-\frac{\lambda(l'-\varepsilon_t)^2}{\varepsilon_t^2}} & if\ l' > \varepsilon_t \end{Bmatrix}$$

Where $l' = |\xi_i \varepsilon_{ij} \xi_j|$; $\xi = (sin\theta, cos\theta)$ in the plane coordinate, shown as $\beta' = |\xi_i \varepsilon_{ij} \eta'|$, $\beta' = |\xi_i \varepsilon_{ij} \eta'_j|$, $\beta'' = |\xi_i \varepsilon_{ij} \eta''_j|$, $\eta' = (cos\theta, -sin\theta)$; $\eta'' = (-cos\theta, sin\theta)$.

When the deformation is within the linear elastic limit, $\varepsilon \le \varepsilon_p$, both the L-bond and the R-bond density are kept constant. As the deformation exceeds the linear elastic limit (ε_p) such

that, $\varepsilon > \varepsilon_p$. The bond density begins to reduce. Therefore, the ε_c should approximately take the value of ε_p.

These equations are successfully adopted by MC-VIB model and the simulations are performed. The stress-strain relationship is observed for this model, which are presented in Chapter 4 and the results based on this study are presented in Chapter 5.

Chapter 3.

VALIDATION OF MC-VIB MODEL

The Modified Concrete Virtual Internal Bond (MC-VIB) model is implemented in the LS-DYNA®. The theory and the history of development of the model is explained in Chapter 2. Now Chapter 3 focuses on the work performed to validate the model based on stress-strain behavior under uniaxial unconfined loading. It is compared with one of the popular standard equations to obtain stress-strain curve for concrete, Hognestad's Equation. The procedure to plot the stress-strain curve for concrete using this equation is explained in brief. Also the chapter explains the procedure followed to perform simulations on single element and cylinder model in LS-DYN® using material models MC-VIB and CDMR3. It also illustrates how the stress-strain curves are obtained in each case and studied for calibration purpose.

3.1 Hognestad's Equation

There are several approximations to predict shape of stress-strain curve for the concrete. Hognestad's Equation is one of the widely accepted equations. It assumes that shape of stress-strain curve before achieving maximum stress is second degree parabola and depends on the strength of concrete represented by Eq. 31.

$$f_c' = f_c" \left[2\left(\frac{\varepsilon_c}{\varepsilon_0}\right) - \left(\frac{\varepsilon_c}{\varepsilon_0}\right)^2 \right] \qquad \text{Eq. 31}$$

Where, the fc" is the maximum peak stress reached for concrete, in this case it is 27.6 MPa (4ksi). The extent of falling branch behavior depends on the remaining useful concrete strain assumed [17] . Modulus of Elasticity Ec =4730√fc'= 24849.387 MPa. The ε_0 is the strain

at which peak stress is achieved, can be given as $\varepsilon_0 = \frac{2f_c''}{E_c} = 0.002\ mm/mm$. The stress value drops linearly to $0.85f_c''$ at strain value of 0.0038.

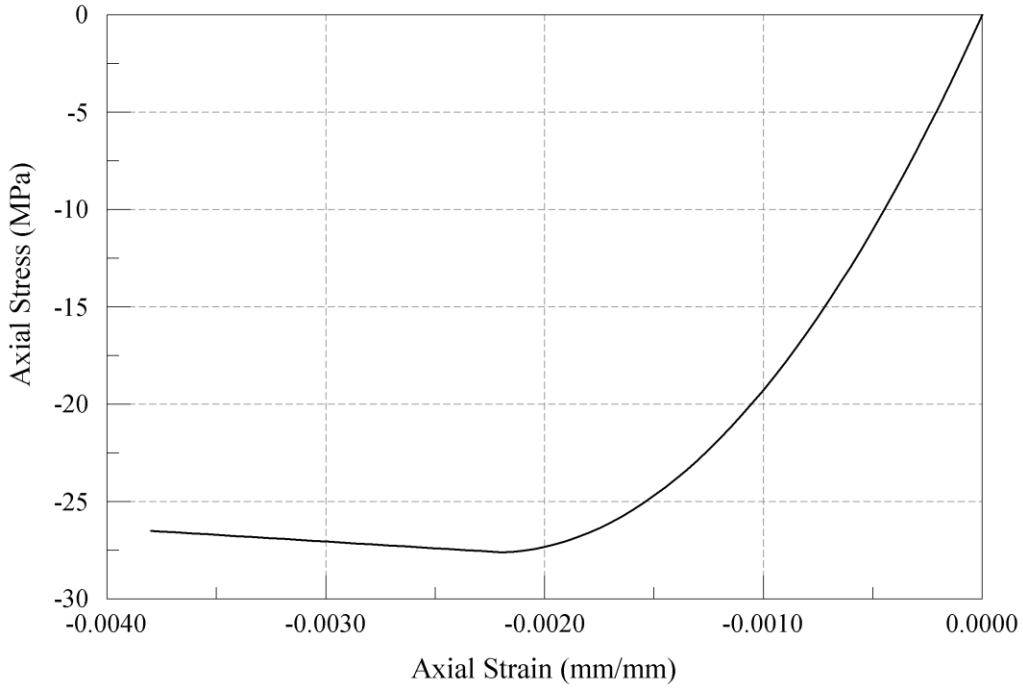

Figure 3-1 Stress-strain curve for fc' = 27.6 MPa concrete obtained using Hognestad's equation

In this thesis, Hognestad's Equation is used to plot stress-strain curve for concrete with fc' of 27.6 MPa (4ksi) and is used to calibrate that obtained from Single element simulation in LS-DYNA® using MC-VIB material model. The stress-strain curve plotted with this procedure is shown in Figure 3-1.

3.2 Numerical Modeling in LS-DYNA®

Modified Concrete Virtual Internal Bond model (MC-VIB) is a user defined material model in LS-DYNA®, modified to be applied to concrete. A general overview is given for LS-DYNA® user interfaces in this section.

3.2.1 User Defined Material Models in LS-DYNA®

The LS-DYNA® is popular in the researchers because of its flexibility. The LS-DYNA® Keyword User Manual [15] guides user to use the program for simulation. The program allows user to input data organized in the logical section it is related to. For example, to reset the LS-DYNA® defaults, control section is used; material section defines constitutive constants and an equation of state; to define element part identifiers and nodal connectivity, element section is used. LS-DYNA® is used for wide range of research involving finite element analysis. It can be applied to concrete undergoing deformation or for crash analysis of a car. For each of these cases, the context and complexity differs and so should the interface. It is impossible and redundant to implement comprehensive changes in the program addressing all its applications. A user defined interface allows researchers to partially change the program by adding their numerical model to the code. The interface can be structural material, Equation of State, structural elements, loading etc. MC-VIB is the one such algorithm, developed or modified by Dr. Ganesh Thiagarajan, discussed in this thesis.

The paper 'An overview of user interfaces in LS-DYNA®' [16] well summarizes the number of such user defined interfaces currently available in the version 971 R5 of LS-DYNA® and process for creating one. A "usermat package" is a compressed archive containing several files such as object files, library files, 'Fortran' files and 'makefile'. The FORTRAN files 'dyn21.f' and 'dyn21b.f' as well as the 'makefile' are most important files for the user. The 'makefile' describes the procedure to derive the target program in LS-DYNA® executables and decides which FORTRAN compiler to use. Once the compiler is installed, the 'make' command starts generating personalized executables for the user, which are called "LS971". This LS971 program can be operated similar to standard version of LS-

DYNA®. After successful translation and linking, users can implement their own algorithms for the features like elements, materials, friction into user subroutines for FORTRAN files dyn21.f and or dyn21b.f. Out of which, material interface has most applications and undergone several sophistication over the period of time. It is used to implement user's own material model. It can be standard constitutive models which compute stresses from strains in solid elements and shells or it can incorporate other material laws such as thermal material properties or failure criteria for standard materials.

When the user defines keyword *MAT_USER_DEFINED_MATERIAL_MODELS in the input file, the main program calls subroutine 'usrmat' in dyn21.f and 'urmathn' subroutine is called for solid elements which in turn calls user subroutine umat41 in order to computer stresses from strains. These subroutines use, material constants as the input arguments and give output in terms of stress variables calculated by particular theory.

This is a brief discussion of how a user defined material model functions. The development or modification of the code is out of the scope of this thesis and was done by Dr. Ganesh Thiagarajan. The Chapter 2 gives overview of theory implemented for MC-VIB. The objective of the study presented in this thesis is to validate the MC-VIB material model as a user. The procedure followed is explained in the successive sections of the Chapter 3.

3.2.2 Model Generation

To get started, the Uniaxial Unconfined Compression (UUC) and Uniaxial Unconfined Tensile (UUT) tests are modelled in LS-DYNA® on Single element and cylinder models. Dimensions for single elements are 25.4 mm x 25.4 mm x 25.4 mm (1" x 1" x1"). Cylinders with three sizes namely 4x8, 8x16 and 16x32 are selected to study effect of specimen dimension on stress-strain behavior. For simplification, the term 4x8 cylinder is used in the

thesis to designate cylinder size, i.e. 101.6 mm (4”) diameter and 203.2 mm (8”) height, similarly 8x16 is used for 203.2 mm x 406.4 mm and 16x32 for 406.4 mm x 812.8 mm. Total six cylinder models are used with varying dimensions and mesh sizes; three 4x8 cylinder models with three different mesh sizes namely coarse, medium and fine as shown in Figure 3-2, two 8x16 cylinder with coarse and medium mesh size (Figure 3-3), whereas coarse mesh is used for the 16x32 cylinder (Figure 3-4). Simulations are performed using both, MC-VIB and CDMR3 material models, and the models in each case is subjected to same velocity loading. The results are used to calibrate the model.

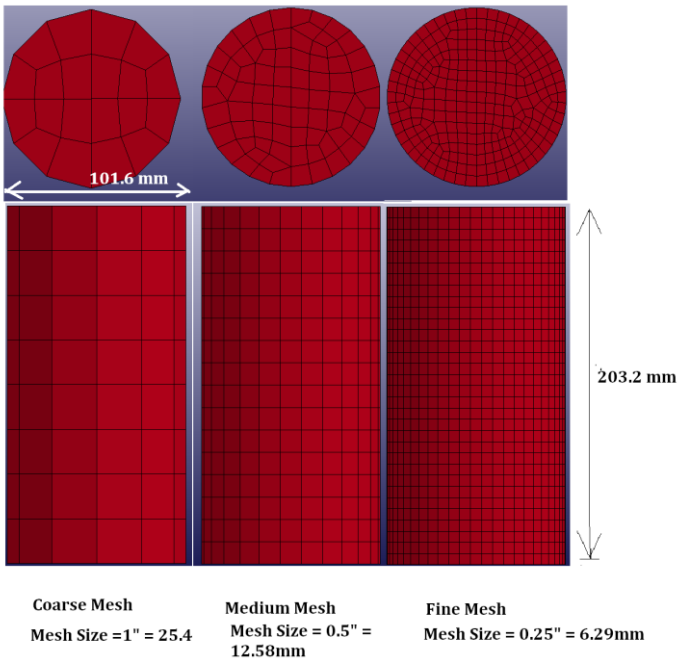

Figure 3-2 Cylinder Models- 4x8 Size with Coarse, Medium and Fine Mesh Sizes

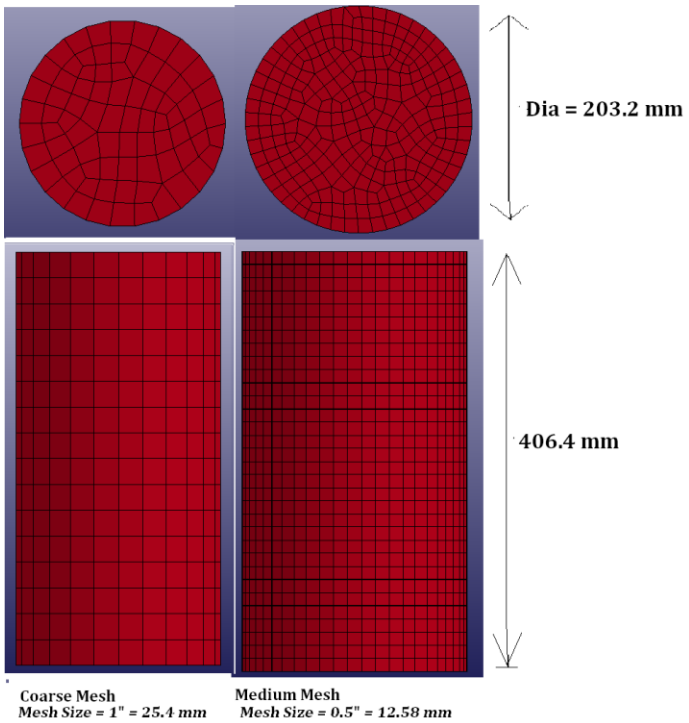

Figure 3-3 8x16 Cylinder Models with Coarse and Medium Mesh Size

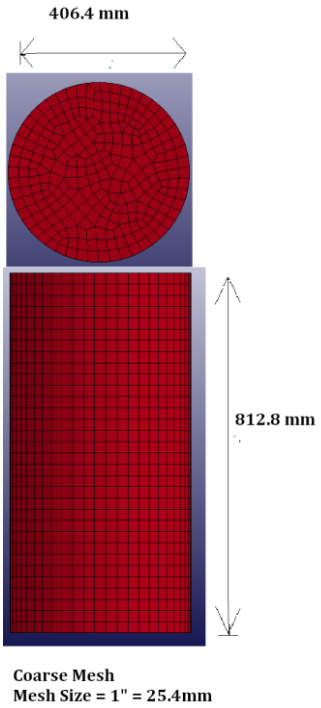

Figure 3-4 Cylinder Model- 16”x32” Size with Coarse Mesh

3.2.3 Material Models

From the LS-DYNA® material library, Concrete_Damage_Model_Release3 (CDMR3) is chosen for this study. As described in LS-DYNA® user manual [15], this model also called as Kargozian & Case (K&C), has origin based on the Pseudo-tensor Model (Material Type 16). It takes relatively simple input and has capability to generate parameters only based on unconfined compressive Strength. It uses three shear failure surfaces, includes damage and strain-rate effects. The K&C Model can capture the key concrete behaviors including post-peak softening, shear dilation, confinement effect, and strain rate effect properly. Structural analyses also show that K&C model is suitable for quasi-static, blast and impact loads and works well only for low confinement situations. Even though this thesis focuses on stress-strain behavior of models under uniaxial unconfined loading, wider scope of the project includes, calibration of MC-VIB based on several aspects such as post-peak softening, confinement effect. Because of its significant properties, the CDMR3 is believed to best serve the purpose of calibration of MC-VIB model. The user defined material MC-VIB is explained in detail in the Chapter 2.

In the LS-DYNA® keyword file, once the part is defined, material model is assigned to that part using parameter ‘mid’ which refers to a specific Material ID, where input is given to specify properties of concrete. The units specified for MCVIB file and CDMR3 files are MPa-mm and psi-in respectively. The Figure 3-5 shows the keyword file input for to assign CDMR3 material model. The material ID mid for CDMR3 is 072R3. The card *MAT_CONCRETE_DAMAGE_REL3 is used to defined the unconfined compressive strength of 4000 psi which is equivalent to 27.6 MPa. All the results obtained from CDMR3 file are converted using unit conversion factor of 1 MPa =145 psi and 1 inch = 25.4 mm.

Poisson’s ratio used is 0.2. Density of concrete is specified as 2.21E-4 lb per cubic inch. All the other parameters are automatically generated by CDMR3 material model. It uses tabulated compaction Equation of State (EOS 8) card to specify pressure-volume strain response [18] as shown in Figure 3-5.

```
$$$$$$$$$$$$$$$$$$$$$$$$$$$$$$$$$$$$$$$$$$$$$$$$$$$$$$$$$$$$$$$$$$$$$$$$$$$$$$$$
$
$   Define Parts, Sections, and Materials
$
$$$$$$$$$$$$$$$$$$$$$$$$$$$$$$$$$$$$$$$$$$$$$$$$$$$$$$$$$$$$$$$$$$$$$$$$$$$$$$$$
$...>....1....>....2....>....3....>....4....>....5....>....6....>....7....>....8
$
*PART
$       pid       sid       mid     eosid      hgid    adpopt
Concrete
          1         1     072R3         8
$
*SECTION_SOLID
$       sid    elform
          1         1
*EOS_TABULATED_COMPACTION
$     EOSID      Gamma          E0       Vol0
8,0.000E+00,0.000E+00,1.00
$     VolStrain01     VolStrain02     VolStrain03     VolStrain04     VolStrain05
0.00000000E+00,-3.6177502,-2.9239512,-2.5180457, -2.2306366
$     VolStrain06     VolStrain07     VolStrain08     VolStrain09     VolStrain10
-1.6709091,-0.1381511,-0.0255410,-0.6941716,-1.1001311
$      Pressure01      Pressure02      Pressure03      Pressure04      Pressure05
0.00000000E+00,958.16,2107.87,3353.33,4311.49
$      Pressure06      Pressure07      Pressure08      Pressure09      Pressure10
7664.83,23382.41,25717.49,35323.02,42915.07
$               Multipliers of Gamma*E
0.000000000E+00,0.000000000E+00,0.000000000E+00,0.000000000E+00,0.000000000E+00
0.000000000E+00,0.000000000E+00,0.000000000E+00,0.000000000E+00,0.000000000E+00
$      BulkUnld01      BulkUnld02      BulkUnld03      BulkUnld04      BulkUnld05
3.37925846E+06,3.37925846E+06,3.42656808E+06,3.59891026E+06,4.28152047E+06
$      BulkUnld06      BulkUnld07      BulkUnld08      BulkUnld09      BulkUnld10
4.96750994E+06,5.65012015E+06,6.16714669E+06,1.38752352E+07,1.68962923E+07
$
*HOURGLASS
        1         5
*MAT_CONCRETE_DAMAGE_REL3
$ID,     RO        PR (units psi)
072R3,2.21e-4,0.2
$F'(t)  A0      A1      A2     B1  OMEGA    A1F
0,-4000
$^    NOUT EDROP RSIZE       UCF  LCRate Locwidth NPTS
0,0,0,1,1
$^1  ^2     ^3       ^4        ^5       ^6        ^7    ^8
0,0,0,0,0,0,0,0
$^9         ^10     ^11 ^12  ^13     B3      A0Y    A1Y
0,0,0,0,0,0
$Eta1 Et2    Et3     Et4  Et5 Et6 Et7 Et8
0,0,0,0,0,0,0,0
$Et9 Et10 Et11 Et12 Et13 B2    A2F      A2Y
0,0,0,0,0,0
```

Figure 3-5 Input for CDMR3 to Define Part, Section and Materials

```
$$$$$$$$$$$$$$$$$$$$$$$$$$$$$$$$$$$$$$$$$$$$$$$$$$$$$$$$$$$$$$$$$$$$$$$$$$$$$$$$
$
$  Define Parts, Sections, and Materials
$
$$$$$$$$$$$$$$$$$$$$$$$$$$$$$$$$$$$$$$$$$$$$$$$$$$$$$$$$$$$$$$$$$$$$$$$$$$$$$$$$
$...>....1....>....2....>....3....>....4....>....5....>....6....>....7....>....8
$
*PART
$      pid       sid       mid     eosid      hgid    adpopt
Concrete
         1         1       001,0,1
$
*SECTION_SOLID
$      sid    elform
         1         1
$
*HOURGLASS
         1         5,0.1
$
*MAT_USER_DEFINED_MATERIAL_MODELS
$      MID        RO        MT       LMC       NHV    IORTHO        IB        IG
01,2.00E-06,41,17,0,0,16,17
$     IVEC     IFAIL       ITHERM    IHYPER    IEOS
         0         0         0         1         0
$         17 material parameters
$       EM        PR      EPS_C     BETA_C     EPS_T     BETA_T   LAMBDA    RLOMIN
0.300E+04,2.00E-01,0.001,0.0006,0.0001,0.00006,1.0,1.0
$   RLOMAX    PHIMIN    PHIMAX  THETAMIN  THETAMAX        EN        EC, BulkMod
1.0,0,1.570796,0.0,6.283185,1.0,0.15,15000
$Shear Mod
2500
```

Figure 3-6 Input for MC-VIB material model

The Figure 3-6 shows sample input to define the user defined material model MC-VIB using *MAT_USER_DEFINED_MATERIAL_MODEL, Material type 41.

Card 1	1	2	3	4	5	6	7	8
Variable	MID	RO	MT	LMC	NHV	IORTHO	IBULK	IG
Type	A8	F	I	I	I	I	I	I
Card 2								
Variable	IVECT	IFAIL	ITHERM	IHYPER	IEOS			
Type	I	I	I	I	I			

Figure 3-7 Figure Showing Two Cards Used to Define User Defined Material Type 41

The user manual for LS-DYNA® [18] gives brief about the parameter input in the cards used to define the *MAT_USER_DEFINED_MATERIAL as shown in Figure 3-7. MID of '01' refers to material identification, RO is mass density of concrete, MT specifies the material type, which is 41 for MC-VIB. LMC is length of material constant array which is equal to number of material constants to be input, which is 17 in this case. LMC is limited to 40 for IORTHO = 1 which is not the case. IROTHO is set to zero as the material is not orthotropic. IBULK and IG are the address of bulk modulus and shear modulus in material constants array holding the values of 16 and 17 for MC-VIB. The "0" value for IVECT turns the vectorization flag off, eliminating the need for vectorized user subroutine to be supplied. The failure flag IFAIL = 1 allows failure of shell and solid elements due to a material failure criterion and deletion of elements. The material fails at an integration point when IFAIL is true. IFAIL = 0 is adopted for this thesis, so the elements are not deleted from the calculation. If temperature flag is on, i.e. ITHERM = 1, it computes the element temperature. In our case both it is turned off by input value of 'zero'. Deformation gradient flag is turned on by defining IHYPER=1 to compute deformation gradient. The equation of state is turned off by defining IEOS = 0.

The MC-VIB model has total 17 input parameters enlisted in the keyword file as EM PR(ν), EPS_C (ε_c), BETA_C(β_c) , EPS_T (ε_t), BETA_T(β_t), LAMBDA (λ),RL_{0min}, RL_{0max},ϕ_{min},ϕ_{max} , θ_{min} θ_{max}, $EN(n)$, $EC(\ c\ )$, B and G. Where, E depends on Elastic Modulus. PR represents Poisson's ratio (ν) and the value is used to be 0.2 consistently. The parameters ε_c and ε_t denote limiting value of elastic strain in compression and tension respectively, where $\varepsilon_t = 0.1(\varepsilon_c)$. These parameters decide the values of another two parameters $\beta_c = 0.5(\varepsilon_c + \nu\,.\,\varepsilon_p)$ and $\beta_t = 0.5(\varepsilon_t + \nu\,.\,\varepsilon_p)$. As explained in section 2.2.2

$\varepsilon = \varepsilon_p$ in respective compression or tension case, as the value of Poisson's ratio is set to $\nu = 0.2$, $\beta_c = 0.5(1 + 0.2)\varepsilon_c = 0.6\varepsilon_c$ and similarly $\beta_t = 0.6\varepsilon_t$. The parameter Lambda (λ) is the coefficient to adjust bond reduction ratio with deformation set to '1'. The minimum and maximum values for radius or length of bond and bond angle are defined by parameters 8th to 13th which are kept constant throughout the project. Where the parameter θ is the angle of L-bond with respect to vertical positive axis and ϕ is the angle of bond in the horizontal plane with respect to vertical axis. Length of bond is fixed to unity and $\phi_{min} = 0, \phi_{max} = \frac{\pi}{2} = 1.57^c, \theta_{min} = 0 \; and \; \theta_{max} = 2\pi = 6.28^c$. EN and EC are the n and c from Eq. 30 respectively. The parameter c denotes coefficient for shear compression part while n represents exponent for shear compression part. The 16th and 17th parameters are bulk modulus (B) and shear modulus (G) of concrete respectively, calculated as $B = \frac{3E}{1-2\nu} = 5E$ and $G = \frac{3E(1-4\nu)}{(1+\nu)(1-2\nu)}$. For this thesis, $\nu = 0.2$. Hence, the formulae become, $B = 5E$ and $G = \frac{E}{1.2}$.

Out of these seventeen parameters, seven parameters are varied and to study their effect on stress-strain curve of concrete. There are five parameters primarily focused namely EM, EPS_C (ε_c), EPS_T (ε_t), EN, EC and The two parameters BETA_C(β_c) and BETA_T(β_t) are basically dependent on the other two parameters EPS_C (ε_c), EPS_T (ε_t). The bulk modulus and Shear modulus changed with changing E.

3.2.4 Boundary Conditions and Loads

Eight-node hexahedral element of size 25.4 mm is defined in LS-DYNA® using the input as shown in Figure 3-8. It also shows the input command to define boundary conditions and loading. Each node has six degrees of freedom. Three in translational and three rotational.

The bottom four nodes are fixed in all the six directions and free at top four nodes are free in translational direction but restrained to rotate as shown in Figure 3-9. The velocity loading is applied at top four nodes using the card *BOUNDARY_PRESCRIBED_MOTION_NODE. The load curve identification (LCID = 1) is assigned to the top four nodes which refers to the load curve defined with the array of time vs velocity of loading at that time.

```
$
$$$$$$$$$$$$$$$$$$$$$$$$$$$$$$$$$$$$$$$$$$$$$$$$$$$$$$$$$$$$$$$$$$$$$$$$$$$$$$$$
$
$   Define Nodes and Elements
$
$$$$$$$$$$$$$$$$$$$$$$$$$$$$$$$$$$$$$$$$$$$$$$$$$$$$$$$$$$$$$$$$$$$$$$$$$$$$$$$$
$...>....1....>....2....>....3....>....4....>....5....>....6....>....7....>....8
$
$
*NODE
$    node               x               y               z      tc
        1    0.000000E+00    0.000000E+00    0.000000E+00
        2    25.400000000    0.000000E+00    0.000000E+00
        3    25.400000000    25.40000E+00    0.000000E+00
        4    0.0000000000    25.40000E+00    0.000000E+00
        5    0.0000000000    0.000000E+00    25.40000E+00
        6    25.400000000    0.000000E+00    25.40000E+00
        7    25.400000000    25.40000E+00    25.40000E+00
        8    0.0000000000    25.40000E+00    25.40000E+00
$
*ELEMENT_SOLID
$    eid     pid      n1      n2      n3      n4      n5      n6      n7      n8
       1       1       1       2       3       4       5       6       7       8
$
$$$$$$$$$$$$$$$$$$$$$$$$$$$$$$$$$$$$$$$$$$$$$$$$$$$$$$$$$$$$$$$$$$$$$$$$$$$$$$$$
$
$   Define Boundary Conditions and Loads
$
$$$$$$$$$$$$$$$$$$$$$$$$$$$$$$$$$$$$$$$$$$$$$$$$$$$$$$$$$$$$$$$$$$$$$$$$$$$$$$$$
$...>....1....>....2....>....3....>....4....>....5....>....6....>....7....>....8
$
*BOUNDARY_SPC_NODE
$ NIC, CID, DOFX, DOFY,DOFZ,ROFX,ROFY,ROFZ
1,0,1,1,1,1,1,1
2,0,1,1,1,1,1,1
3,0,1,1,1,1,1,1
4,0,1,1,1,1,1,1
$5,0,0,0,0,1,1,1
$6,0,0,0,0,1,1,1
$7,0,0,0,0,1,1,1
$8,0,0,0,0,1,1,1
$$$$$$$$$$$$$$$$$$$$$$$$$$$$$$$$$$$$$$$$$$$$$$$$$$$$$$$$$$$$$$$$$$$$$$$$$$$$$$$$
$
$   Define Boundary Loads
$
$$$$$$$$$$$$$$$$$$$$$$$$$$$$$$$$$$$$$$$$$$$$$$$$$$$$$$$$$$$$$$$$$$$$$$$$$$$$$$$$
$...>....1....>....2....>....3....>....4....>....5....>....6....>....7....>....8
*BOUNDARY_PRESCRIBED_MOTION_NODE
$      nid       dof       vad      lcid        sf       vid
         5         3         0         1 1.000E+00
         6         3         0         1 1.000E+00
         7         3         0         1 1.000E+00
         8         3         0         1 1.000E+00
$
*DEFINE_CURVE
$     lcid      sidr      scla      sclo      offa      offo
         1
$           abscissa            ordinate
               0.000          0.0000
             0.10000          -5.0
*END
```

Figure 3-8 Keyword File for Single Element Showing Input to Define Boundary Conditions and Loading

3.2.5 Theory to Obtain Stress-strain Curve

3.2.5.1 Illustration for Single Element

The following example explains the correlation between loading input and output obtained in the form of stress, displacement and strain values.

Consider the eight node hexahedral single element with size 25.4 mm as shown in Figure 3-9. The element is defined using *NODE card as shown in Figure 3-8.

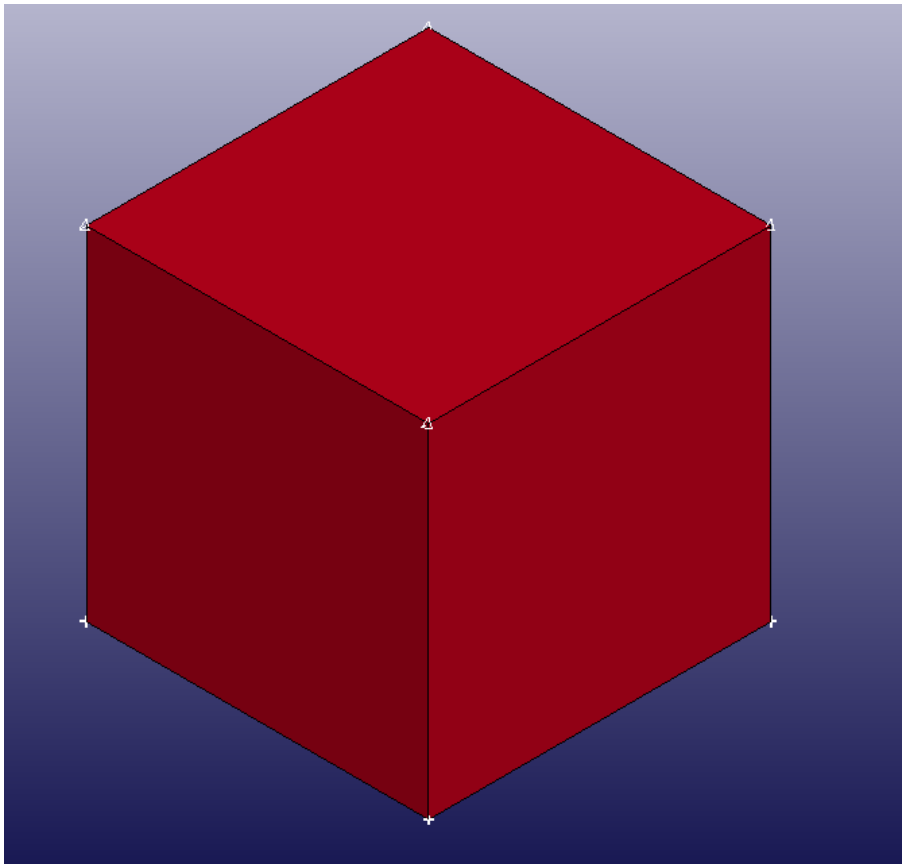

Figure 3-9 Single Element showing Boundary Conditions and Loading

The loading is defined as shown in Figure 3-8. The time duration of simulation is t= *0.1 sec* where $t_0 = 0$. Velocity loading is defined using load curve as shown in Figure 3-10

where, initial velocity, $u_0 = 0\, mm/\sec$ and final velocity $u_1 = 3.5\, mm/\sec$ (+ve for tension and –ve for compression).

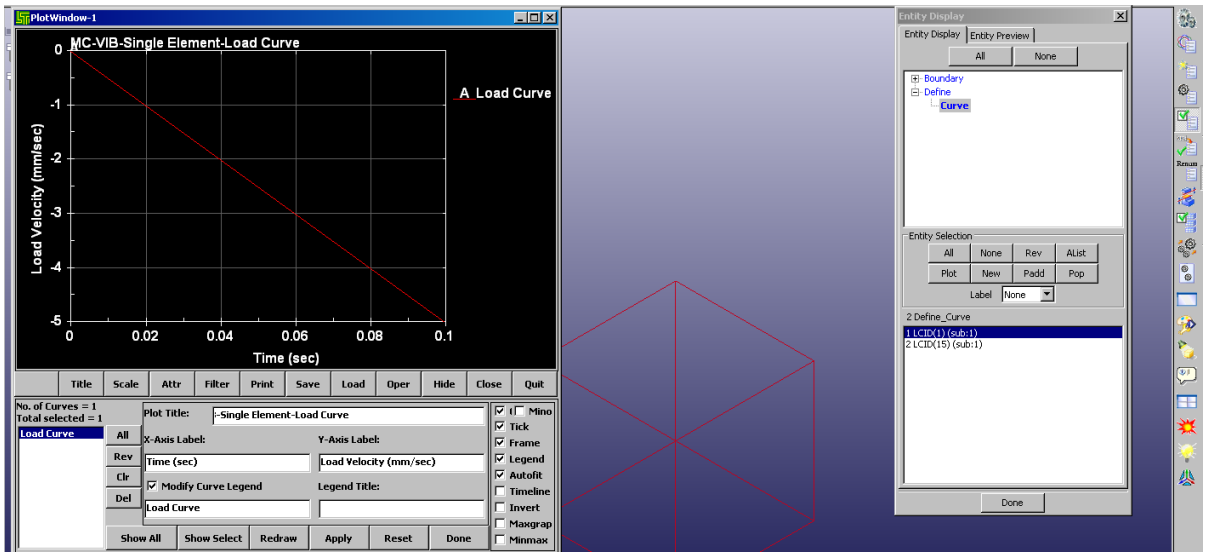

Figure 3-10 Load Curve Defined in LS-DYNA® for Single Element

The acceleration given is calculated as, $a = \frac{u-u_0}{t} = \frac{\frac{3.5mm}{sec} - \frac{0mm}{sec}}{0.1sec} = \frac{35mm}{sec^2}$. Using Newton's equation of motion, compression or Displacement can be given as $s=s_0+u_0t+\frac{1}{2}at^2=\frac{1}{2}(35)(0.1)^2=17.5(0.01)=0.175$mm. Hence the Strain produced is, $\varepsilon=\frac{\text{displacement}}{\text{length}}=\frac{0.175}{25.4}=\frac{0.007\text{mm}}{\text{mm}}$. Lateral strain = Poisson's Ratio x axial strain = $0.2(0.007)=0.0014\frac{\text{mm}}{\text{mm}}$. The

Figure 3-11 and

Figure 3-12 show initial and deformed shape of the single element under this accelerated velocity loading in isometric and front views.

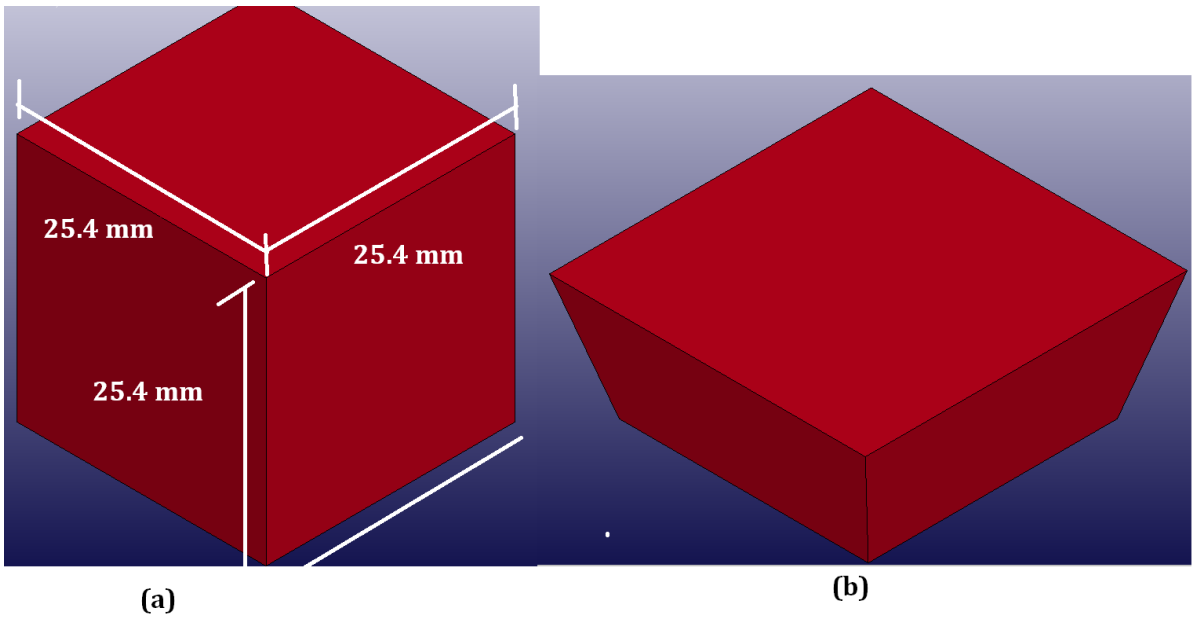

Figure 3-11 Isometric View of Single Element (a) at t= 0 sec (b) at t = 0.1 sec showing deformed shape

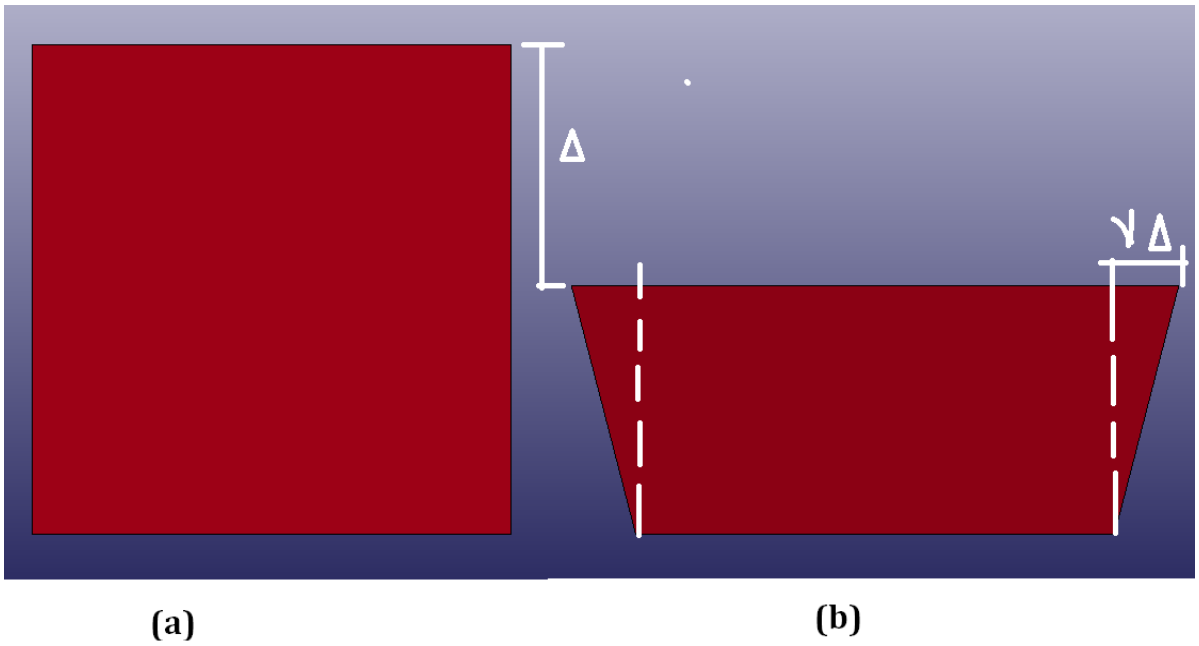

Figure 3-12 Front View of Single Element (a) at t = 0 sec Showing Original Shape (b) at t = 0.1 sec Showing Deformed Shape

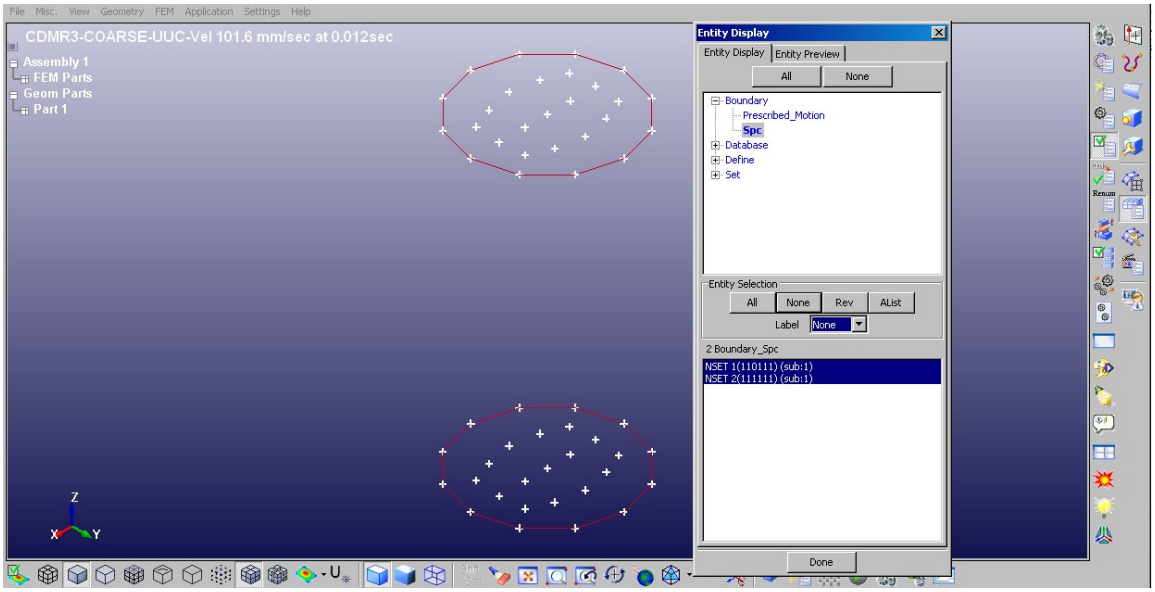

Figure 3-13 Cylinder Model Showing Restrained Nodes at Top and Bottom Surfaces

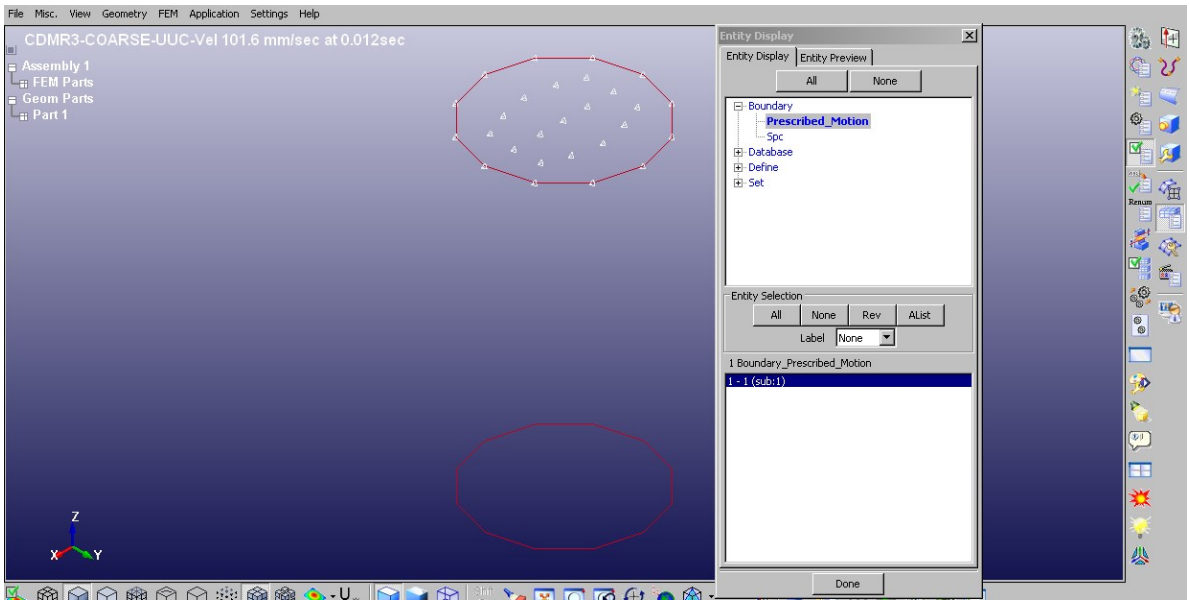

Figure 3-14 Cylinder Model: Showing Set of Nodes Subjected to Velocity Loading

3.2.5.2 Illustration Calculation for Cylinder Model

The Uniaxial Unconfined Compression test on cylinder is simulated using LS-DYNA®. The loading is applied as velocity loading with acceleration on the top surface of the cylinder. In LS-PREPOST the z-stress and z-strain using green-St.Venant strain tensor graph is plotted for element near mid-height of the cylinder. The axial displacement (z-direction), strain and stress are obtained with theoretical calculations using Newton's laws, and Hognestad's equation. The curves obtained by using LS-DYNA® are then calibrated against theoretical curves.

The calculations are illustrated with following example:

In this case, Accelerated velocity loading of 0.5/sec is applied to 4 x 8 cylinder (101.6mm x 203.2mm). As the stress and strain values are plotted at mid-height of the cylinder all the calculations are done with respect to half the height of cylinder that is 101.6 mm. The force applied can be defined using "vad" parameter in *BOUNDARY_PRESCRIBED_MOTION_SET. "Zero" value for "vad" denotes the loading is defined in terms of velocity. Using *DEFINE_CURVE card, the velocity load applied at different time interval can be given as input as an array of(t_n, v_n). If v_0 is zero then the loading applied is accelerated loading. The velocity value of 101.6 mm/sec indicates displacement of 101.6 mm produced per second for total height of Cylinder that is 203.2 mm. Rate of strain produced per second is 101.6/203.2 = 0.5/sec. For half the cylinder the strain rate remains the same and loading velocity value is reduced t half, that is 50.8 mm/sec. In this case initial velocity is zero and final velocity at end time of 0.012sec is 50.8 mm/sec. The acceleration is

$a = \frac{v-u}{t} = \frac{50.8-0}{0.012} = 4233.33 \frac{mm}{sec^2}$. Compressive strength of concrete is 27.6mpa (4 ksi). Elastic modulus of concrete is given as Ec = 4730√fc' = 24849.4 MPa.

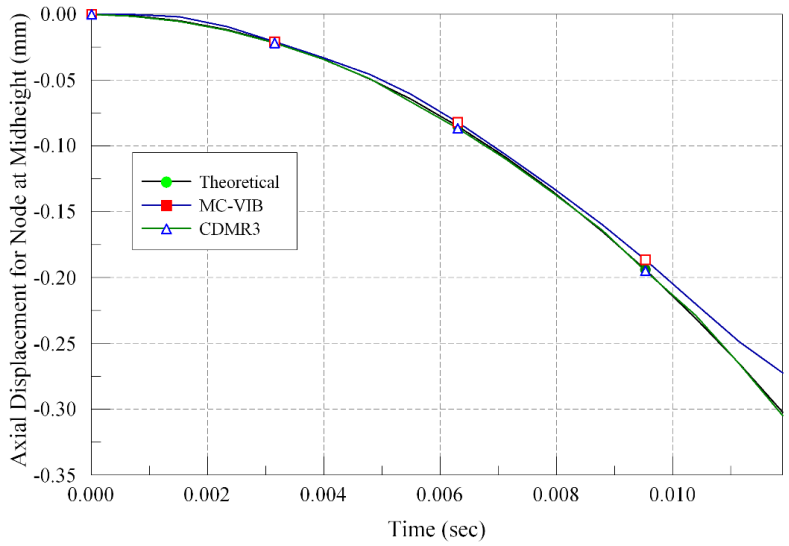

Figure 3-15 Comparison of Theoretical Axial Displacement at Mid-height Node with MC-VIB model and CDMR3

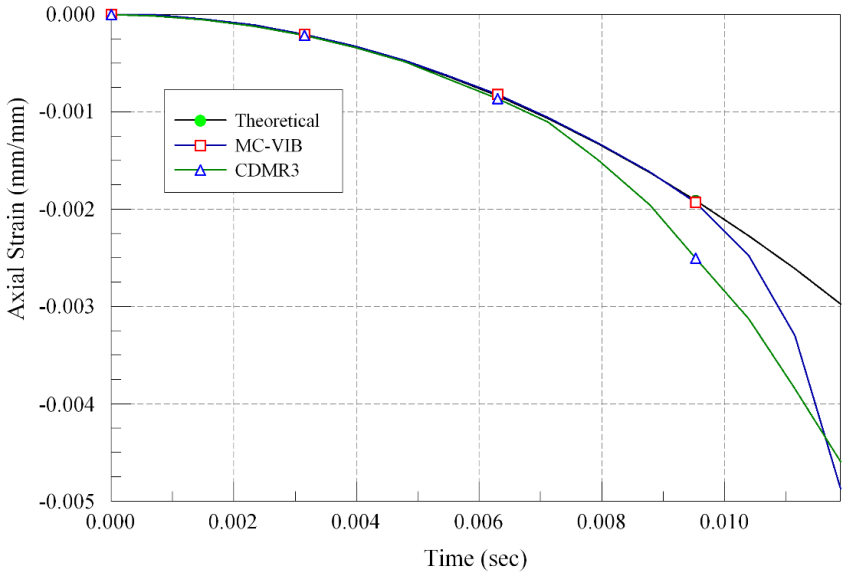

Figure 3-16 Axial Strain at Mid-height of the Cylinder - Comparison of Theoretical Curve with MCVIB and CDMR3

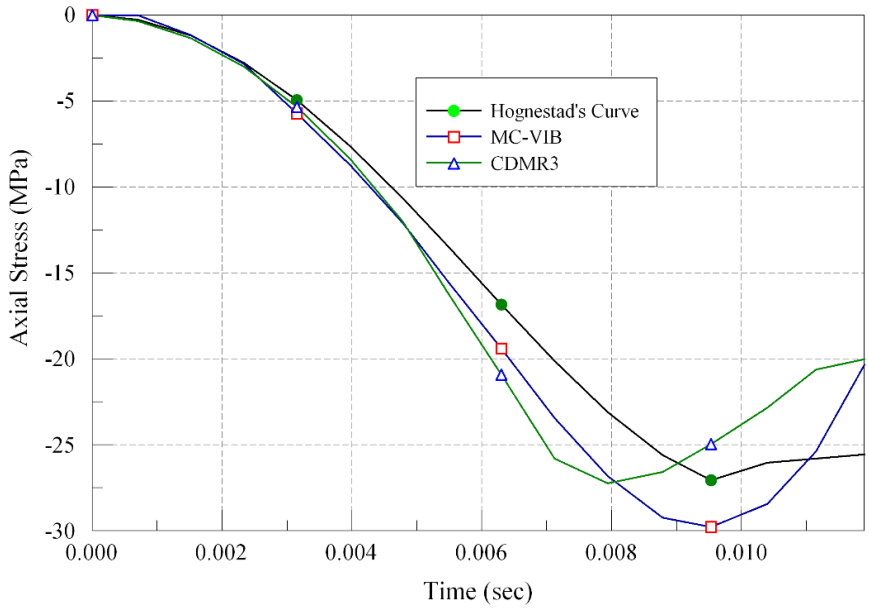

Figure 3-17 Axial Stress at Mid-height of the Cylinder - Comparison of Theoretical Curve with MCVIB and CDMR3

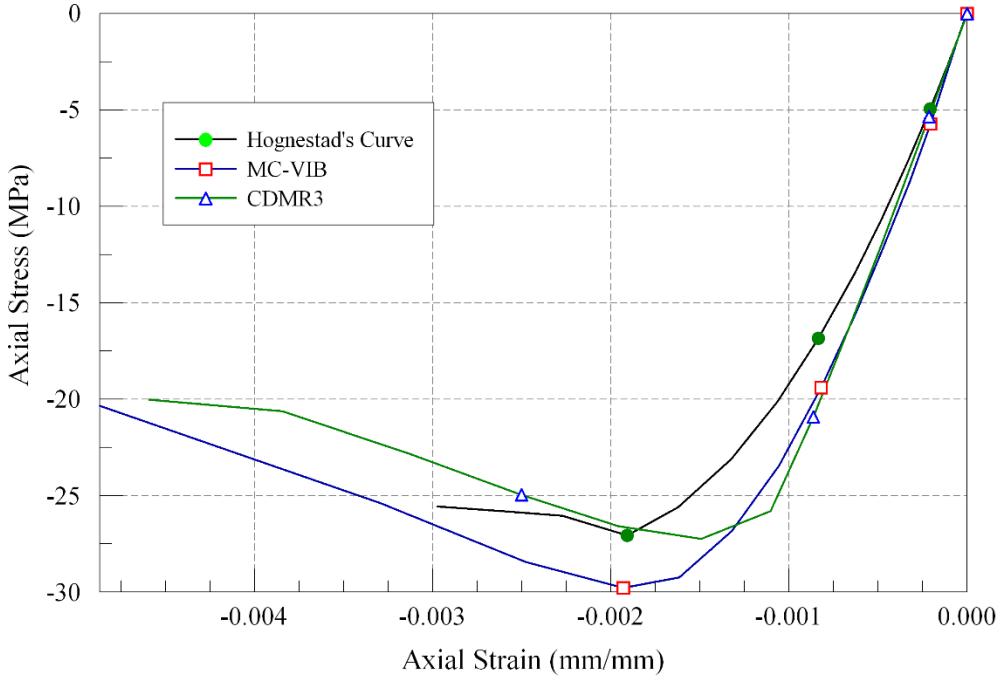

Figure 3-18 Axial Stress-strain Curve for Cylinder- Comparison of Theoretical Curve with MC-VIB and CDMR3

The Observations are as follows:

Table 3-1 Summary of Results for 4x8 Cylinder Accelerated velocity loading of 0.5 (mm/mm)/s

	Time (Sec)	Strain (mm/mm)	Stress (MPa)
Hognestad's Eqn		0.00191	27.59
CDMR3	0.0079393	0.00154	27.23
MC-VIB	0.0095290	0.00193	29.79

The displacement values obtained with LS-DYNA® for MC-VIB model are consistent with those with Theoretical calculations. Stress values for MC-VIB model are 10% higher than those for Hognestad's curve .When compared to CDMR3, percentage error in stress value is within 5% within elastic limit. After that, the parabolic curve shows up to 20% higher peak stress than that of CDMR3. Strain at which peak stress is achieved in MC-VIB model is depicted more accurately compared to CDMR3.

3.3 Studying Effect of Changing Parameters in MC-VIB

Objective of the study is to obtain a set of parameters in MC-VIB material model which can approximate the behavior of 27.6 MPa (4 ksi) concrete. The single element is subjected to accelerated velocity loading. The strain rate at end time is 0.0197 per second. The parameters under primary consideration are E, EPS_C, EN and EC. While studying one parameter, the other parameters are kept constant. Study of each parameter is described in successive sections.

3.3.1 Effect of Changing E

As explained earlier, the effect of change in E on stress-strain is studied. The Figure 3-19 and Figure 3-20shows stress-strain curves obtained from single element simulations with changing value of E or UUC and UUT respectively. The other parameters under consideration

are same for all these simulations. It is observed that, as E depends on Elasticity Modulus, it changes the initial slope of the curve within elastic limit. For the simulations performed for different values of E form 1000 to 5000, with increments of 1000.

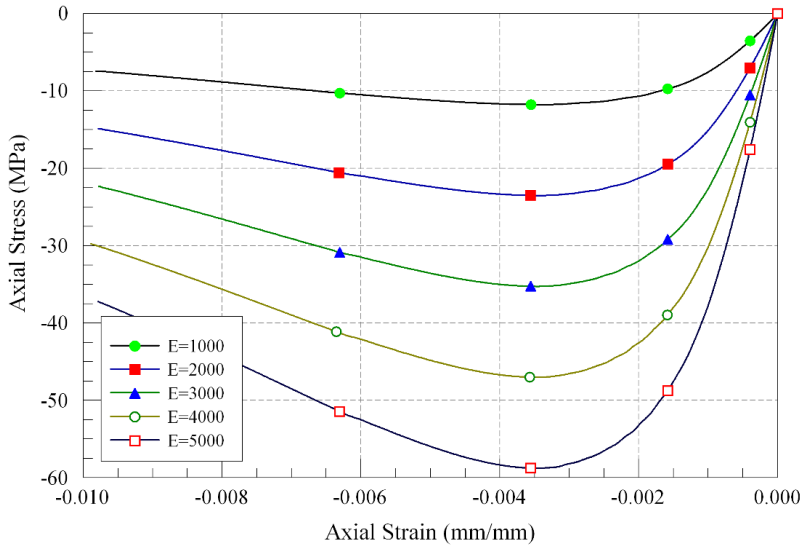

Figure 3-19 Single Element-UUC-Effect of changing E on Stress-strain curve

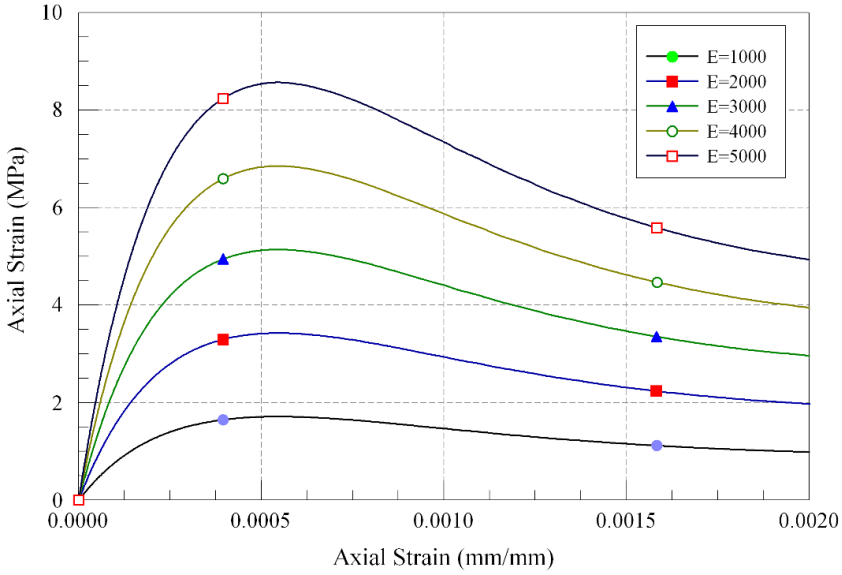

Figure 3-20 Single Element-UUT-Effect of changing E on Stress-strain Behavior

The initial slope of values of these curves are plotted against the corresponding E value in

Figure 3-21 for UUC and

Figure 3-22 for UUT respectively. It is observed to have a linear relationship. The slope of the curve increases linearly with increasing value of E.

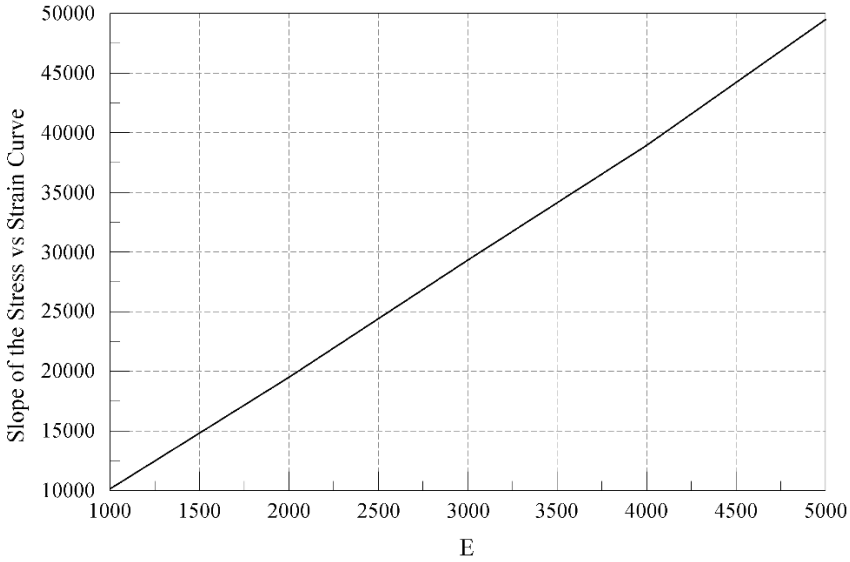

Figure 3-21 MC-VIB-Single Element-UUC-Graphical relation between initial slope of the stress-strain curves and E

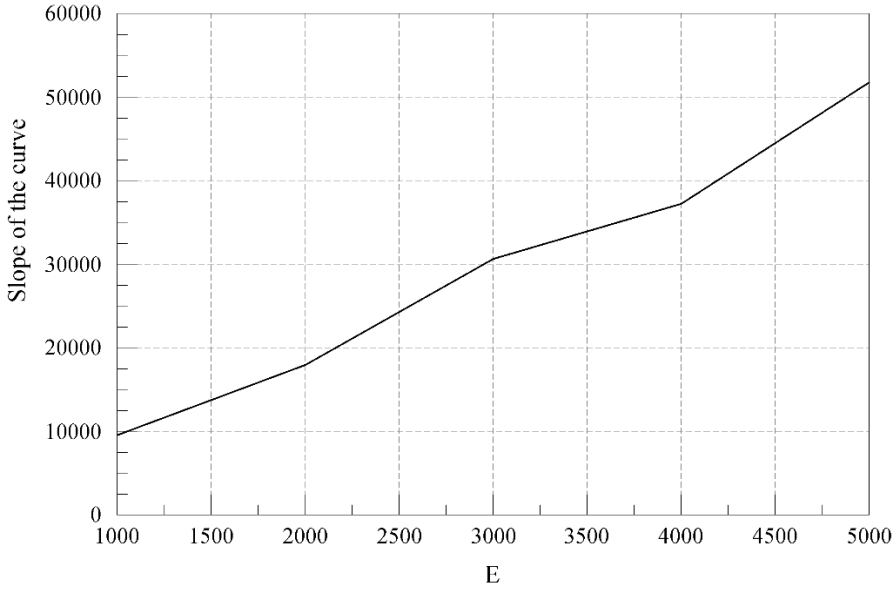

Figure 3-22 MC-VIB-Single Element-UUT-Graph showing trend of the initial slope of Stress-strain curve with changing E

3.3.2 Effect of Change in EPS_C in UUC

When EPS_C is changed, the value of other three dependent parameters EPS_T, BETA_C and BETA_T are changed accordingly. The

Figure 3-23 and Figure 3-24 represent stress-strain curves for UUC and UUT respectively for varying EPS_C and EPS_T value respectively. To observe changes in Peak stress and corresponding strain value with respect to EPS_C in case of UUC are indicated in

Figure 3-25 and Figure 3-26. Whereas those for UUT with respect to EPS_T are shown in Figure 3-27 and Figure 3-28 respectively. The variation shows linear relation.

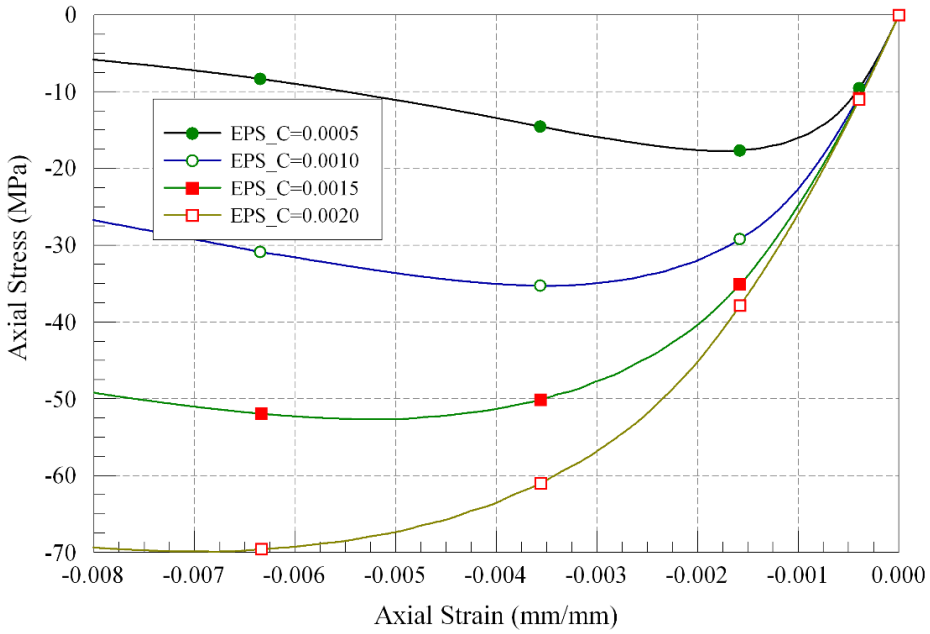

Figure 3-23 Single Element –UUC-Effect of changing EPS_C on Stress-strain Behavior

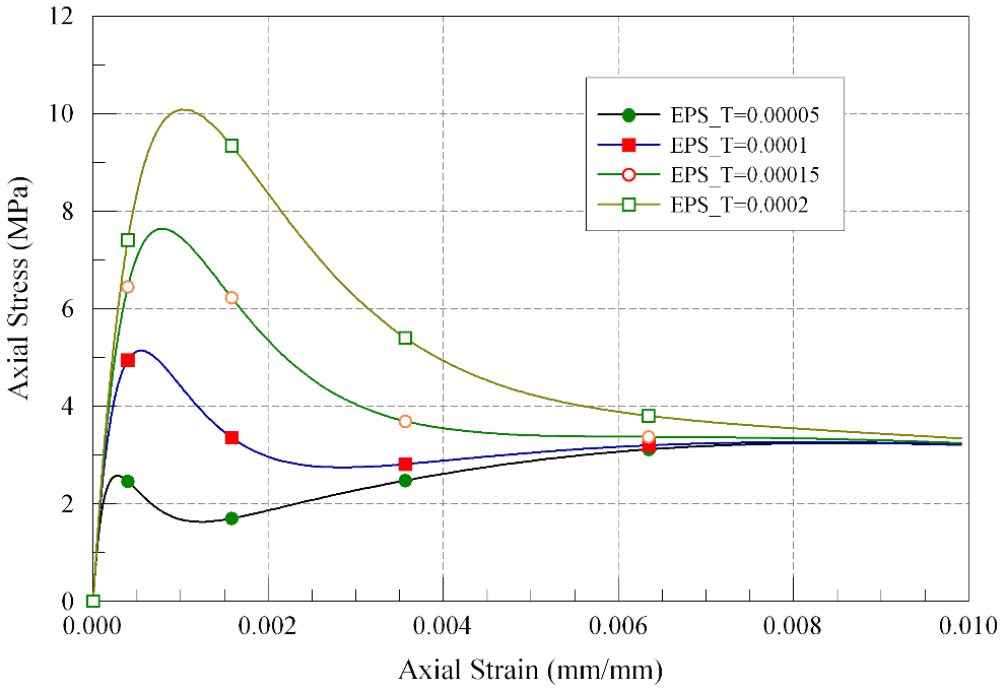

Figure 3-24: Single Element-MC-VIB-UUT-Effect of changing EPS_T on Stress-strain Behavior

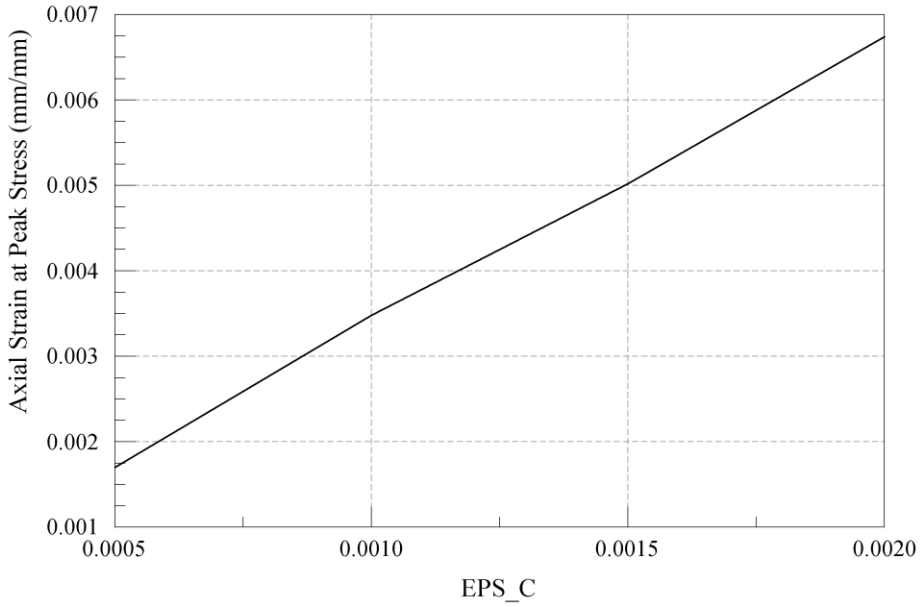

Figure 3-25 MC-VIB-Single Element-UUC-Effect of EPS_C on Axial Strain values at Peak corresponding Axial Peak Stress

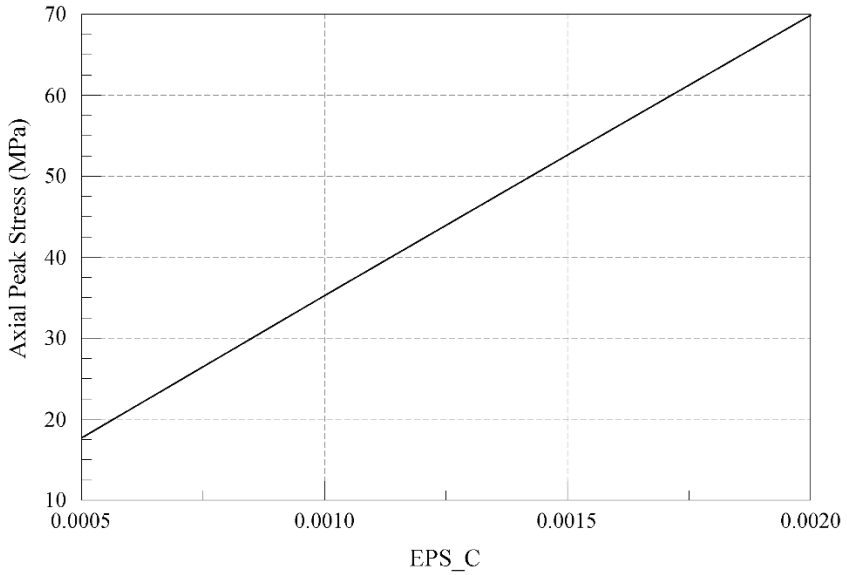

Figure 3-26 MC-VIB-Single Element-UUC- Axial Peak Stress value for Corresponding EPS_C value

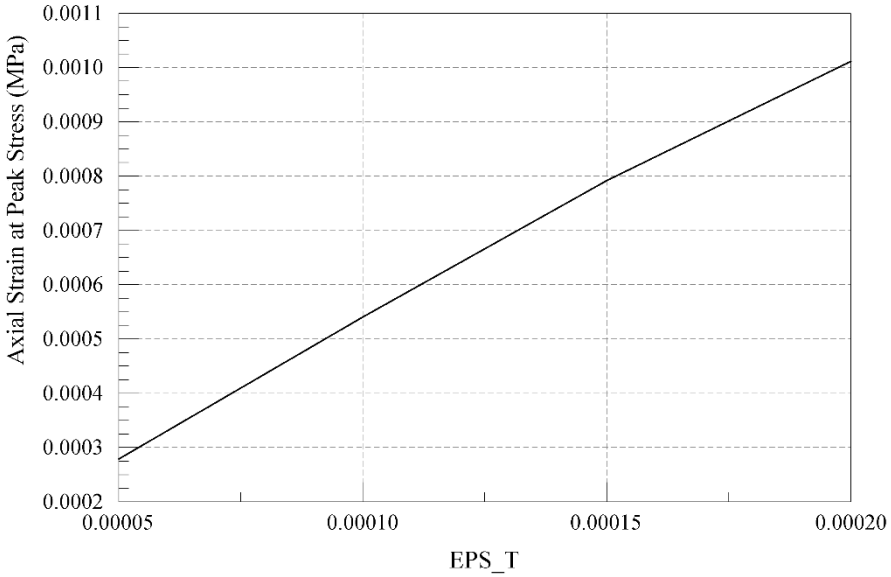

Figure 3-27 MC-VIB-Single Element-UUT-Axial Strain at Peak Stress plotted against corresponding value of EPS_T

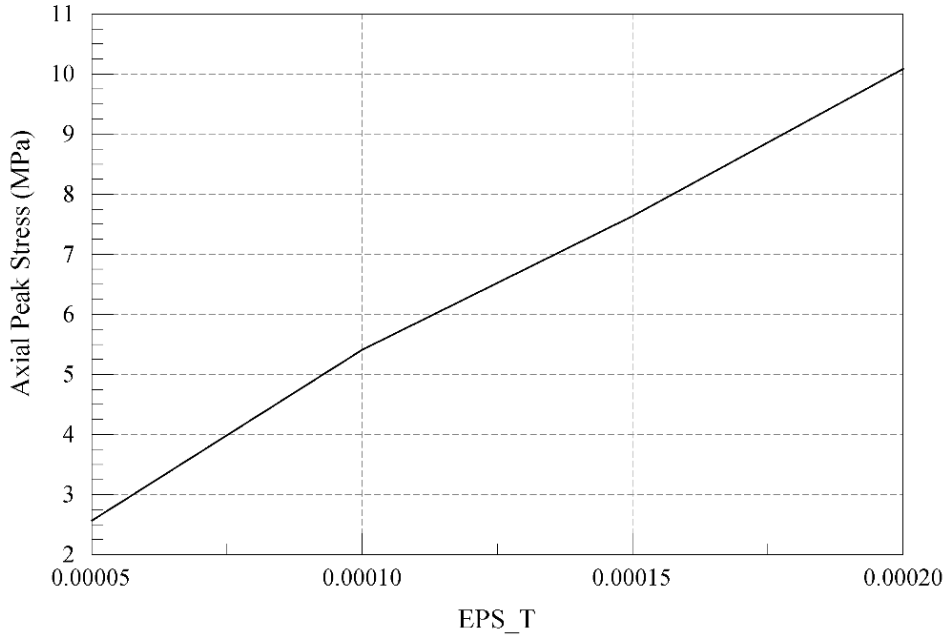

Figure 3-28 MC-VIB-Single Element-UUT-Axial Peak Stress plotted against corresponding value of EPS_T

When EPS_C is changed keeping other parameters (EM, EC, EN) constant, the slope of the curve remains same but, the value of max stress and corresponding strain value change in proportion to value of EPS_C .For example, whereas for EPS_C = 0.002, the max stress is 6928 psi which is double than Max stress of 3468 psi at EPS_C = 0.001 same is for the strain values. The trend of Max stress versus EPS_C and strain at max stress versus EPS_C is linear with slope of one.

3.3.3 Effect of Change in EN

Single element simulations are performed with EN value changing from 0.5 to 2.5 for UUC and UUT. The

Figure 3-29 and

Figure 3-30 show stress-strain curves plotted in UUC and UUT respectively. For given set of simulations, the other parameters are set to E = 3000, EPS_C = 0.001, EC = 0.15.

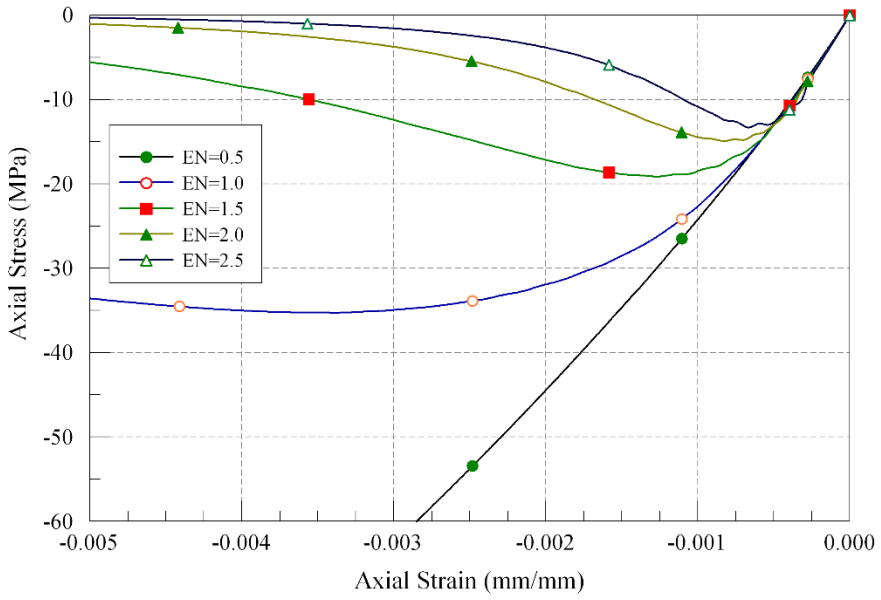

Figure 3-29 Effect of change of EN on stress-strain curves in UUC

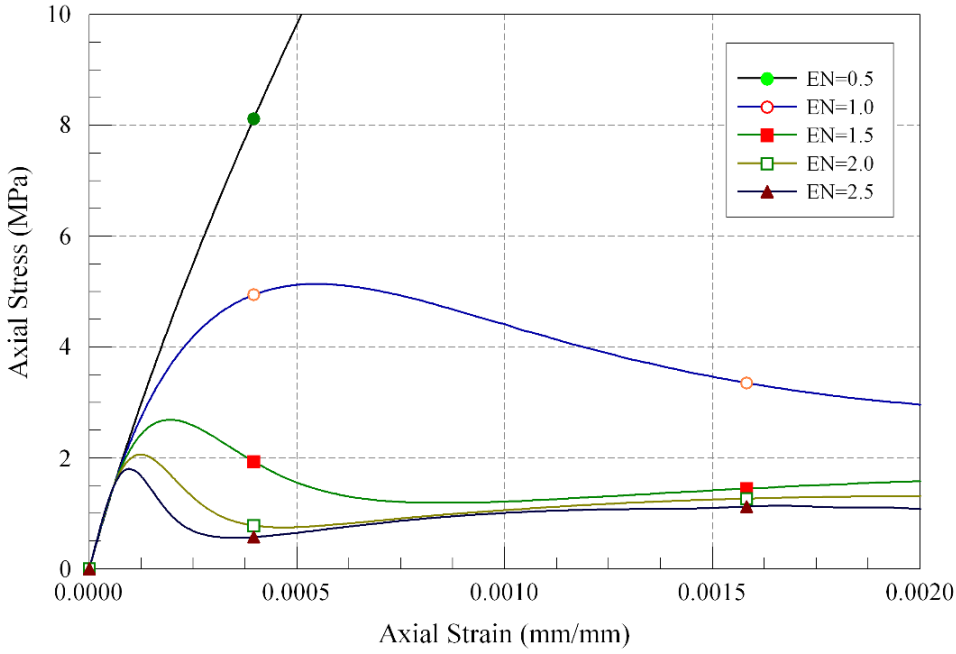

Figure 3-30 Effect of change of EN on stress-strain curves in UUT

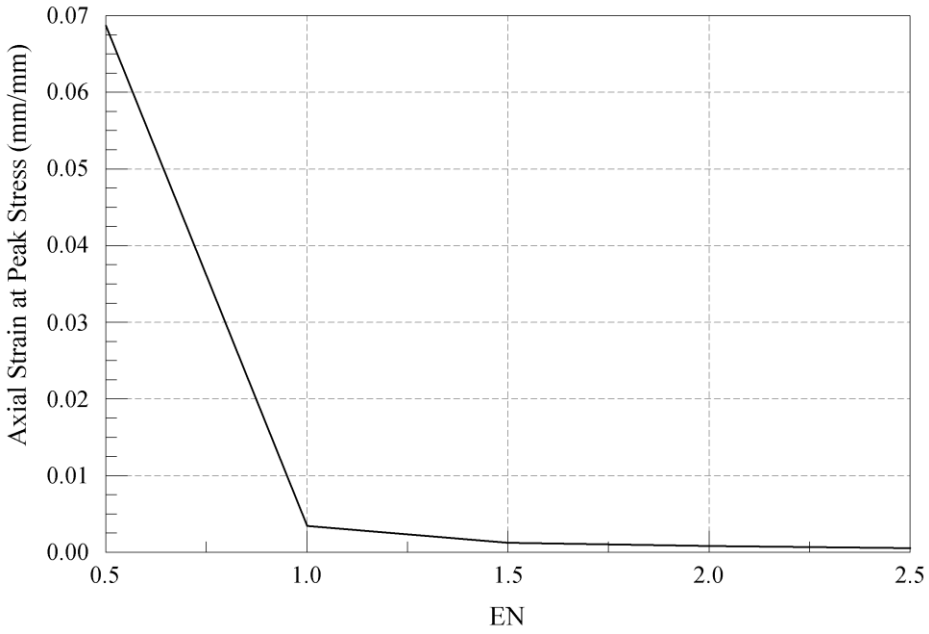

Figure 3-31 MC-VIB-Single Element-UUC-Trend showing Axial Strain at Peak Stress for Corresponding EN value

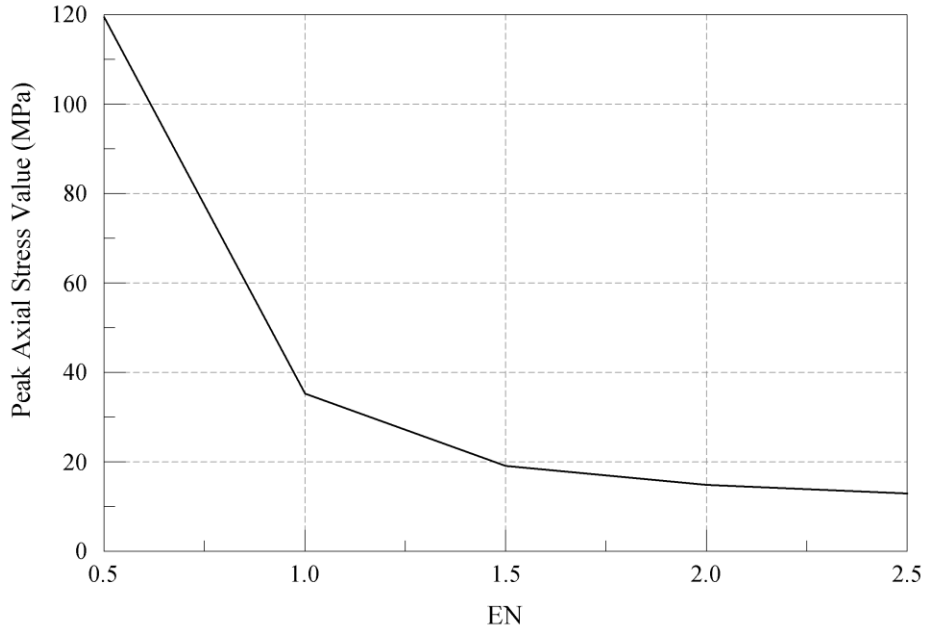

Figure 3-32 MC-VIB-Single Element-UUC-Trend showing Peak Axial Stress for Corresponding EN Value

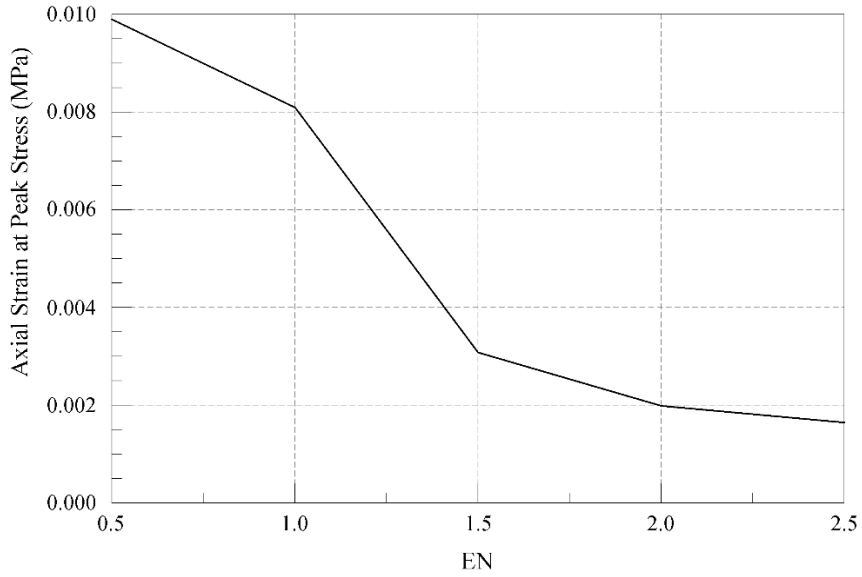

Figure 3-33 MC-VIB-Single Element-UUT-Trend showing Axial Strain at Peak Stress for corresponding EN

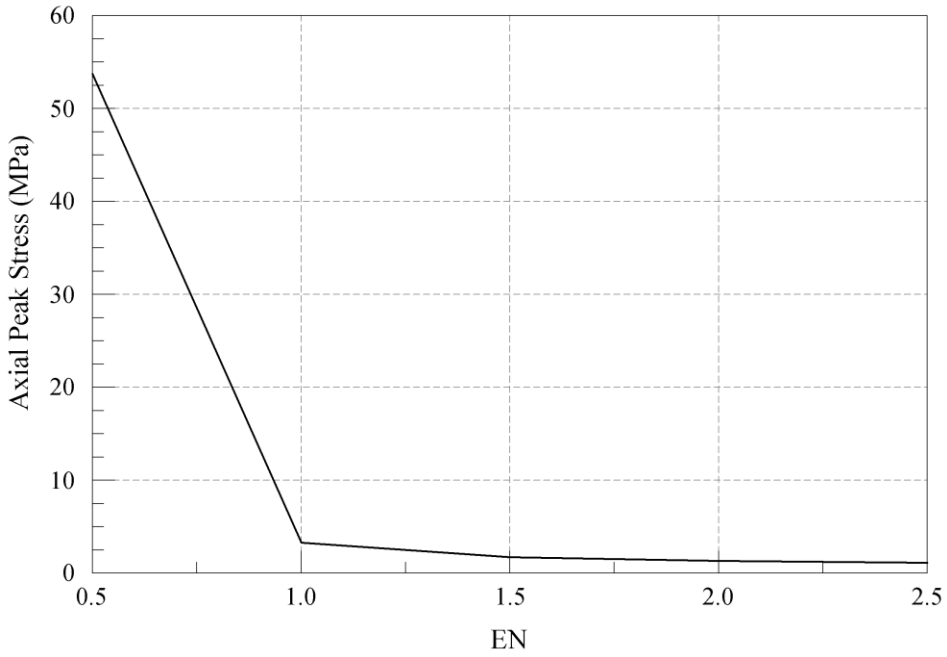

Figure 3-34 MC-VIB-Single Element-UUT-Trend showing Axial Peak Stress for corresponding EN Value

The peak stress and corresponding strain in each case are noted. These values are plotted against the corresponding EN values as shown in

Figure 3-31 to Figure 3-34. Change in peak stress and corresponding strain are inversely proportional to that in EN. The plots stress vs. EN and strain vs. EN, show changing slope.

The stress-strain curve shows more ductile behavior as EN value is reduced. It shows higher peak stress and sustained strain. The failure becomes gradual showing reduced brittleness. These observations are in agreement with the Zhang and Ge work [15] which concludes brittleness is increased with increasing EN value.

3.3.4 Effect of Change in EC

In this set of single element simulations, EC is varied from 0.1 to 0.3 for both UUC and UUT. The other parameters are kept constant and the same velocity loading is applied to have consistency in the results. The

Figure 3-35 and Figure 3-36 show comparison of these graphs for UUC and UUT respectively. The peak stress and corresponding strain values are plotted against respective EC value as shown in figures from Figure 3-37 to Figure 3-40. The observation shows that increasing EC reduces the peak stress and its corresponding strain value. This observation is in accordance with Zhang and Ge study [15] .

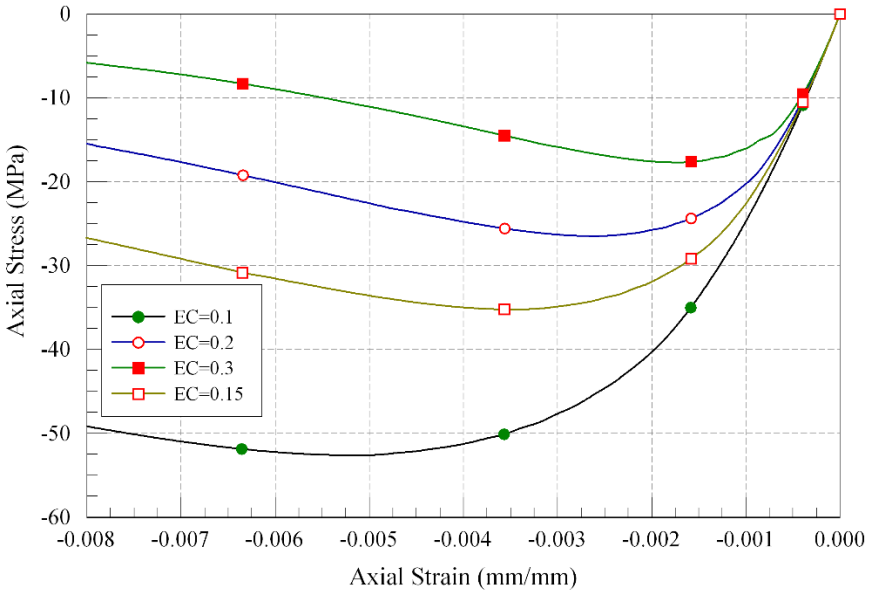

Figure 3-35 Effect of change in EC on stress-strain curves (UUC)

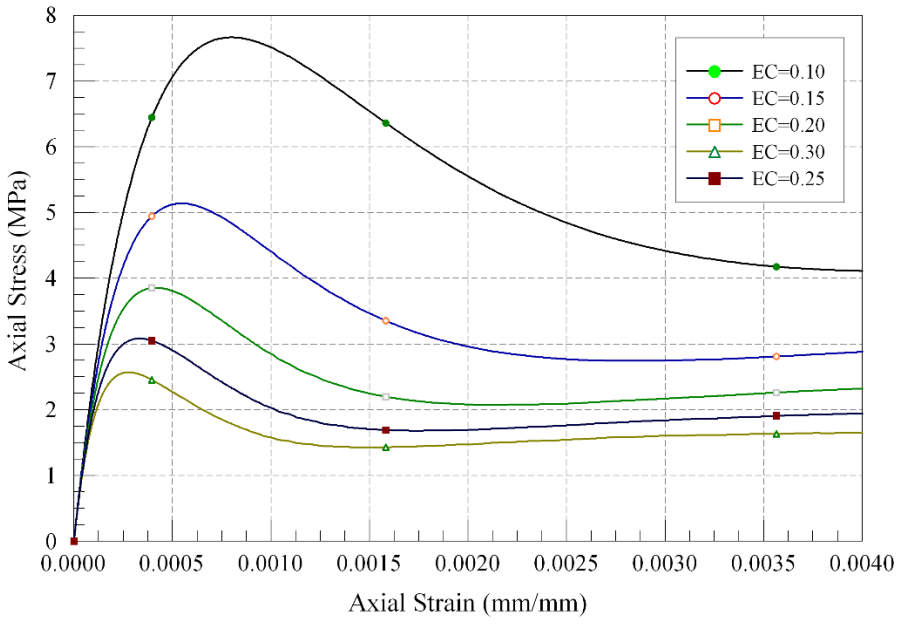

Figure 3-36 Single Element-MC-VIB-UUT-Effect of change in EC on stress-strain curves

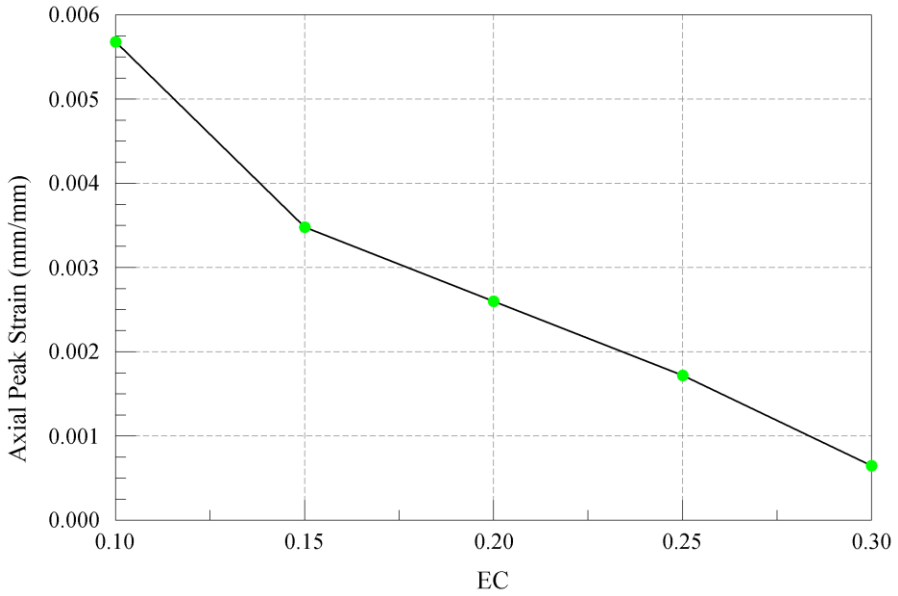

Figure 3-37 MC-VIB-Single Element-UUC-Trend showing effect of axial strain at peak stress with respect to EC

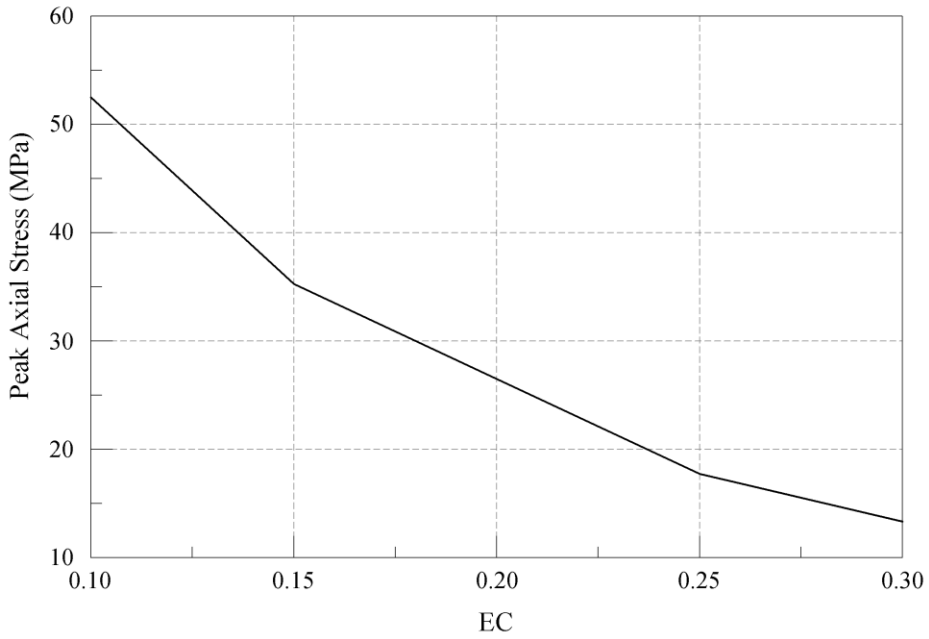

Figure 3-38 MC-VIB-Single Element-UUC-Trend showing effect of axial Peak Stress with respect to EC

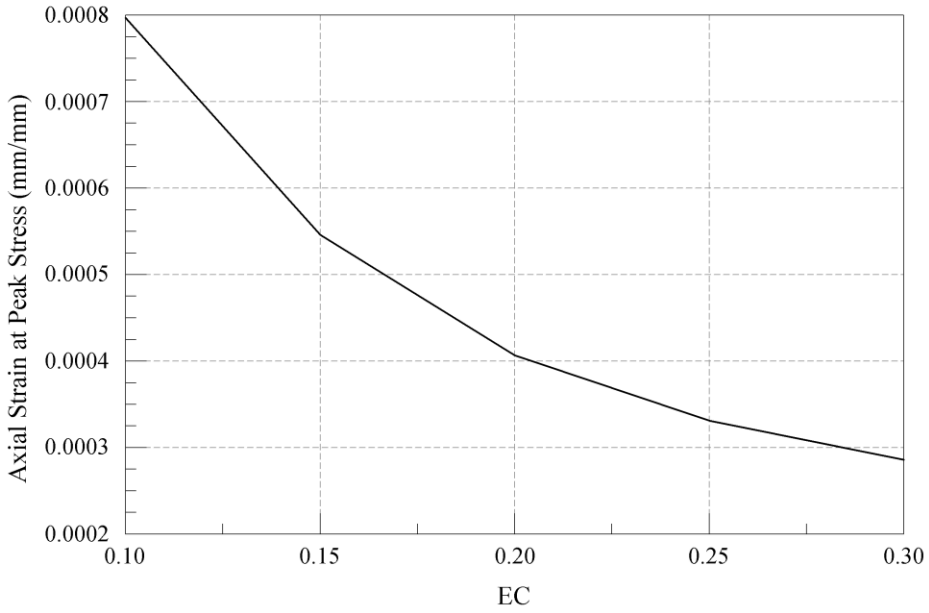

Figure 3-39 MC-VIB-Single Element-UUT-Trend showing effect of axial strain at peak stress with respect to EC

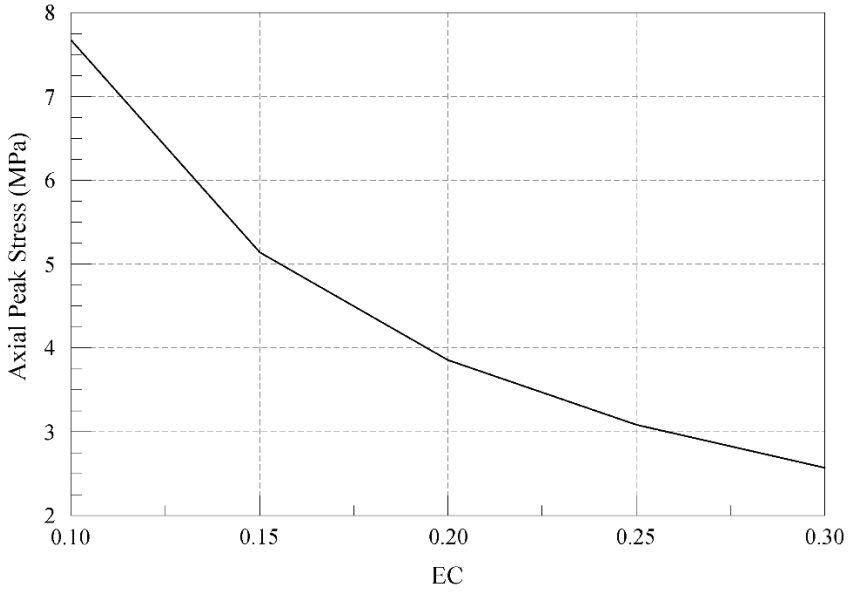

Figure 3-40 MC-VIB-Single Element-UUT-Trend showing effect of axial peak stress with respect to EC

3.3.5 Trial And Error Method

To study every parameter, a number of simulations are performed. Out of which, only few samples are presented in the section 3.3. The stress-strain curve obtained from Hognestad's equation and CDMR3 are used as the references for study. These graphs are compared with MC-VIB stress-strain curves, while modifying each parameter. At the beginning, efforts were made to achieve a parameter combination by changing one parameter at one time. For instance, the value of E is varied and it is observed that the graph with E = 3000 has initial slope equivalent to that of standard curves. It is easy to manipulate the peak stress value by changing EPS_C considering its direct proportion. But EN and EC also affect the peak stress and strain values considerably. The stress-strain curve is affected by combination of all the parameters in a set. So number of trial simulations are performed to serve the purpose. Three sample trial curves for UUC and UUT are plotted in

Figure 3-41 and Figure 3-42 respectively.

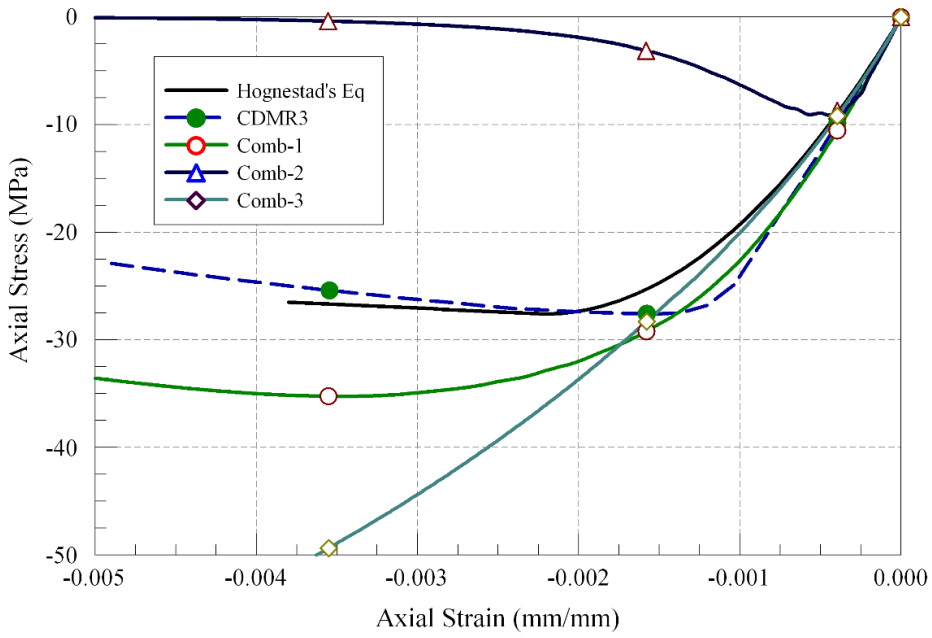

Figure 3-41 MC-VIB-single element-UUC-sample trial

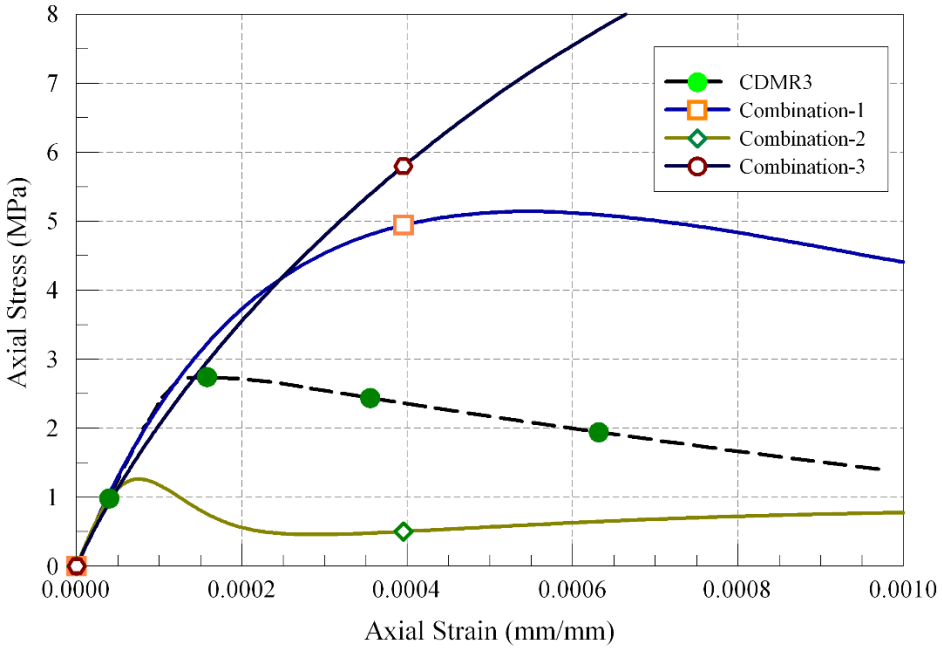

Figure 3-42 MC-VIB-single element-UUT-Sample trials

The peak stress and corresponding strain values are tabulated in Table 3-2 and Table 3-3 for UUC and UUT respectively. All the three combinations have E set to 3000, hence the bulk modulus and shear modulus are 15000 and 2500 respectively. But it is clearly seen that, initial part of these curves do not coincide exactly, because it is affected by other parameters in the set. The combination-3 has lowest EN value that is 0.5, hence shows higher peak stress and higher strain at peak stress value. The EPS_C value is doubled from 0.0005 for Combination-2 to 0.001 for Combination-1. The peak stress value is increased from 9 MPa to 35 MPa but is not 18 MPa exactly double as explained in 3.3.2. Because of reduced value of EN, the peak stress value is increased beyond 35 MPa and again reduced to 35 MPa due to increased EC value. Same logic applies to strain at which peak stress is achieved.

Table 3-2 MC-VIB-Single element –UUC – Sample trials-comparison with standard results

	E	EPS_C	EN	EC	Strain at peak stress (mm/mm)	Peak stress (MPa)	% difference from Hognestad's Eqn results	
							Strain at peak stress (mm/mm)	Peak stress (MPa)
Hognestad's Eqn					0.0022	27.59		
CDMR3					0.0015	27.62	-32%	0%
MC-VIB								
Comb-1	3000	0.001	1	0.15	0.00347	35.26	58%	28%
Comb-2	3000	0.0005	2	0.1	0.00045	9.12	-80%	-67%
Comb-3	3000	0.001	0.5	0.3	0.00985	80.34	348%	191%

Table 3-3 MC-VIB-Single element-UUT-Sample trials-comparison with standard results

		EPS_C	EPS_T	EN	EC	Strain at peak stress (mm/mm)	Peak stress (MPa)	% error with standard results	
								Strain at peak stress (mm/mm)	Peak stress (MPa)
Standard						0.0002	3.27		
CDMR3						0.00015	2.74	-25%	-16%
MC-VIB									
Comb-1	3000	0.001	0.0001	1	0.15	0.00054	5.14	171%	57%
Comb-2	3000	0.0005	0.00005	2	0.1	0.00007	1.25	-64%	-62%
Comb-3	3000	0.001	0.0001	0.5	0.3	0.00489	14.4425	2347%	341%

When compared to standard values, the Combination-1 used for both the cases, is observed to have minimum percentage difference. It depicts a desired shape of stress-strain behavior for concrete. The combination-1 is used for further study in cylinder simulations. It is discussed in Chapter 4.

Chapter 4.

STUDY OF STRESS-STRAIN BEHAVIOR

The simulations are performed on cylinder models and stress-strain curves are obtained as per procedure already explained in section 3.2.3. The stress-strain behavior of cylinder under UUC and UUT are presented under three sections in this chapter. First is to compare these curves with their respective case for CDMR3 and Hognestad's Curve. The other two cases are to study mesh size effect and cylinder size effect respectively.

4.1 Comparison With Standard Results

There are six cases for compression loading and six cases for tension loading. The results are presented in the form of graphs in this section.

The cylinder with diameter 101.6 mm and height 203.2 mm is termed as 4 x 8 cylinder. The nodes at top surface of the cylinder are subjected to velocity loading such that it produces strain of 101.6 mm/mm in one second. Two simulations are performed with two different material models namely CDMR3 and MC-VIB assigned to this cylinder. While running MC-VIB model different solver is selected. This solver is the LS-971 executable file, modified by Dr. Ganesh Thiagarajan.

The binary file is opened in LS-PREPOST which shows the analysis results after processing the file. An element is selected at the height101.6 mm. The history card is used to plot z-stress and green St. Venant-z-strain for this element. These stress and strain curves are crossed using XYPLOT button. The stress-strain data is written in the "csv" format. These arrays of data can be used to combine the curves in one graph and compare with each other.

The

Figure 4-1 to Figure 4-6 show a smooth curve obtained using MC-VIB showing stress-strain relationship of concrete for uniaxial unconfined compression loading (UUC). The peak stress value for Hognestad's curve is 27.6 MPa (4 ksi) at strain value of 0.0022 mm/mm. The overall behavior of the stress-strain curves obtained using MC-VIB show good agreement with those plotted using CDMR3.

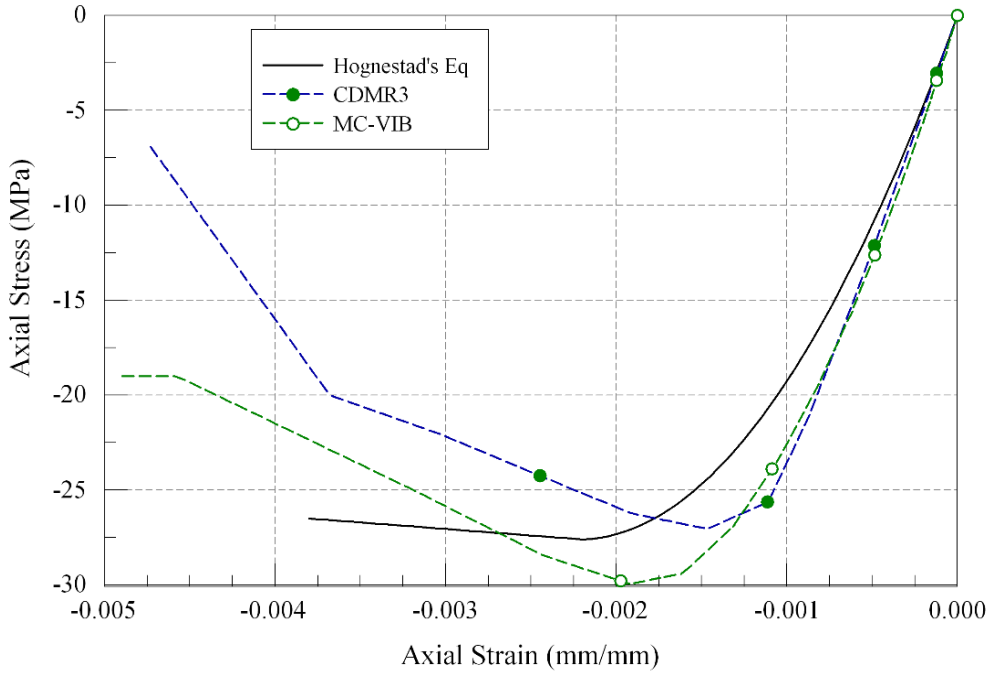

Figure 4-1: UUC-4x8 Cylinder-Stress-strain Curve Comparison with Standard

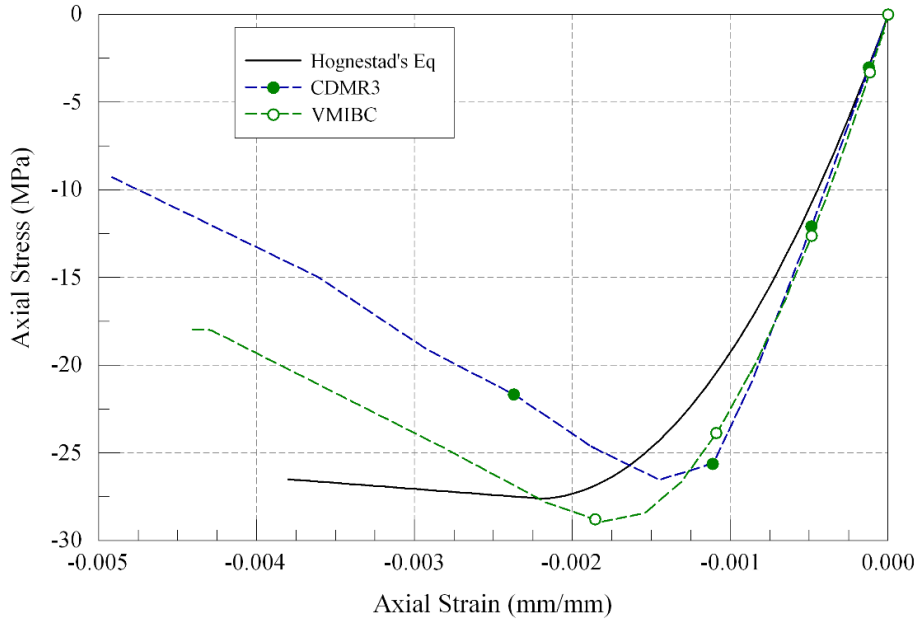

Figure 4-2: UUC-4x8 Cylinder Stress-strain Curve-Comparison with Standard curves

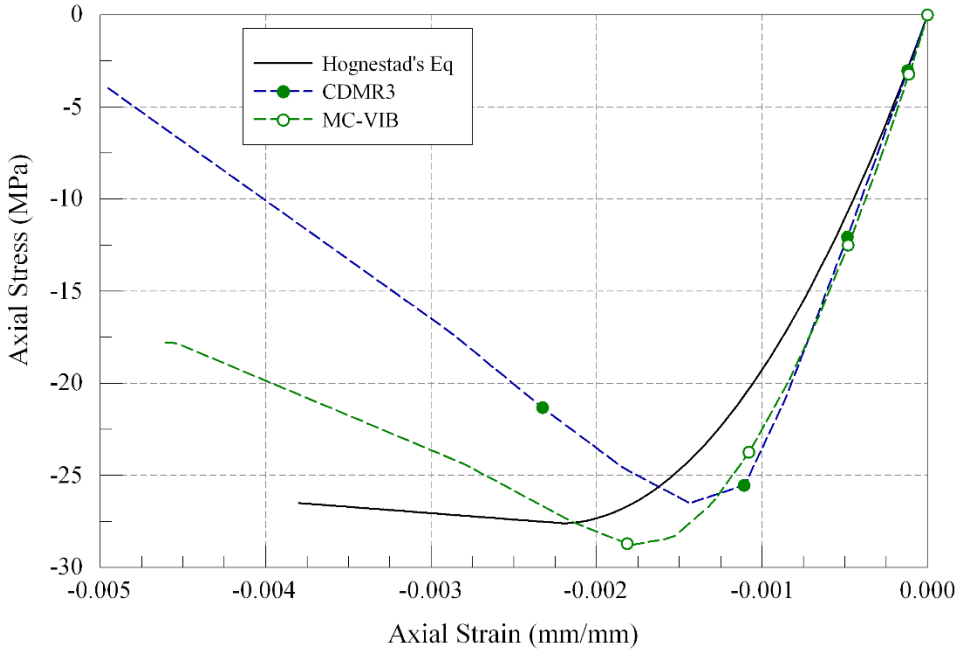

Figure 4-3: UUC-4x8 Cylinder- Fine Mesh - Stress-strain Curve-Comparison with standard curves

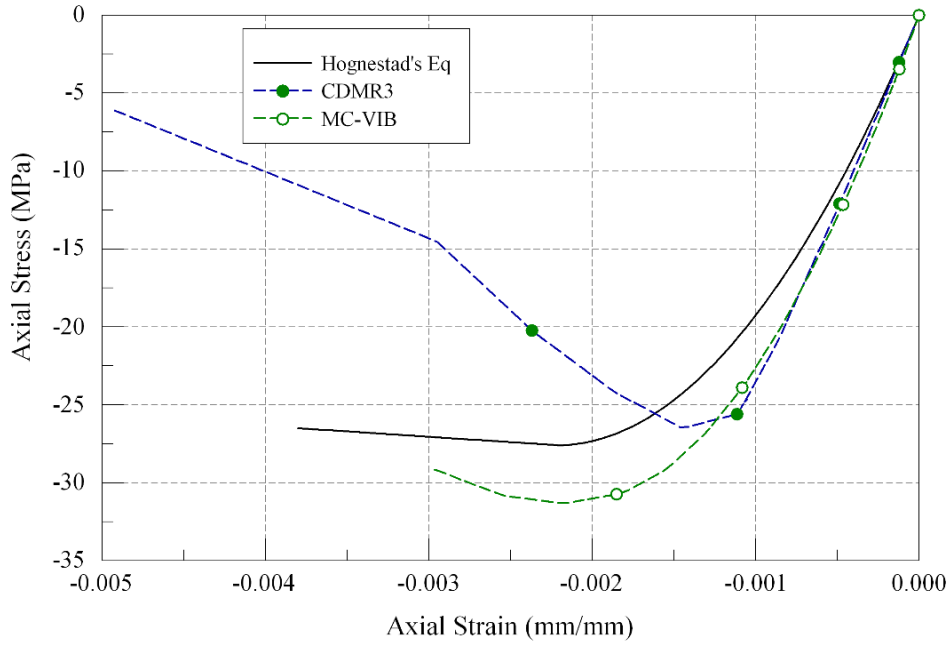

Figure 4-4: UUC-8x16 Cylinder-Coarse Mesh-Stress-strain Curve-Comparison with Standard curves

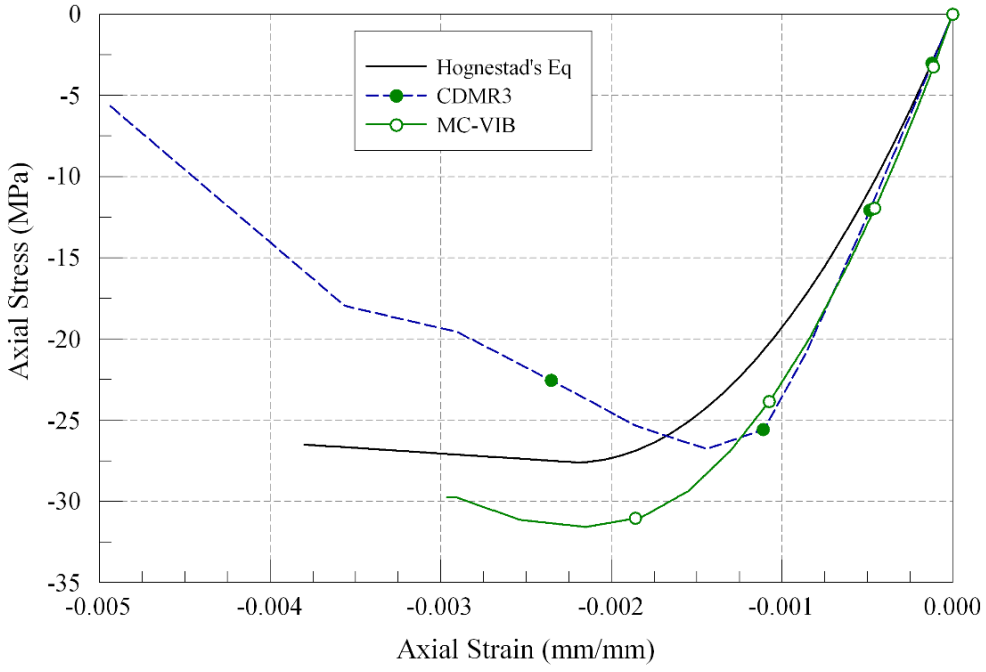

Figure 4-5 UUC-8x16 Cylinder-Medium Mesh-Stress-strain Curve-Comparison with Standard

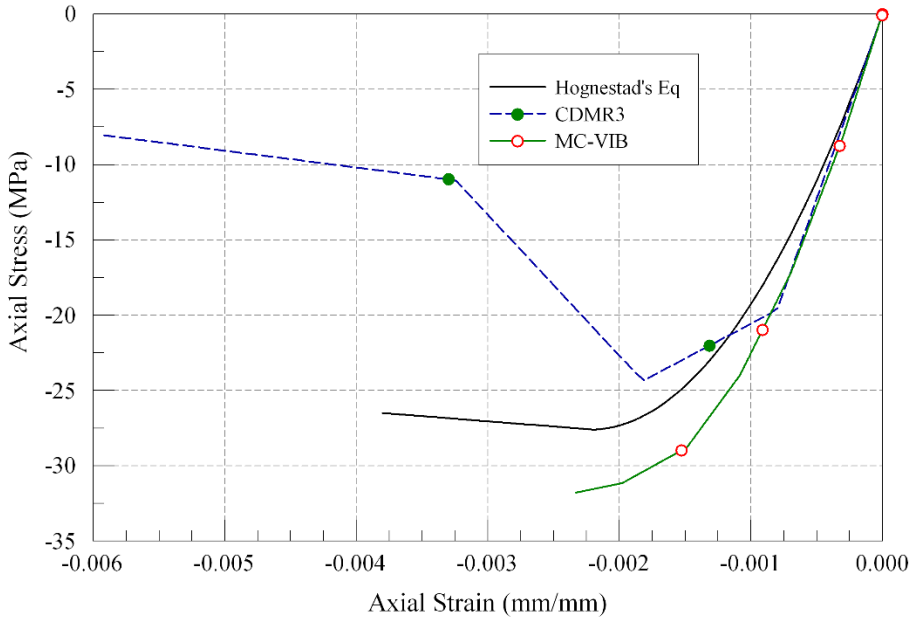

Figure 4-6 UUC-16x32 Cylinder-Fine Mesh-Stress-strain Curve-Comparison with Standard

Table 4-1 UUC- MCVIB and CDMR3 comparison with standard results

Cylinder Size		Results and Corresponding % Difference w.r.t. Hognestad's Results							
		CDMR3 Results				MC-VIB Results			
Dimension (dia. X height)	Mesh Size	Strain at peak stress (mm/mm)		Peak stress (MPa)		Strain at peak stress (mm/mm)		Peak stress (MPa)	
4x8	Coarse	0.00147	-27%	27.04	-2%	0.00192	-4%	29.95	8%
	Medium	0.00145	-28%	26.52	-4%	0.00181	-10%	28.92	5%
	Fine	0.00144	-28%	26.49	-4%	0.00179	-11%	28.77	4%
8x16	Coarse	0.00144	-28%	26.77	-3%	0.00215	8%	31.57	14%
	Medium	0.00145	-28%	26.5	-4%	0.00217	9%	31.33	14%
16x32	Coarse	0.00145	-28%	26.55	-4%	0.00233	11%	31.79	15%

Using Hognestad's equation the peak stress of 27.6 MPa is achieved at the strain 0.002 mm/mm. The peak stress and corresponding strain values are noted down and summarized in Table 4-1. It depicts the percentage difference of predicted values from peak stress and strain vales of Hognestad's Curve. The MC-VIB curve shows higher peak stress value than

Hognestad's Curve. The percentage difference increases with increase in cylinder height. It is observed that, strength of concrete is increased with the increase in size of the cylinder. The peak stress value predicted with CDMR3 is very close to that with Hognestad's curve whereas, CDMR3 shows the strain value at peak stress as 0.00145 mm/mm which is 28% lower when compared to Hognestad's Curve. This difference for strain prediction is approximately within 10% for MC-VIB.

The similar cylinder sizes and mesh sizes of cylinder are subjected to uniaxial unconfined tension (UUT) test. Velocity of loading is to produce tensile strain of 0.5 mm/mm per second in the cylinder. The simulations are performed and the stress vs strain curves are plotted with the similar procedure followed for UUC as shown in

Figure 4-7 to Figure 4-12. For this case, it is observed that stress-strain curves obtained for both CDMR3 and MC-VIB show instable results after a certain point. The CDMR3 shows a linear behavior, whereas the MC-VIB curve shows a good parabolic behavior. The modulus of rupture for 27.6 MPa concrete is obtained by the standard formula, $f_r = 7.5\sqrt{f_c'}psi = 474\ psi = 3.27\ MPa.$, where $1\ MPa = 145\ psi.$ MC-VIB shows continuously increasing value of stress beyond 3.27 MPa, with increase in strain produced. As the behavior of curve is smooth, it is believed that, modification of some material parameters, can refine the results.

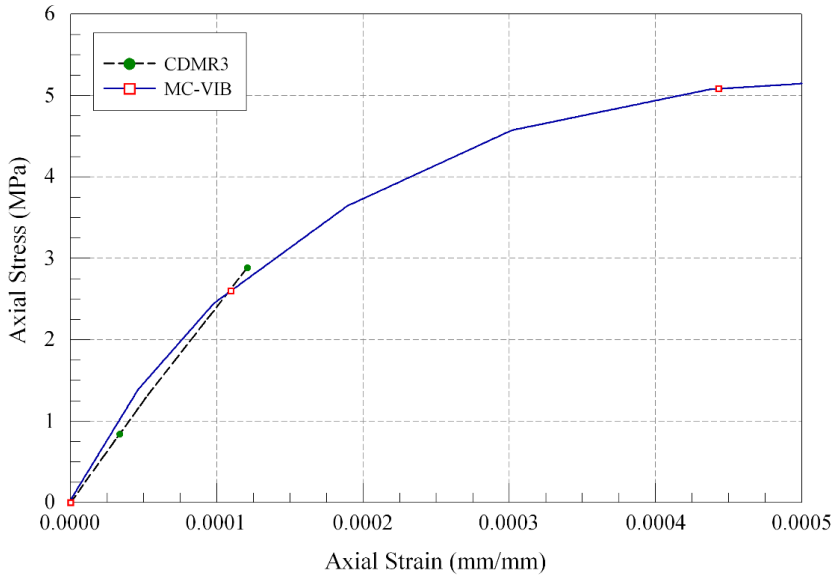

Figure 4-7 UUT-4x8 Cylinder Coarse Mesh – Stress-strain Curve

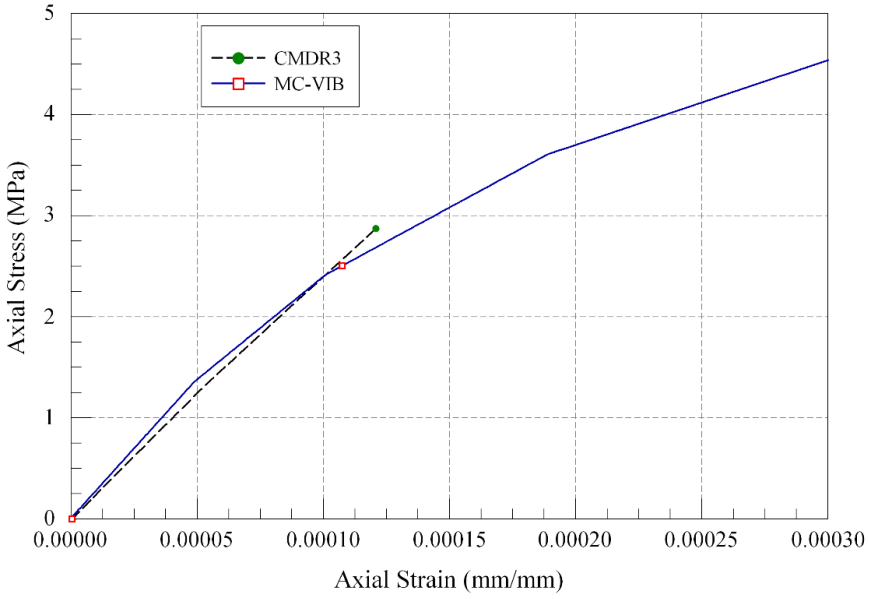

Figure 4-8 UUT- 4x8 Cylinder-Medium Mesh-Stress-strain Curve

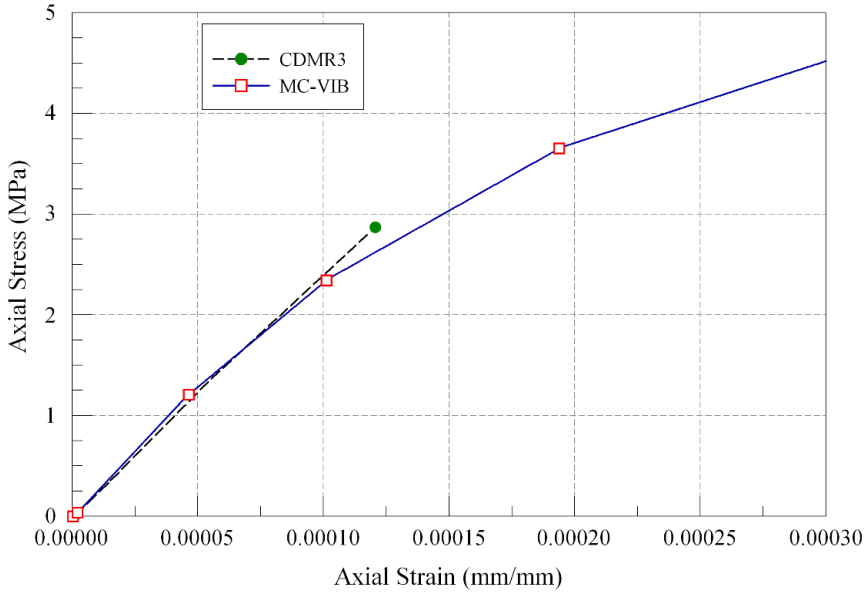

Figure 4-9 UUT- 4x8 Cylinder-Fine Mesh-Stress-strain Curve

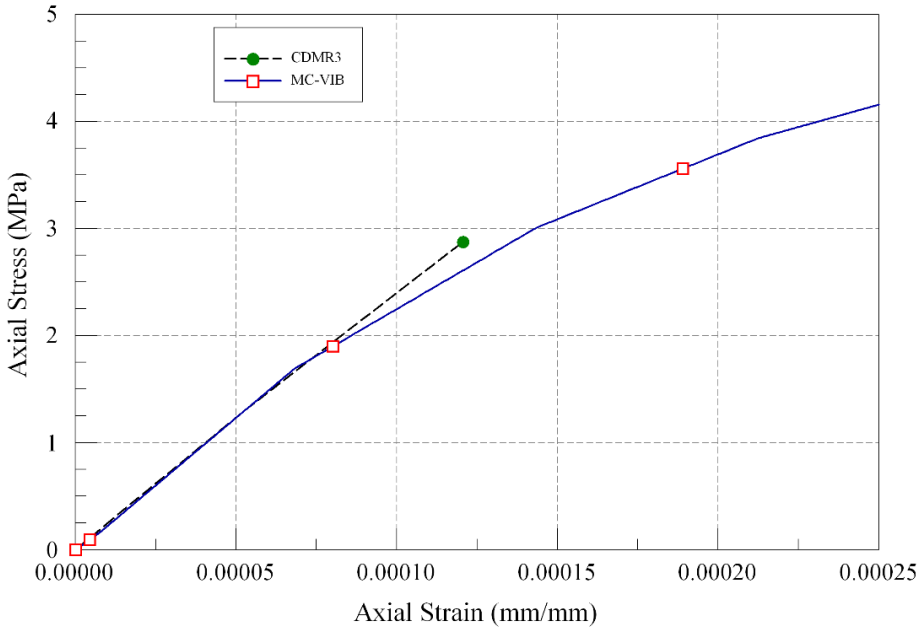

Figure 4-10 UUT-8x16 Cylinder-Coarse Mesh – Stress Strain curves

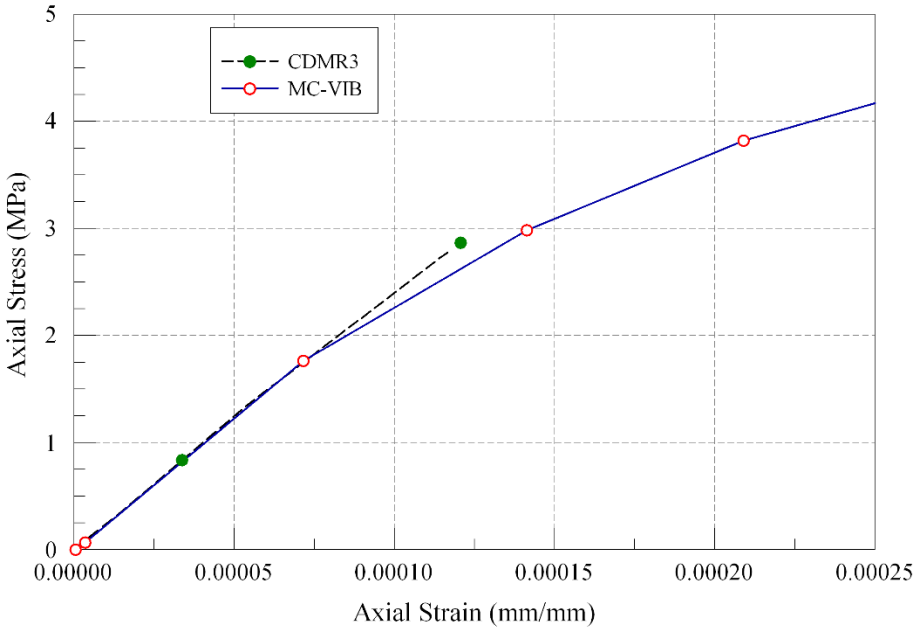

Figure 4-11 UUT-8x16 Cylinder- Medium Mesh – Stress-strain Curve

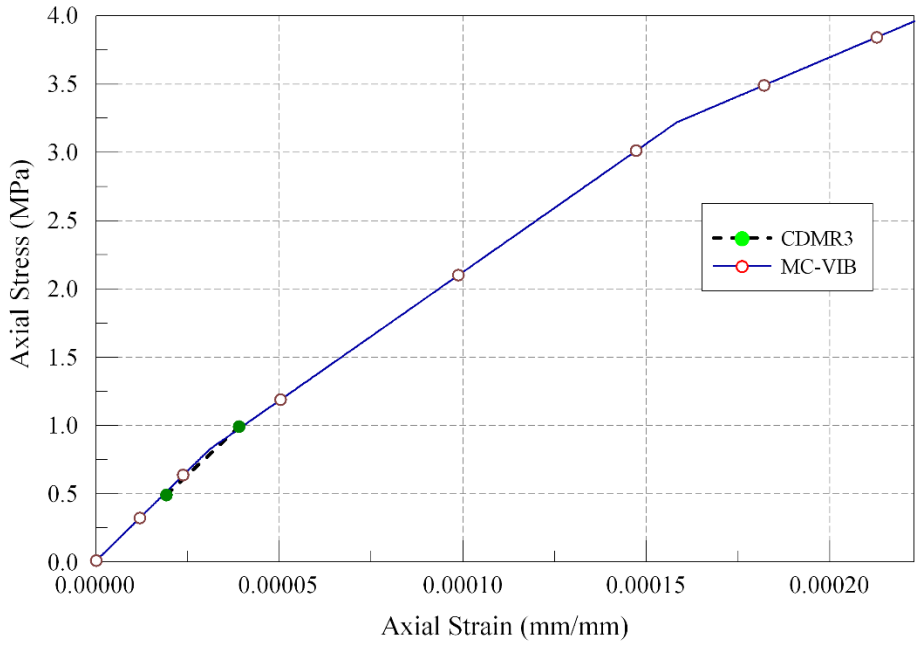

Figure 4-12 UUT-16x32 Cylinder-Coarse Mesh- Stress-strain Curve

4.2 Effect of Mesh Size

In this section the criterion used to compare the stress-strain curves is mesh size of the model. The cylinder 101.6 mm x 203.2 mm (4" x 8") is modelled using three mesh sizes namely coarse (25.4 mm or 1"), medium (12.7 mm or 0.5") and fine (6.35 mm or 0.25"). They cylinder model 203.2 mm x 406.4 mm (8"x 16") is modelled in coarse and medium mesh size. For a cylinder size, the stress-strain curves obtained using three mesh sizes are compared with each other for both the material models. The comparison is shown in this section from

Figure 4-13 to Figure 4-20 for UUC and UUT.

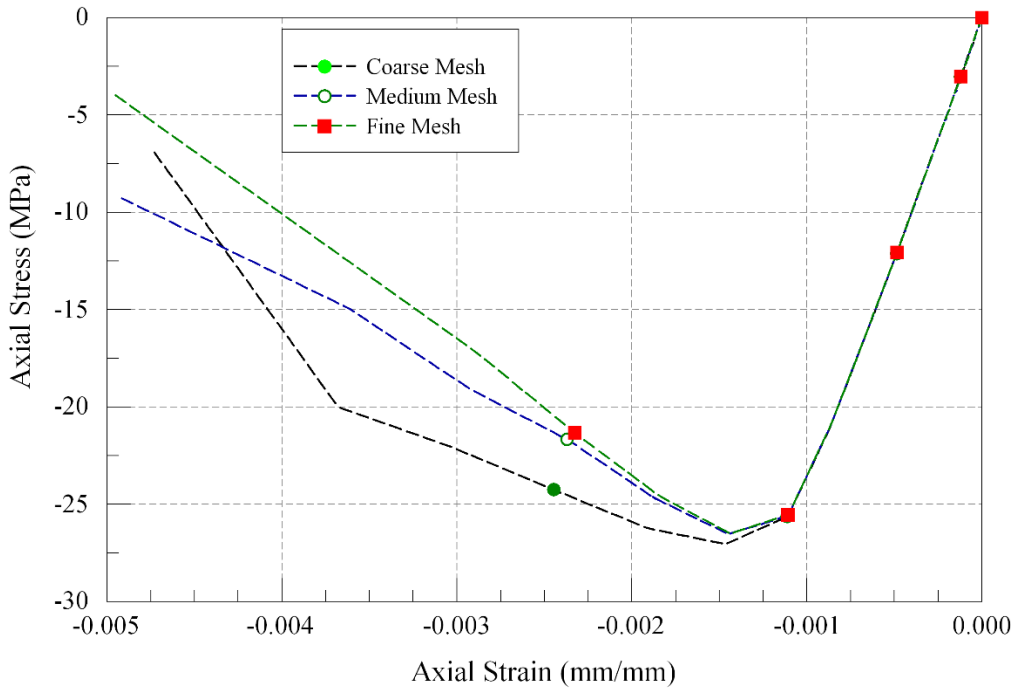

Figure 4-13 UUC- CDMR3-4x8 Cylinder-Effect of Mesh Size

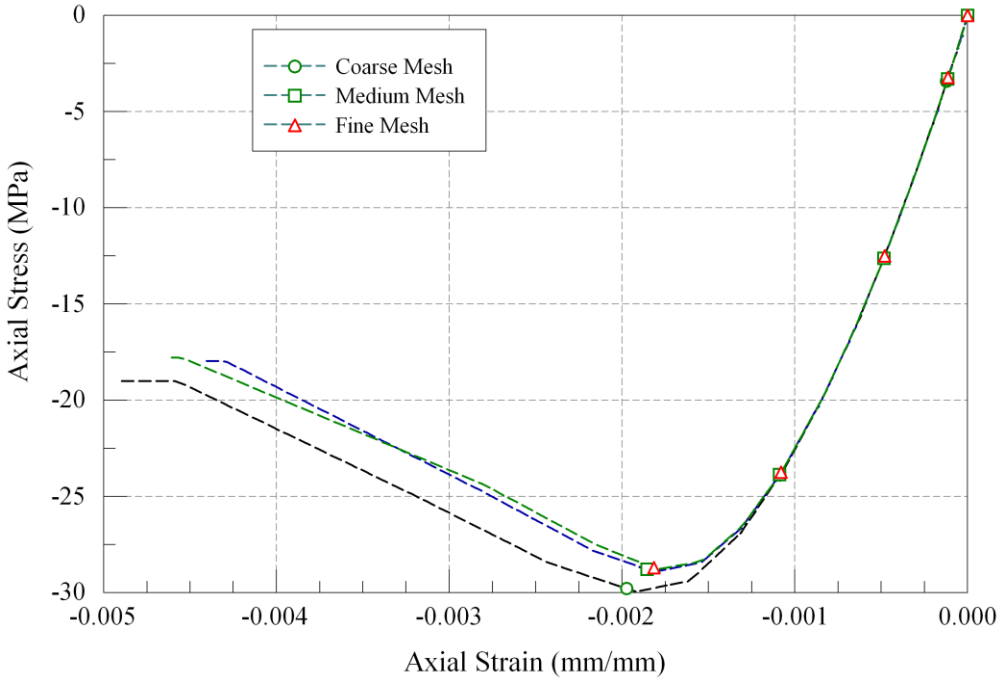

Figure 4-14 UUC-MC-VIB-4x8 Cylinder-Effect of Mesh Size

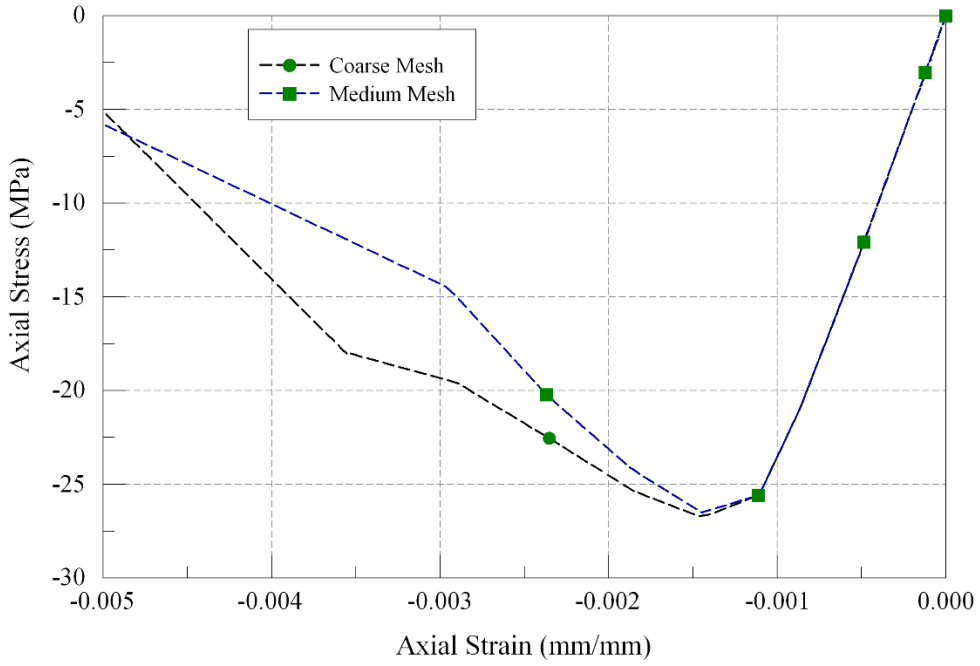

Figure 4-15 UUC-8x16-CDMR3-Effect of Mesh Size

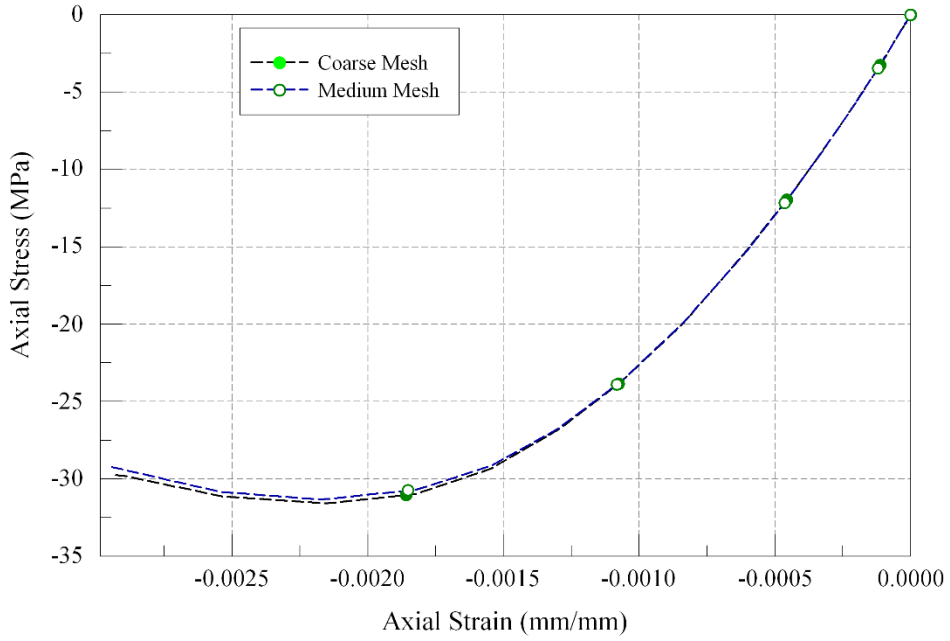

Figure 4-16 UUC-8x16-MC-VIB-Effect of Mesh Size

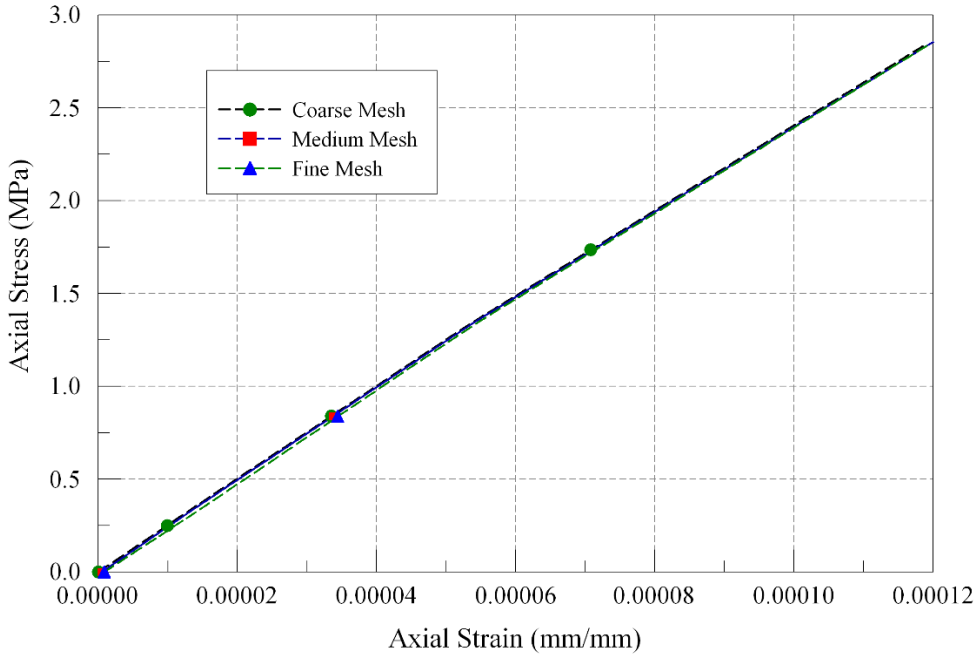

Figure 4-17 UUT-4x8 Cylinder-CDMR3-Effect of Mesh Size

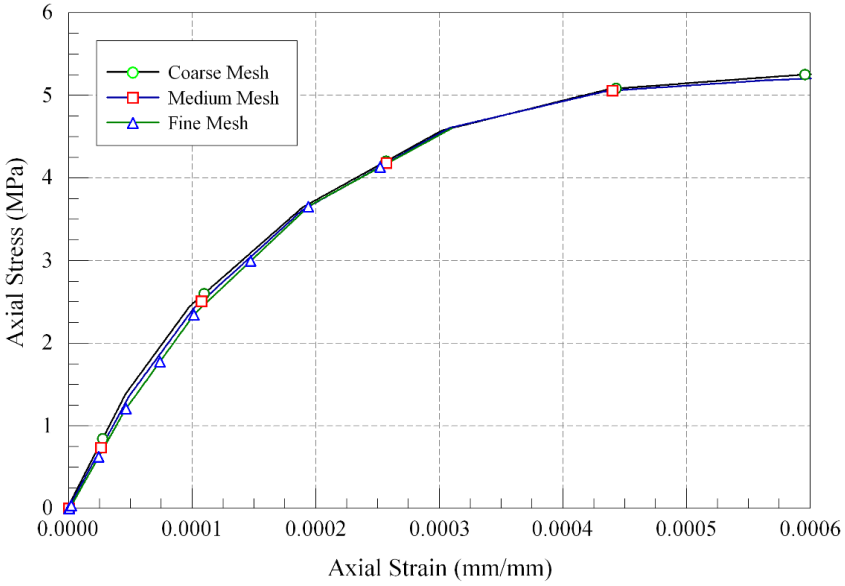

Figure 4-18 UUT-4x8-Cylinder-MC-VIB-Effect of Mesh Size

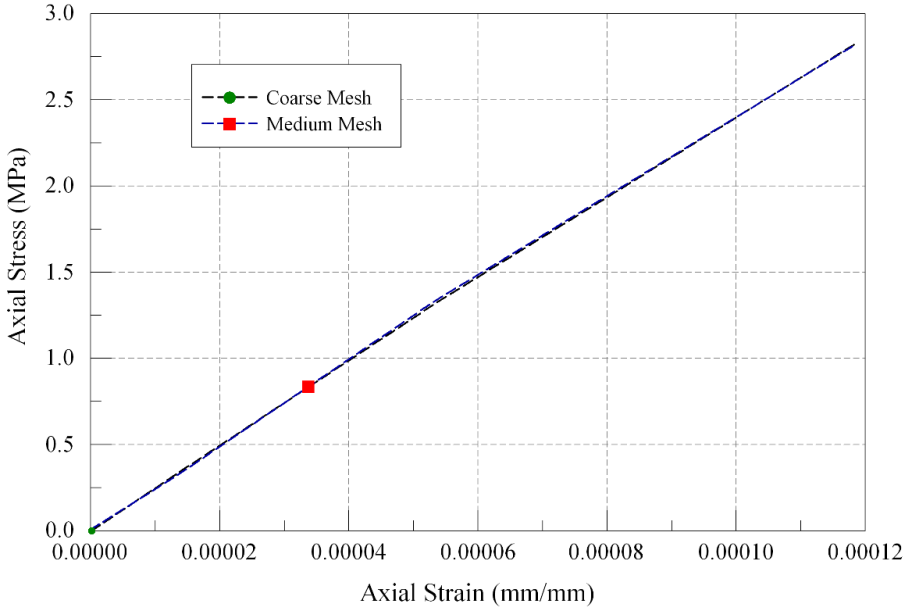

Figure 4-19 UUT-CDMR3-8x16-Effect of Mesh Size

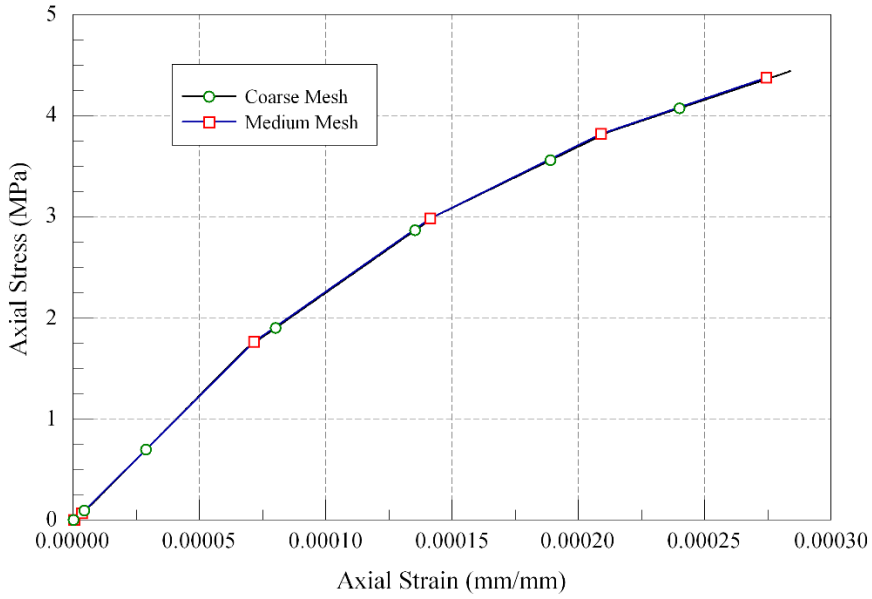

Figure 4-20 UUT-MC-VIB-8x16 Cylinder-Effect of Mesh Size

Table 4-2 CDMR3-UUC-Cylinder-Effect of mesh size on stress-strain results

Cylinder Size	Mesh Size	Mesh Size (mm)	Strain at peak stress (mm/mm)	Peak stress (MPa)	% Change w.r.t coarse mesh	
					Strain at peak stress (mm/mm)	Peak stress (MPa)
4x8	Coarse	25.4	0.00147	27.0447		
	Medium	12.7	0.00145	26.5159	-1%	-2%
	Fine	6.35	0.00144	26.4947	-2%	-2%
8x16	Coarse	25.4	0.00144	26.768		
	Medium	12.7	0.00145	26.499	1%	-1%

Table 4-3 MC-VIB-UUC-Cylinder-Effect of mesh size on stress-strain results

Cylinder Size	Mesh Size	Mesh Size (mm)	Strain at peak stress (mm/mm)	Peak stress (MPa)	% Change w.r.t coarse mesh	
					Strain at peak stress (mm/mm)	Peak stress (MPa)
4x8	Coarse	25.4	0.00192	29.9456		
	Medium	12.7	0.00181	28.9182	-6%	-3%
	Fine	6.35	0.00179	28.7686	-7%	-4%
8x16	Coarse	25.4	0.00215	31.5694		
	Medium	12.7	0.00217	31.3299	1%	-1%

To study effect of refining the mesh size on peak stress and strain values prediction is studied by comparing those values with results from coarse mesh. The values and their percentage change with mesh size change for UUC are tabulated for CDMR3 and MC-VIB in Table 4-2 and Table 4-3 respectively. The peak stress and peak strain value is reduced by 1% with reduced mesh size in CDMR3. It is observed that when mesh size is reduced, the stiffness of the model is reduced due to increased degrees of freedom. Same is observed for MC-VIB. For the coarse mesh 4 x 8 cylinder, the peak stress is 29.9 MPa. It is reduced to 28.9 MPa for medium mesh and to 28.8 MPa for fine mesh. This percent reduction in peak stress value is within 5%, which is a satisfactory prediction.

4.3 Effect of Cylinder Size

The velocity of loading is kept constant for all the specimen. The stress-strain curves plotted using the cylinder models with same mesh size, but different dimensions are compared together in this section. The Figure 4-21 and Figure 4-23 show stress strain curve comparison under UUC loading with CDMR3 cylinders using coarse mesh and medium mesh respectively. The initial part of the curve is linear and coincident for all sizes of cylinder. The peak stress value is observed to be reducing with increase in cylinder size. It is assumed that, the strength of concrete increases with increase in cylinder size due to lateral confinement effect. But for CDMR3 the observation is contradictory to this assumption. Refer to Figure 4-22 and Figure 4-24 for MC-VIB cylinder results with coarse and medium mesh respectively. The peak stress is observed to be increasing with increase in cylinder size which is in agreement with the assumption. The Figure 4-25 to Figure 4-28 show the stress strain curves comparison for UUT.

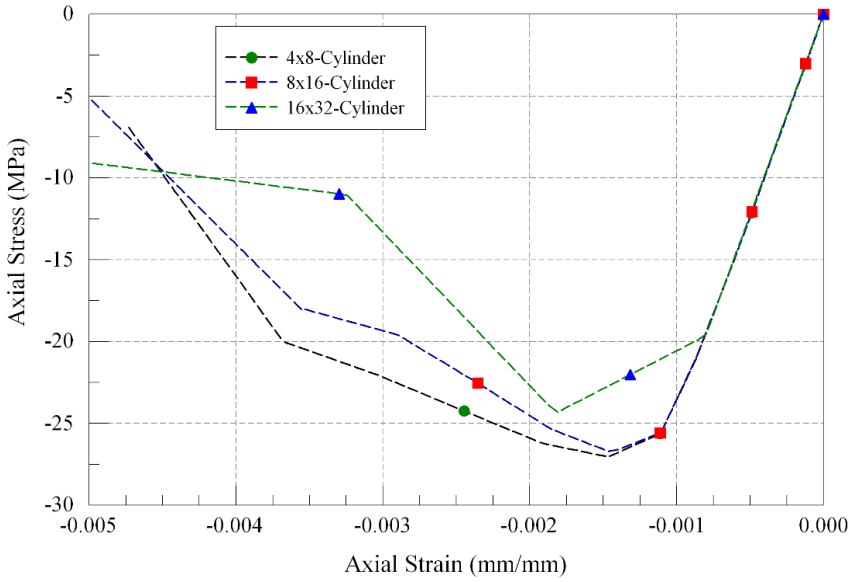

Figure 4-21 UUC- CDMR3-Coarse Mesh- Cylinder-Effect of Cylinder Size

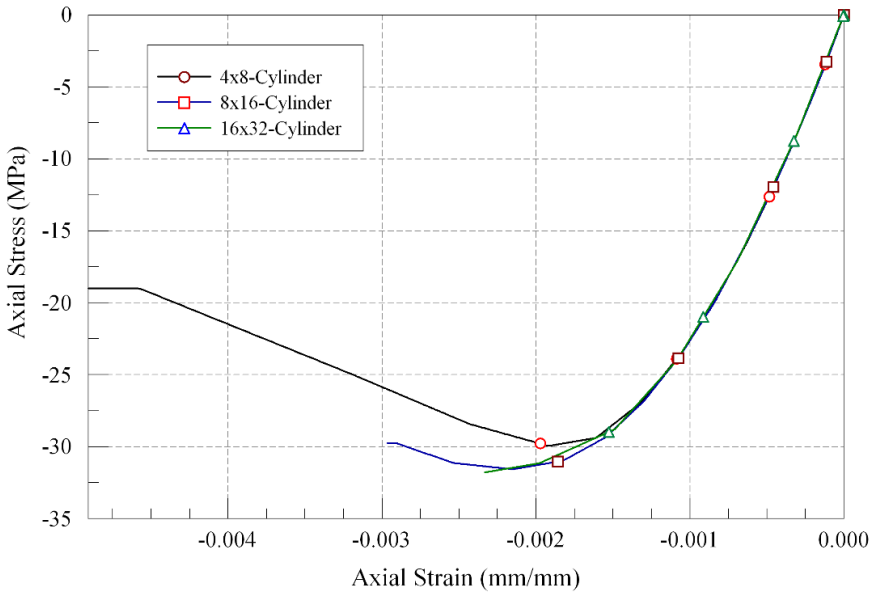

Figure 4-22 UUC-MC-VIB-Coarse Mesh-Effect of Cylinder Size

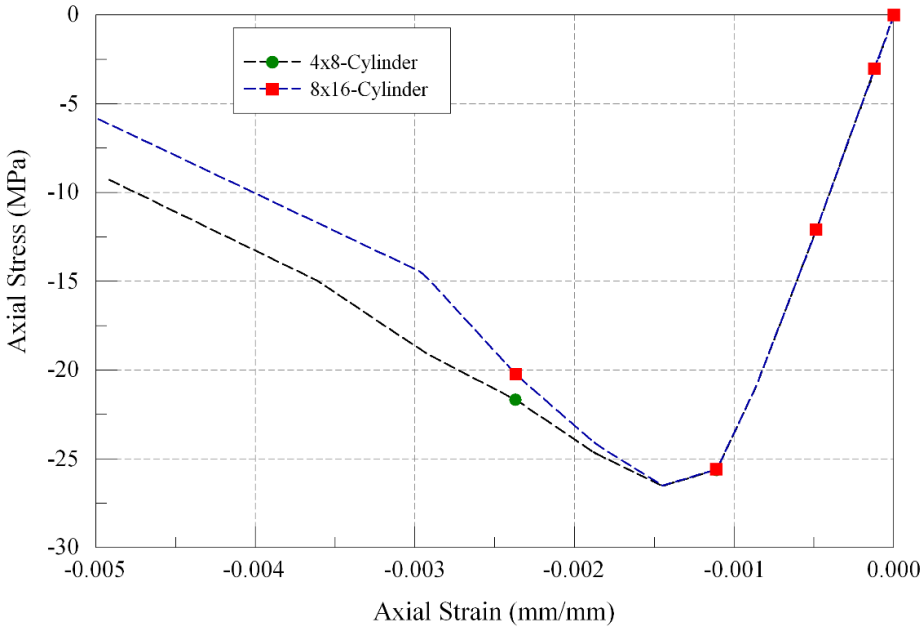

Figure 4-23 UUC-CDMR3-Medium Mesh-Stress-strain Curve

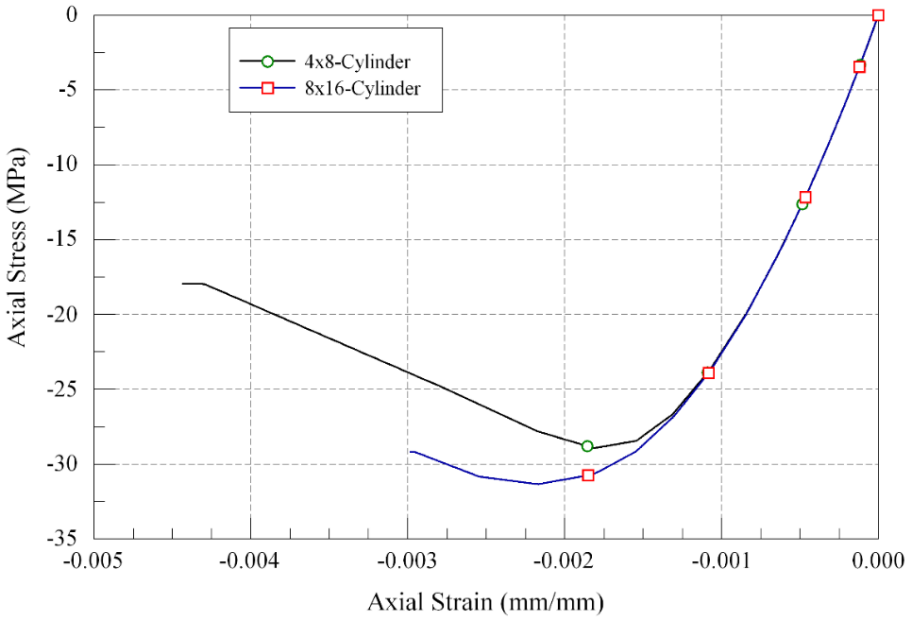

Figure 4-24 UUC-MC-VIB-Medium Mesh-Stress-strain Curve

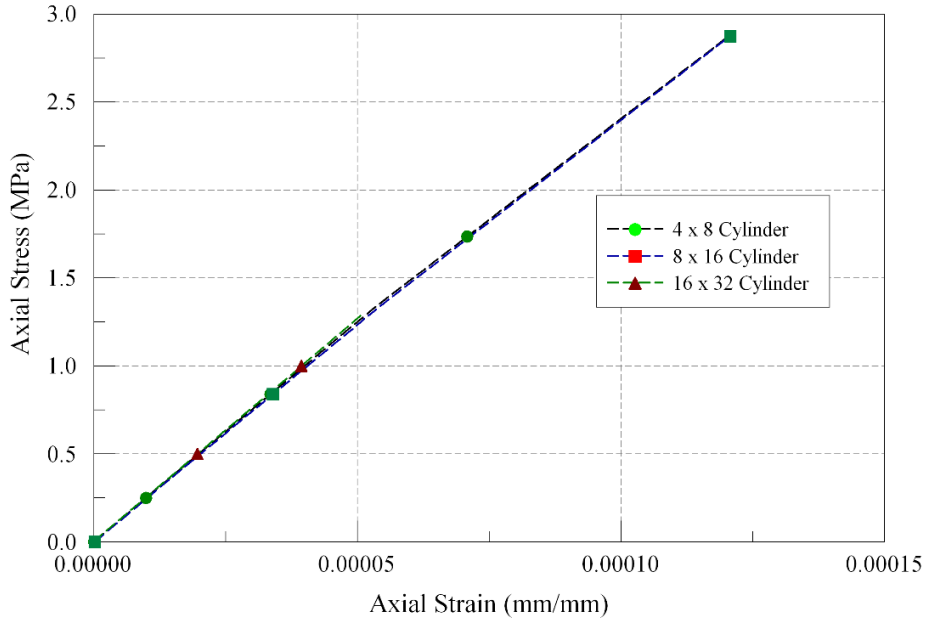

Figure 4-25 UUT-CDMR3-Coarse Mesh-Effect of Cylinder Size on Stress-strain Curve

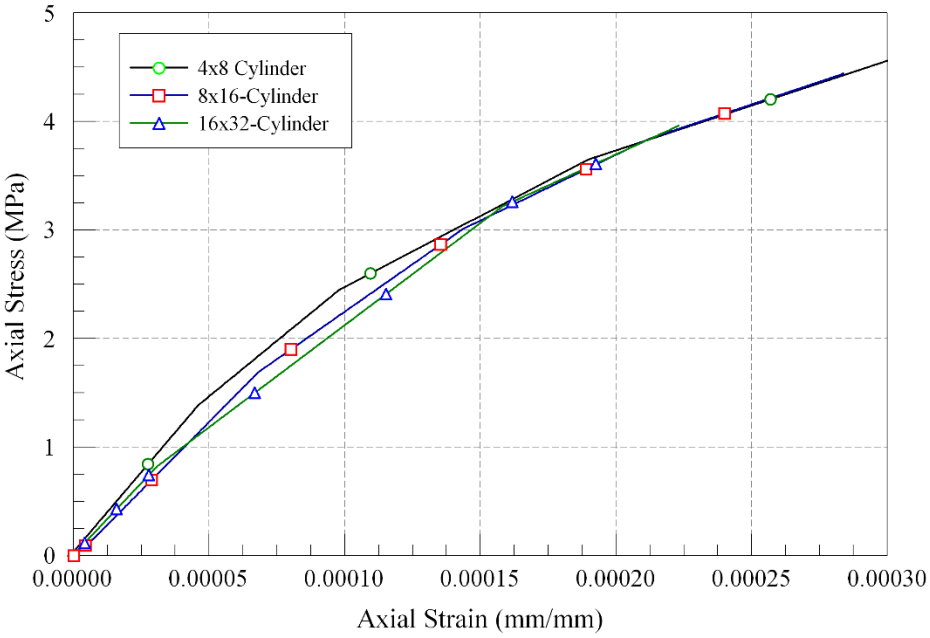

Figure 4-26 UUC-MC-VIB-Coarse Mesh-Effect of Cylinder Size on Stress-strain Curve

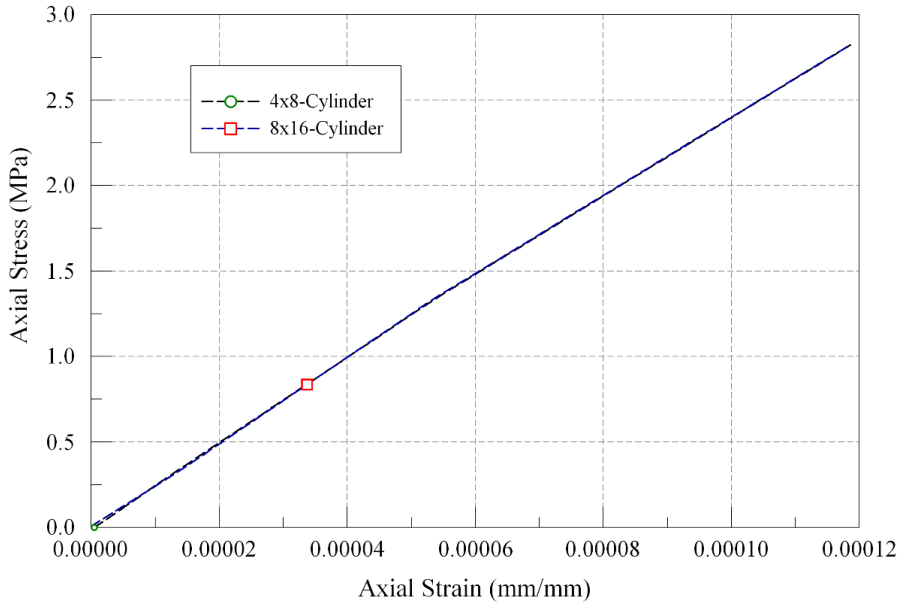

Figure 4-27 UUT-CDMR3-Medium Mesh-Effect of Cylinder Size on Stress-strain Curve

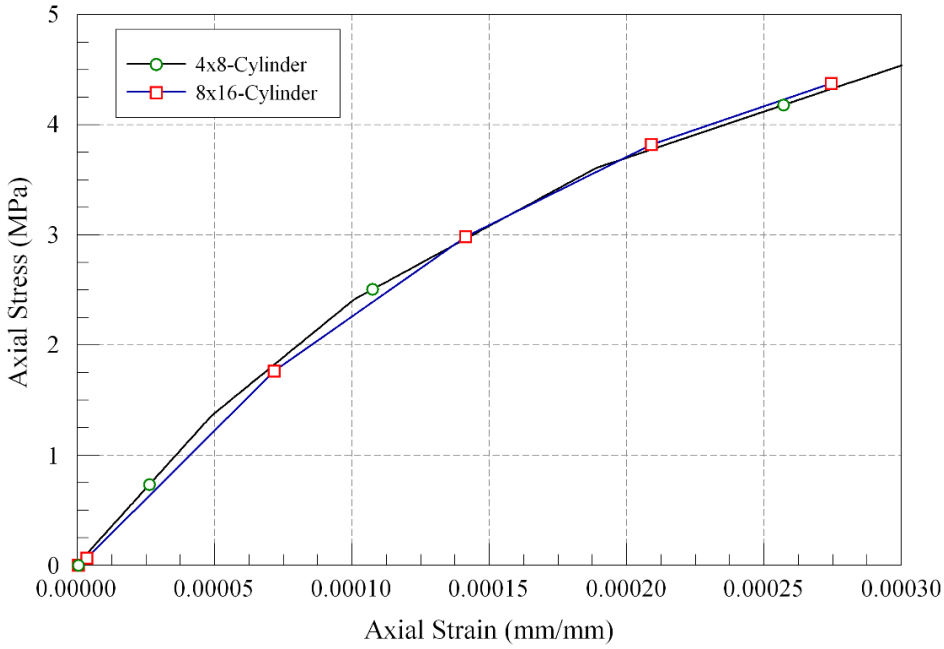

Figure 4-28 UUT-MC-VIB-Medium Mesh-Effect of Cylinder Size on Stress-strain Curve

Table 4-4 CDMR3-UUC-effect of cylinder size on stress-strain results

Cylinder Size	Mesh Size	Diameter (mm)	Height (mm)	Strain at peak stress (mm/mm)	Peak stress (MPa)	% Change w.r.t 4x8 cylinder values	
						Strain at peak stress (mm/mm)	Peak stress (MPa)
4x8	Coarse	101.6	203.2	0.00147	27.0447		
8x16	Coarse	203.2	406.4	0.00144	26.768	-2%	-1%
16x32	Coarse	406.4	812.8	0.00145	26.545	-1%	-2%
4x8	Medium	101.6	203.2	0.00145	26.52		
8x16	Medium	203.2	406.4	0.00145	26.5	0%	0%

Table 4-5 MC-VIB-UUC-effect of cylinder size on stress-strain results

Cylinder Size	Mesh Size	Diameter (mm)	Height (mm)	Strain at peak stress (mm/mm)	Peak stress (MPa)	% Change w.r.t 4x8 cylinder values	
						Strain at peak stress (mm/mm)	Peak stress (MPa)
4x8	Coarse	101.6	203.2	0.00192	29.95		
8x16	Coarse	203.2	406.4	0.00215	31.57	12%	5%
16x32	Coarse	406.4	812.8	0.00233	31.79	21%	6%
4x8	Medium	101.6	203.2	0.00181	28.92		
8x16	Medium	203.2	406.4	0.00217	31.33	20%	8%

The effect of cylinder size on peak stress and strain values are shown in tabulated format in Table 4-4 and Table 4-5 for CDMR3 and MC-VIB respectively. The peak stress and strain values are unchanged for medium mesh cylinder in CDMR3 whereas, reduced by 2% with coarse mesh cylinder. This observation is in contrast with the assumption made. The increase in peak stress value with cylinder size for coarse mesh is within 6% and 8% for medium mesh, when using MC-VIB model. This is in agreement with the assumption and believed to be acceptable.

4.4 Revision of Trials

It is observed that for cylinder simulations, the peak stress and corresponding strain values are higher than the desired values. It is possible to modify the available parameter combination and achieve the parameter combination which can give more accurate prediction. For example, efforts are made to revise the set of parameter and observe the changes in stress-strain curve for single element.

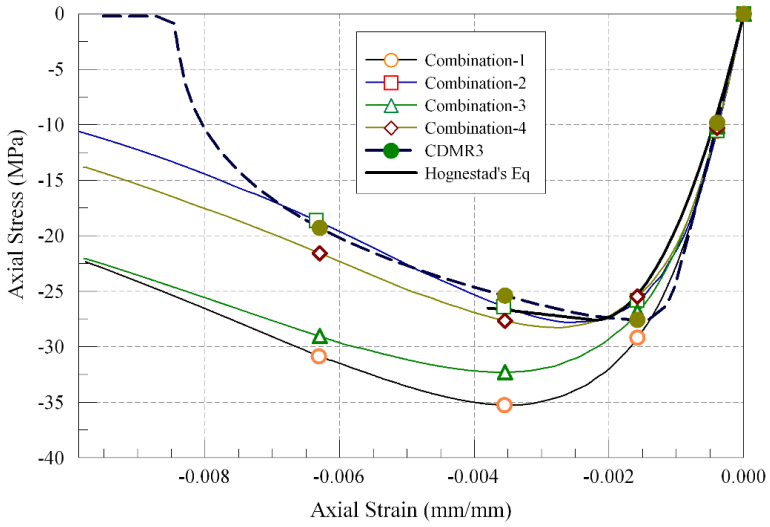

Figure 4-29 MC-VIB –Single element – Trials revision- comparison with Standard results

Table 4-6 MC-VIB-Single element-summary of revised trials for UUC

	E	EPS_C	EN	EC	Strain at peak stress (mm/mm)	Peak stress (MPa)	% error with Standard Results	
							Strain at peak stress (mm/mm)	Peak stress (MPa)
Hognestad's Eqn					0.0022	27.597		
CDMR3					0.0015	27.626	-32%	0%
Comb-1	3000	0.001	1	0.15	0.00347	35.2615	58%	28%
Comb-2	3000	0.001	1.1	0.16	0.00264	27.7908	20%	1%
Comb-3	3000	0.001	0.9	0.2	0.00361	32.2924	64%	17%
Comb-4	3000	0.0008	1	0.15	0.00282	28.2514	28%	2%

Four trial combinations are presented in this section for UUC. The Figure 4-29 depicts the comparison of MC-VIB trial stress-strain curves with Hognestad's Equation and CDMR3. The results tabulated in Table 4-6 clearly show that, the combination-3 and combination-4 yield the graphs which show closer approximation of Hognestad's Equation. The strain at peak stress value with combination-1 is 58% higher than that for Hognestad's Equation. But with combination-2, this difference is reduced to 20% which is lesser than, 32%, the percentage error for CDMR3. The peak stress for MC-VIB –Combination-2 shows 1% error from Hognestad's Equation.

The combinations used for UUC are used for single element UUT. But to reduce the error from standard value further, the sub combinations are tried. Where, EPS_C and hence BETA_C values are remain unchanged; only EPS_T and BETA_T values are modified to see the difference. Remarkable difference is observed as shown in Figure 4-30. In the Table 4-7 it is evident that, each combination with suffix 'a' show reduced error than the original combination results. Combination-2a can be said to have minimum error in peak stress value (39%) and corresponding strain (6%).

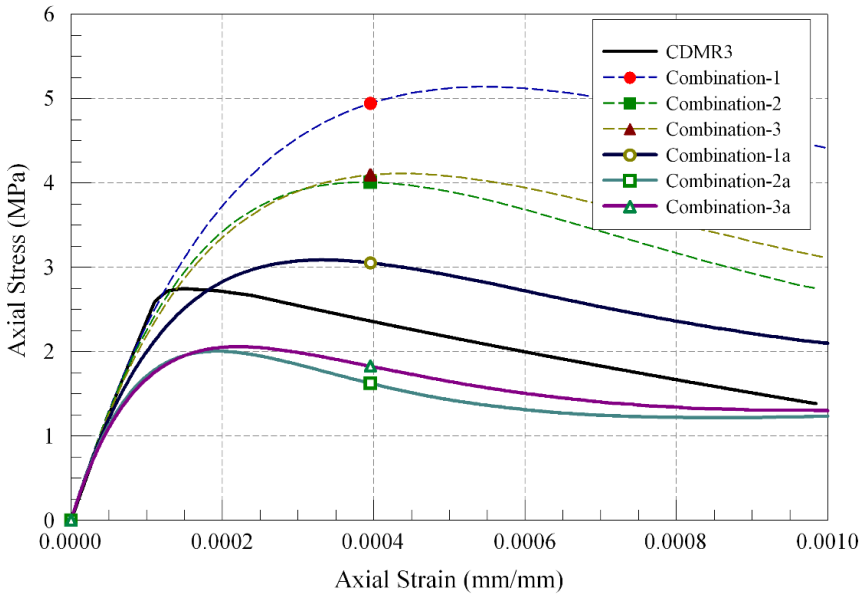

Figure 4-30 MC-VIB-Single Element-UUT-Revised trials- comparison with standard results

Table 4-7 MC-VIB-Single Element-Trials-UUT comparison with standard results

	E	EPS_C	EPS_T	EN	EC	Strain at peak stress (mm/mm)	Peak stress (MPa)	% error with Standard	
								Strain at peak stress (mm/mm)	Peak stress (MPa)
Standard						0.0002	3.27		
CDMR3						0.00015	2.75	-25%	-16%
MC-VIB									
Comb-1	3000	0.001	0.0001	1	0.15	0.00054	5.14	171%	57%
Comb-1a	3000	0.001	0.00006	1	0.15	0.00033	3.09	66%	-6%
Comb-2	3000	0.001	0.0001	1.1	0.16	0.00039	4.01	94%	23%
Comb-2a	3000	0.001	0.00005	1.1	0.16	0.00019	2	-6%	-39%
Comb-4	3000	0.0008	0.00008	1	0.15	0.00044	4.11	122%	26%
Comb-4a	3000	0.0008	0.00004	1	0.15	0.00021	2.06	7%	-37%

This leads to the future work for the project. The next chapter summarizes the conclusions form the results and future scope of the work.

Chapter 5.

CONCLUSIONS AND FUTURE WORK

In this project, the MC-VIB material model is successfully used to simulated elastic behavior of 27.6 MPa (4 ksi) concrete in both, Unconfined Uniaxial Compression as well as in Unconfined Uniaxial Tension. The comparison of the axial stress vs axial strain behavior of the concrete to that using CDMR3 and Hognestad's Equation show satisfactory results. The peak stress and corresponding strain value are primary objects of this study.

The study performed for individual parameters shows, effect of the parameters E, EPS_C, EPS_T, EN, and EC on the stress vs strain behavior of concrete. It is helpful to modify the parameters so as to get a best match with the standard results. The revised trials results shown in Chapter 4 show that there is scope to refine the parameters. Effects of change in loading velocity or strain rate is also an important aspect to study in comparison with the CDMR3 model.

The scope of this thesis is limited to Elastic behavior of stress-strain curve. Subsequent stages involve introducing plasticity in the model. That is to modify the subroutine and implementing equations to generate results for Elasto-plastic failure of the concrete after achieving peak stress. Simulations can be done with the focus on post peak behavior and failure of concrete. In similar manner the study can be done for different strength of concrete say 8ksi. The parameters then can be generalized to define a concrete with specific compressive strength.

REFERENCES

[1] G. Thiagarajan, "Dynamic Fracture Simulation of Concrete Using a Virtual Internal Bond Model," *Journal of Enigneering Mechanics,* vol. 133, no. 5, p. 514, 2007.

[2] H. Gao, "A Theory of Local Limiting Speed in Dynamic Fracture," *Journal of Mechanics and Physics of Solids,* vol. 44, no. 9, pp. 1453-1474, 1996.

[3] H. Gao, "Elastic Waves in a Hyperelastic Solid Near Its Plane Srain," *Philosophical Magazine Letters,* vol. 76, pp. 307-314, 1997.

[4] P. Klein and H. Patrick and Gao, "Crack Nucleation and Growth as Strain Localization in Virtual Internal Bond Continuum," *Engineering Fracture Mechanics,* vol. 61, pp. pp 21-48, 1998.

[5] P. Zhang, P. Klein, H. Y. Y., H. Gao and P. D. Wu, "Numerical Simulation of Cohesive Fracture by The Virtual Internal Bond Method," *Computational Modeling in Engineering and Science,* vol. 3, pp. 263-278, 2002.

[6] G. Thiagarajan, k. J. Hsia and Y. Huang, "Finite Element Implementation of Virtual Internal Bond Model for Simulating Crack Behavior," *Engineering Fracture Mechanics,* vol. 71, pp. 401-423, 2004.

[7] G. Thiagarajan and A. Misra, "Fracture Simulation for Anisotropic Materials Using Virtual Internal Bond Model," *International Journals of Solids and Structures,* vol. 41, pp. 2919-2938, 2004.

[8] Z. Zhang and X. Ge, "Micromechanical Consideration of Tensile Crack Behavior Based on Virtual Internal Bond in Contrast to Cohesive Stress," *Theoretical and Applied Fracture Mechanics,* vol. 43, pp. 342-359, 2005.

[9] Z. Zhang, X. Ge and Y. Li, "A Multiscale Mechanical Model for Materials Based on Virtual Internal Bond Theory," *Acta Mechanica Solida Sinica,* vol. 19, no. 3, pp. 196-202, 2006.

[10] J. K. Gran, Y. M. Gupta and A. L. Florence, "An Experimental Method to Study Dynamic Tensile Failure of Brittle Geologic Materials," *Mechanical Materials,* vol. 6, pp. 113-125, 1987.

[11] Z. N. Zhang, "Multiscale Simulation of Fracture Propagation in Heterogeneous Materials using Virtual Multidimensional Internal Bonds," *Theoretical and Applied Fracture Mechanics,* vol. 49, pp. 233-241, 2008.

[12] Z. Zhang, "Numerical Simulation of Crack Propagation with Equivalent Cohesive Zone Method Based on Virtual Internal Bond Theory," *International Journal of Rock Mechanics and Mining Sciences,* vol. 46, pp. 307-314, 2009.

[13] Z. Zhang and Y. Chen, "Simulation of Fracture Propagation Subjected to Compressive and Shear Stress Field Using Virtual Multidimensional Internal Bonds," *International Journal of Rock Mechanics and Mining Sciences ,* vol. 46, pp. 1010-1022, 2009.

[14] Z. Zhang, "Discretized Virtual Internal Bond Model for Nonlinear Elasticity," *International Journal of Solids and Strcutures,* vol. 50, pp. 3618-3625, 2013.

[15] Z. G. X. R. Zhang, "Multiscale Shear Fracture of Heterogeneous Material Using the Virtual Internal Bond," *Theoretical and Applied Fracture Mechanics,* vol. 47, pp. 185-191, 2007.

[16] C. Chang, T. Wang, L. Sluys and J. Van Mier, "Fracture Modeling Using a Micro-Structural Mechanics Approach-I. Theory and Formulation," *Engineering Fracture Mechanics,* vol. 69, no. 17, pp. 1941-1958, 2002.

[17] R. Park and T. Paulay, "Stress-strain Relationships for Concrete and Steel," in *Reinforced Concrete Structures*, A Wiley-Interscience Publication, 1975, pp. 12-16.

[18] LSDYNAV970, "971 Keyword Manual Vol. 1 and Vol. 2,.," Livermore Software Technology Corporation, Livermore, CA.

[19] T. Erhart, "An Overview of User Defined Interfaces in LS-DYNA(R)".

[20] J. B. Mander, M. J. N. Priestley, R. Park and A. Fellow, "Theoretical Stress-Strain Model For Confined Concrete".

[21] J. Crawford and S. Lan, "Design and Implementation of Protective Technologies for Improving Blast Resistance of Buildings ,," in *Encasing Building Security Seminar Proceedings*, Singapore, 2005.

[22] L. Schwer and M. L. Javior, "Simplified Concrete Modeling with *MAT_CONCRETE_DAMAGE_REL3," in *JRI LS-DYNA USER WEEK*, 2005.

[23] G. Thiagarajan, H. Y. Y and K. J. Hsia, "Fracture Simulation Using an Elasto-Viscoplastic Virtual internal Bond Model With Finite Elements," *Journal of Applied Mechanics,* vol. 71, no. 1, 2004.

[24] H. Gao and P. Klein, "Numerical Simulation of Crack Growth in an Isotropic Solid with Randomized Internal Cohesive Bonds," *Journal of Mechanics and Physics of Solids,* vol. 46, no. 2, pp. 187-218, 1998.

[25] D.o.D, "Unified facility criteria (UFC), DoD minimum antierrorism standards for buildings," Department of Defense, UFC 4-010-01, 2007.

VITA

Mayuri Rajendra Patil was born in Mumbai, in the state of Maharashtra, India on February 12, 1990. She got Bachelors in Civil engineering from Veermata Jijabai Technological Institute in 2011. She worked with Vadalkar & Associates in Mumbai, India as Design Structural Engineer. She earned valuable experience in analysis and design. She joined University of Missouri-Kansas City for masters in Civil and Structural Engineering in fall 2012. She started to work as Graduate Research Assistant with Dr. Ganesh Thiagarajan. The research thesis focuses on implementing modified virtual internal bond for concrete under dynamic loading. She is currently working with Desai/Nasr Consulting Engineers, Detroit, Michigan as a Structural Engineer and interested to pursue her career in the Structural Engineering.